

The Role of Dlc-2 in Ceramide Signaling to PGP Synthase

By CAROLINE SHIELDS

A Thesis Submitted to  
The Faculty of Graduate Studies  
of  
The University of Manitoba

In Partial Fulfillment of the Requirements for the Degree of  
MASTER OF SCIENCE

Department of Biochemistry and Medical Genetics  
University of Manitoba  
Winnipeg, Manitoba, Canada

Copyright © 2010 Caroline Shields

## **ABSTRACT**

The purpose of this project was to determine how Dlc-2 and Rho signaling modulate the ceramide induction of PGP synthase. Dlc-2 is a tumor-suppressor gene with RhoGAP, START, and SAM domains. The RhoGAP domain allows Dlc-2 to inactivate Rho proteins, namely RhoA and Cdc42. Rho proteins act as molecular switches that are involved in cellular processes such as cytoskeletal arrangements, cell morphology, cell migration, enzymatic activities, and signal transduction pathways. Ceramide is a sphingolipid that can regulate differentiation, growth suppression, cell senescence, and apoptosis. PGP synthase is the enzyme in the committed step of cardiolipin synthesis. Cardiolipin is a mitochondrial membrane phospholipid that is important to the structure and function of the mitochondria, and is an important docking lipid involved in apoptosis.

The ceramide induction of PGP synthase was studied at the transcriptional, post-transcriptional, and post-translational levels using cell culture, Real-Time RT-PCR, protein purification, phage display, and western blotting techniques.

We have demonstrated that the PGP synthase gene is not controlled at the transcriptional level by ceramide and Rho, nor is the mRNA stability of PGP synthase affected. However, the PGP synthase protein level is affected by ceramide and Rho.

The relationships between Dlc-2 (and Rho), ceramide, and PGP synthase (and CL) are important to understand. All three are involved in cancer and apoptotic responses. The knowledge gained by the experiments discussed in this thesis will contribute to an understanding of how these proteins and lipids interact. This knowledge may then be used in the future to develop cancer treatments.

## ACKNOWLEDGEMENTS

This thesis marks the end of the very long “school” phase of my life. I have learned a great deal, and gained a lot of experience. However, I do look forward to the future of homework-free evenings and weekends without journal articles.

Firstly, I would like to thank my family and friends for their unwavering support and patience. I greatly love and appreciate them all. I owe my parents a great deal. Without them, I would never have had the thought to pursue a Master’s degree, nor the means to do so. They have supported me with all of my life’s endeavours. A very large thank you is due to Jonathan for always supporting and encouraging me. He has been very patient, and has been there with me the whole time I have pursued this degree. I am truly lucky to have him in my life. I would also like to thank the Graham family for their support, especially Bonnie for her guidance. I would like to thank Angela, Carly, Marissa, Jenny H., Jenny M., and Aleks for being wonderful friends. I have known them all for a very large portion of my life, and they have stuck with me through the good and the frustrating times. A special thanks goes to Angela for being my phone call buddy and thesis-writing party pal. I would like to thank Lisa and Des. They are two wonderful friends I have met while in the Biochemistry and Medical Genetics department. Our Friday lunches were the highlight of my week many times. I owe a special thanks to Lisa for her encouragement in writing this thesis on our many writing dates. As well, I would like to thank Vanessa, Jamie, and the other members of Dr. Eisenstat’s lab for making me feel like part of their lab family. It is very important to have good neighbours, and I

could not ask for any better lab neighbours. Also, an extra thanks to Vanessa and Jamie, as our monthly culture outings and reality TV polls were very welcome breaks from academia that allowed me to re-energize and keep working towards my goal of completing this thesis.

I would like to thank all of the past and present members of the Mowat lab. I owe a large thanks to Yuan and Shannon for their help with the experiments in this thesis. As well, thank you to Heather, Cordula, Sabbir, Meenal, Rachelle, and Ray for making the lab such a nice place to be every day. Also, I owe a great deal to Lauren for her tremendous protein work during the last push to complete this project.

I would like to thank the people of the Biochemistry and Medical Genetics Department. A special thanks to Tuntun and Jan for all of their organization and guidance in the necessary non-science aspects of this degree. As well, I would like to thank Dr. Leygue for all of his help and guidance in putting together presentations. I would like to thank my committee members Dr. Davie and Dr. Hatch for their support and friendly faces when I was always nervous about giving presentations. Their questions always made me think, and they helped me a great deal in this project.

I would also like to thank the Manitoba Health Research Council and the CancerCare Manitoba Foundation for their funding, without which I would not have been able to even begin this project, let alone complete it.

Finally, I would like to thank Dr. Mowat for his patience and guidance throughout this long process. I am very grateful, as without him, this project – this immense accomplishment in my life – would not have been possible.

Sincerely Yours,

Caroline Shields

## **TABLE OF CONTENTS**

<b><u>ABSTRACT</u></b> .....	ii
<b><u>ACKNOWLEDGEMENTS</u></b> .....	iv
<b><u>LIST OF TABLES</u></b> .....	xi
<b><u>LIST OF FIGURES</u></b> .....	xii
<b><u>LIST OF ABBREVIATIONS</u></b> .....	xiv

### **CHAPTER 1 – LITERATURE REVIEW AND BACKGROUND INFORMATION**

1.1	Introduction.....	1
1.2	Rho GTPase-Activating Proteins (RhoGAPs) .....	1
1.3	Deleted in liver cancer-1 (Dlc-1), -2 (Dlc-2), and -3 (Dlc-3) .....	8
1.3.1	Dlc-1 .....	11
1.3.2	Dlc-2 .....	13
1.3.3	Dlc-3 .....	14
1.4	Ceramide .....	15
1.5	Sphingolipid Metabolism.....	19
1.6	Other Sphingolipids .....	26
1.7	Basics of Apoptosis.....	28
1.8	Ceramide and Apoptosis .....	31

1.9	Phosphatidylglycerolphosphate (PGP) Synthase .....	35
1.10	Cardiolipin .....	36
1.11	Cardiolipin Localization and Synthesis .....	39
1.12	Cardiolipin Functions.....	41
1.13	Cardiolipin and Apoptosis .....	42
1.14	Cardiolipin and Disease .....	44
1.15	Previous Laboratory Work.....	46
1.16	Antibody Production Using Phage Display .....	50
1.17	Project Rationale.....	52
1.18	Hypotheses .....	53

## **CHAPTER 2 – MATERIALS AND METHODS**

2.1	Transcriptional and Post-Transcriptional Control Experiments.....	55
2.1.1	Cell Culture Conditions .....	55
2.1.2	Cell Treatments .....	56
2.1.3	RNA Extraction .....	57
2.1.4	DNase Treatment.....	58
2.1.5	cDNA Synthesis .....	59
2.1.6	Real-Time RT-PCR .....	60
2.1.7	Agarose Gels .....	61

2.2	Post-Translational Control .....	62
2.2.1	Cloning of PGP Synthase into <i>E. coli</i> .....	62
2.2.2	Mini-Preparation.....	62
2.2.3	Protein Induction .....	64
2.2.4	Protein Purification.....	65
2.2.4.1	BugBuster Protein Purification Protocol.....	65
2.2.4.2	Urea Protein Purification Protocol .....	68
2.2.5	Bicinchoninic Acid Protein Assay.....	70
2.2.6	SDS-PAGE.....	71
2.2.7	Coomassie Blue Staining.....	72
2.2.8	Drying the gels .....	73
2.2.9	PGP Synthase Peptide Design .....	73
2.2.10	Protein Cross-Linking .....	74
2.2.10.1	Amino Group Preparation .....	74
2.2.10.2	Sulfhydryl Group Preparation .....	75
2.2.10.3	Crosslinking .....	76
2.2.11	Peptide Phage Display .....	76
2.2.12	Enzyme-Linked Immunosorbent Assay (ELISA) .....	89
2.2.13	Production of Soluble Antibody Fragments .....	92
2.2.14	Western Blotting.....	93

### **CHAPTER 3 – RESULTS**

3.1	Overview .....	98
3.2	Transcriptional Control .....	99
3.3	Post-Transcriptional Control .....	106
3.4	Post-Translational Control .....	112

### **CHAPTER 4 – DISCUSSION**

4.1	Introduction .....	147
4.2	Transcriptional Control .....	147
4.3	Post-Transcriptional Control .....	148
4.4	Post-Translational Control .....	149
4.5	Future Directions .....	156
4.6	Conclusions .....	157

### **CHAPTER 5 – LITERATURE CITED**

**LIST OF TABLES**

Table 1: Phage Display Day-to-Day Schedule ..... 84

## LIST OF FIGURES

Figure 1: The Rho GTPase cycle.....	4
Figure 2: Dlc-1 and Dlc-2 protein domains.....	10
Figure 3: Ceramide .....	16
Figure 4: Sphingolipid Metabolism.....	20
Figure 5: Cardiolipin Structure.....	38
Figure 6: Cardiolipin Metabolism .....	40
Figure 7: U3NeoSV1 Viral Vector .....	47
Figure 8: Multiplex RT-PCR of CHO-K1 cell lines.....	49
Figure 9: Phage Display Schematic.....	83
Figure 10: Real-Time RT-PCR.....	100
Figure 11: Cl22 Agarose Gel.....	102
Figure 12: E91 Agarose Gel .....	103
Figure 13: RSC6 Agarose Gel.....	104
Figure 14: RhoMT2 Agarose Gel.....	105
Figure 15: Cl22 Real-Time RT-PCR.....	108
Figure 16: E91 Real-Time RT-PCR .....	109
Figure 17: RSC6 Real-Time RT-PCR.....	110
Figure 18: RhoMT2 Real-Time RT-PCR.....	111

Figure 19: Mini-Preparation Agarose Gel.....	113
Figure 20: Induced Sample A Using the BugBuster Protein Purification Method .....	116
Figure 21: Induced Sample B Using the BugBuster Protein Purification Method.....	117
Figure 22: Non-Induced Sample Using the BugBuster Protein Purification Method ...	118
Figure 23: Induced Sample Using the BugBuster Protein Purification with Inclusion Body Purification Method.....	120
Figure 24: Non-Induced Sample Using the BugBuster Protein Purification with Inclusion Body Purification Method.....	121
Figure 25: Induced Sample Using the Urea Protein Purification Method.....	123
Figure 26: Non-Induced Sample Using the Urea Protein Purification Method .....	124
Figure 27: 16-mer Peptide, Tomlinson Phage Library I ELISA .....	127
Figure 28: 16-mer Peptide, Tomlinson Phage Library J ELISA .....	128
Figure 29: 25-mer Peptide, Tomlinson Phage Library I ELISA .....	129
Figure 30: 25-mer Peptide, Tomlinson Phage Library J ELISA .....	130
Figure 31: Western Blots from First Batch of 1-hour Cell Treatments.....	133
Figure 32: Western Blots from Second Batch of 1-hour Cell Treatments .....	137
Figure 33: Western Blots from First Batch of 4-hour Cell Treatments.....	141
Figure 34: Western Blots from Second Batch of 4-hour Cell Treatments .....	145

## LIST OF ABBREVIATIONS

$\alpha$ -MEM	$\alpha$ -Minimum Essential Medium
Acyl	fatty acid
AD	actinomycin D
AIF	apoptosis-inducing factor
AMP	adenosine monophosphate
Amp <sup>R</sup>	ampicillin resistance gene
ANOVA	analysis of variance
APAF-1	apoptotic protease activating factor-1
APS	ammonium persulfate
ATP`	adenosine triphosphate
B1	thiamine hydrochloride
Bax	B-cell lymphoma gene-2-associated X protein
BCA	bicinchoninic acid
Bcl-2	B-cell lymphoma gene-2
BH3	B-cell lymphoma gene-2 homology 3
Bid	B-cell lymphoma gene-2 homology 3 interacting domain death agonist
BLAST	Basic Local Alignment Search Tool
BSA	bovine serum albumin
C1P	ceramide-1-phosphate
C <sub>2</sub> -ceramide	N-acetyl-D-sphingosine
Ca <sup>2+</sup>	calcium

CaCl <sub>2</sub>	calcium chloride
CAPK	ceramide-activated protein kinase
CAPP	ceramide-activated protein phosphatase
CARD	caspase-recruitment domain
Cdk	cyclin-dependent kinase
cDNA	complementary deoxyribonucleic acid
CDP-DG	cytidine-diphosphate-1,2-diacyl- <i>sn</i> -glycerol
CERT	ceramide transfer protein
CHO	Chinese hamster ovary
CL	cardiolipin
CO <sub>2</sub>	carbon dioxide
CoA	coenzyme A
cten	C-terminal tensin-like protein
CTP	cytidine-5'-triphosphate
<i>C. parvum</i>	<i>Cryptosporidium parvum</i>
ddH <sub>2</sub> O	double distilled water
Dlc-1	deleted in liver cancer-1
Dlc-2	deleted in liver cancer-2
Dlc-3	deleted in liver cancer-3
DNA	deoxyribonucleic acid
DNase	deoxyribonuclease
dNTP	deoxyribonucleotide triphosphate
dsDNA	double-stranded deoxyribonucleic acid

DTT	dithiothreitol
<i>E. coli</i>	<i>Escherichia coli</i>
ECL	Enhanced Chemiluminescence
EDTA	ethylenediaminetetraacetic acid
EF1A1	eukaryotic elongation factor 1A1
ELISA	Enzyme-Linked Immunosorbent Assay
ER	endoplasmic reticulum
EtBr	ethidium bromide
ETC	electron transport chain
FAT	focal adhesion-targeting
FBS	fetal bovine serum
G3P	glycerol-3-phosphate
G418	neomycin antibiotic
GAPDH	glycerol-3-phosphate dehydrogenase
GDI	guanine nucleotide dissociation inhibitor
GDP	guanosine diphosphate
Golgi	Golgi apparatus
GTP	guanosine triphosphate
GTPase	guanosine triphosphatase
HIV	human immunodeficiency virus
HRP	horse radish peroxidase
IgG	immunoglobulin G
IMM	inner mitochondrial membrane

immunotube	Maxisorp immuno test tube
IPTG	isopropyl- $\beta$ -D-thiogalactopyranoside
JNK	c-Jun N-terminal kinase
KCH <sub>3</sub> COO	potassium acetate
KCl	potassium chloride
KH <sub>2</sub> PO <sub>4</sub>	potassium phosphate monobasic
K <sub>2</sub> HPO <sub>4</sub>	potassium phosphate dibasic
LB	lysogeny broth
LTR	long terminal repeat
MAP	mitogen-activated protein
MAPK	mitogen-activated protein kinase
MLCLAT	monolysocardiolipin acyltransferase
MLCL	monolysocardiolipin
MEK	mitogen-activated protein/extracellular-signal-regulated kinase
Mg <sup>2+</sup>	magnesium
MgCl <sub>2</sub>	magnesium chloride
MgSO <sub>4</sub>	magnesium sulphate
Mn <sup>2+</sup>	manganese
mRNA	messenger ribonucleic acid
NaCl	sodium chloride
NADH	nicotinamide adenine dinucleotide
NaF	sodium fluoride
NaH <sub>2</sub> PO <sub>4</sub>	sodium phosphate monobasic

Na <sub>2</sub> HPO <sub>4</sub>	sodium phosphate dibasic
NaHCO <sub>2</sub>	sodium bicarbonate
NaOH	sodium hydroxide
NCBI	National Center for Biotechnology Information
NF-κB	nuclear factor-κB
NGF	nerve growth factor
(NH <sub>4</sub> ) <sub>2</sub> SO <sub>4</sub>	ammonium sulfate
NMR	nuclear magnetic resonance
NO	nitric oxide
NP-40	nonidet P 40 substitute
OD280	absorbance at 280 nm
OD450	absorbance at 450 nm
OD600	absorbance at 600 nm
OD650	absorbance at 650 nm
OH	hydroxide
OMM	outer mitochondrial membrane
Ori	origin of replication
PA	phosphatidic acid
PAGE	polyacrylamide gel electrophoresis
PBR	polybasic region
PBS	phosphate buffered saline
PC	phosphatidylcholine
PCTP	phosphatidylcholine transfer protein

PEG	polyethylene glycol
PG	phosphatidylglycerol
PGP	phosphatidylglycerolphosphate
PH	pleckstrin homology
phage	bacteriophage
PI3-kinase	phosphatidylinositol 3-kinase
PI(4,5)P <sub>2</sub>	phosphatidylinositol-4,5-bisphosphate
PIP3	phosphatidylinositol (3,4,5)-triphosphate
PKC $\delta$	protein kinase C $\delta$
PLA <sub>2</sub>	phospholipase A <sub>2</sub>
PMSF	phenylmethanesulfonyl fluoride
PP1	protein phosphatase 1
PP2A	protein phosphatase 2A
PS	phosphatidylserine
PtdIns4P	phosphatidylinositol-4-monophosphate
PVDF	polyvinylidene fluoride
Rb	retinoblastoma protein
RBD	RhoA-binding domain
Rho	Rho GTPase
RhoGAP	Rho GTPase activating protein
RhoGEF	Rho GTPase guanine nucleotide exchange factor
RISC	ribonucleic acid-induced silencing complex
RNA	ribonucleic acid

RNase	ribonuclease
ROCK	Rho-associated kinase
ROS	reactive oxygen species
RT-PCR	reverse transcriptase-polymerase chain reaction
S1P	sphingosine-1-phosphate
SAM	sterile alpha motif
SAM2	sterile alpha motif domain of deleted in liver cancer-2
SAPK	stress-activated protein kinase
scFv	single chain variable fragment
SDS	sodium dodecyl sulfate
SDS-PAGE	sodium dodecyl sulfate polyacrylamide gel electrophoresis
SH2	Src homology 2
SH3	Src homology 3
shRNAi	short hairpin ribonucleic acid interference
siRNA	short interfering ribonucleic acid
SK	sphingosine kinase
SR	serine/arginine-rich protein
SRE	serum response element
SRF	serum response factor
StAR	steroidogenic acute regulatory protein
StARD8	steroidogenic acute regulatory protein-related lipid transfer protein 8
StARD13	steroidogenic acute regulatory protein-related lipid transfer protein 13
START	steroidogenic acute regulatory protein-related lipid transfer

sulfo-MBS	sulfo- <i>m</i> -maleimidobenzoyl- <i>N</i> -hydroxysuccinimide ester
TAE	tris-acetate-ethylenediaminetetraacetic acid
tBid	t-B-cell lymphoma gene-2 homology 3 interacting domain death agonist
TBS	tris-buffered saline
TCF	ternary complex factor
TEMED	tetramethylethylenediamine
TG1	T-phage resistant <i>Escherichia coli</i> .
TMB	3,3',5,5'-tetramethylbenzidine
TNF- $\alpha$	tumor necrosis factor- $\alpha$
UV	ultraviolet radiation
VH	variable region of the heavy chain of immunoglobulin
VL	variable region of the light chain of immunoglobulin
xg	times gravity

# **CHAPTER 1 – LITERATURE REVIEW AND BACKGROUND INFORMATION**

## **1.1 Introduction**

This thesis discusses the role of the Deleted in liver cancer-2 (Dlc-2) gene in ceramide signaling to phosphatidylglycerolphosphate (PGP) synthase. What follows is a description of Dlc-2 and other Rho GTPase (Rho) activating proteins (RhoGAPs). As well, a discussion of ceramide and other sphingolipids will be given, including their functions, metabolism, and roles in apoptosis. A short explanation on the basics of apoptosis will be given. PGP synthase and its role in cardiolipin (CL) synthesis will be addressed, followed by the role of CL in disease and apoptosis. A discussion of previous work from our laboratory will be given followed by the major techniques used in this project. Finally, a reflection on the future implications of this project is presented.

## **1.2 Rho GTPase-Activating Proteins (RhoGAPs)**

RhoGAPs, such as Deleted in liver cancer-1 (Dlc-1), Dlc-2, and Deleted in liver cancer-3 (Dlc-3), are proteins that inactivate specific Rho proteins by stimulating their intrinsic guanosine triphosphatase (GTPase) activity, converting it to the inactive guanosine diphosphate (GDP)-bound form (Moon and Zheng 2003). The RhoGAP domain is a loop structure that consists of nine  $\alpha$ -helices and a highly conserved arginine residue (Moon and Zheng 2003). RhoGAPs are multi-domain proteins (Moon and Zheng 2003; Jaffe and Hall 2005). For example, many RhoGAP proteins contain Src homology

2 and 3 (SH2 and SH3) domains (Moon and Zheng 2003; Jaffe and Hall 2005). The addition of other domains with the RhoGAP domain adds another level of regulation to these proteins, and thus, specific Rho GTPase proteins are highly regulated (Moon and Zheng 2003; Jaffe and Hall 2005).

Rho GTPases are part of the Ras superfamily of GTPases (Bourne, Sanders et al. 1991). The Ras superfamily is divided into five major branches based on sequence and functional similarities: Ras, Rab, Ran, Arf, and Rho (Wennerberg, Rossman et al. 2005). The Ras branch of proteins is involved in cell proliferation, differentiation, and survival (Wennerberg, Rossman et al. 2005). The Rab branch is involved in regulation of membrane trafficking, intracellular vesicular transport, and protein trafficking (Wennerberg, Rossman et al. 2005). The Ran branch is involved in regulation of nucleocytoplasmic transport of ribonucleic acid (RNA) and proteins (Wennerberg, Rossman et al. 2005). The Arf branch is involved in regulation of vesicular transport (Wennerberg, Rossman et al. 2005). The Rho branch is involved in regulation of actin, cell polarity, cell movement, cell shape, cell-cell and cell-matrix interactions, and cell cycle progression (Wennerberg, Rossman et al. 2005).

There are twenty-two mammalian Rho GTPase genes: RhoA, RhoB, RhoC, Rac-1, Rac-2, Rac-3, Cdc42, RhoD, Rnd1, Rnd2, RhoE/Rnd3, RhoG, TC10, TCL, RhoH/TTF, Chp, Wrch-1, Rif, RhoBTB1, RhoBTB2, Miro-1, and Miro-2 (Aspenstrom, Fransson et al. 2004). Rho GTPase proteins act as binary switches: they are active when bound to guanosine triphosphate (GTP) and inactive when bound to GDP (Bourne,

Sanders et al. 1991; Moon and Zheng 2003; Jaffe and Hall 2005). The Rho GTPase cycle can be seen in Figure 1. Rho GTPase guanine nucleotide exchange factors (RhoGEFs) catalyze the exchange of GDP for GTP, activating the Rho GTPase protein – the RhoGEFs act as the “on” switch (Moon and Zheng 2003; Jaffe and Hall 2005). RhoGAPs stimulate Rho’s intrinsic GTPase activity, causing the loss of a phosphate group from GTP to form GDP, inactivating the Rho GTPase protein – RhoGAPs act as the “off” switch (Moon and Zheng 2003; Jaffe and Hall 2005). Guanine nucleotide dissociation inhibitors (GDIs) bind to the GDP-bound inactive Rho GTPase proteins, stabilizing them in the cytoplasm and localizing them to where they have to be within the cell (Moon and Zheng 2003; Jaffe and Hall 2005).

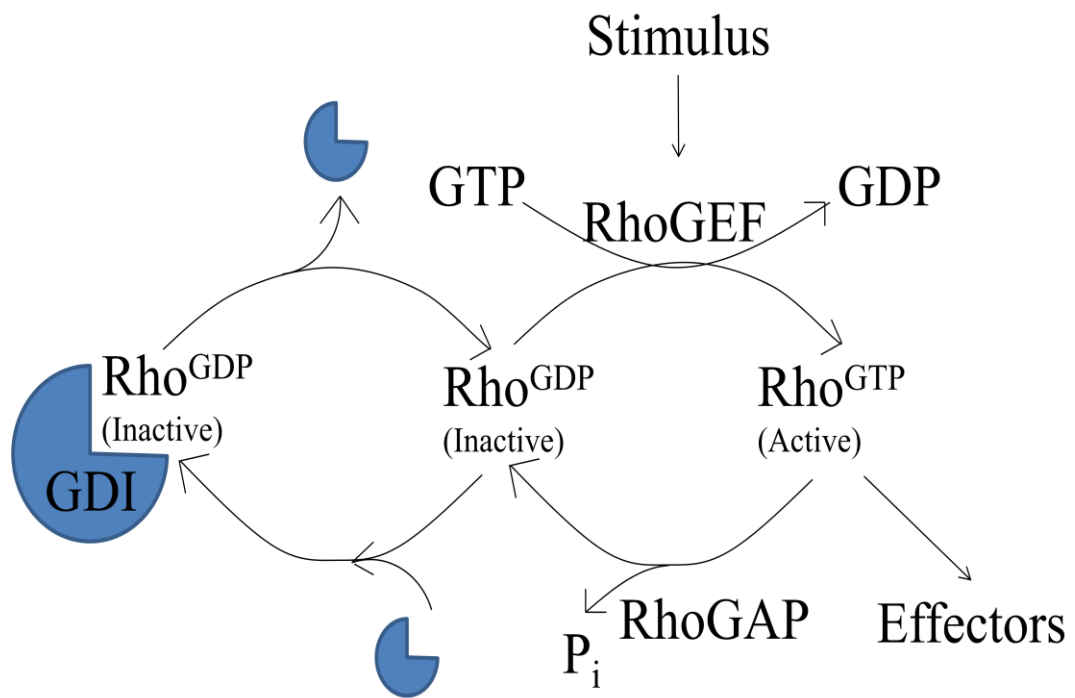


Figure 1: The Rho GTPase cycle

Adapted from: Jaffe and Hall 2005

Rho GTPases have many diverse effects on the cell (Jaffe and Hall 2005). If the proteins remain in either their active or inactive configurations, cellular processes will either keep occurring or will not occur at all (Jaffe and Hall 2005). Therefore, RhoGAPs and RhoGEFs are critical in keeping the balance in cellular processes (Jaffe and Hall 2005). Rho, Rac, and Cdc42 activation leads to actin cytoskeleton assembly (Jaffe and Hall 2005). Rho also affects microtubule dynamics (Jaffe and Hall 2005). Rho GTPases control aspects of the G<sub>1</sub> and M phases of the cell cycle (Jaffe and Hall 2005; Villalonga and Ridley 2006). During the G<sub>1</sub> phase, Rho affects cyclin-dependent kinases (Cdks), which are enzymes that control G<sub>1</sub> progression (Jaffe and Hall 2005; Villalonga and Ridley 2006). Inhibition of Rho, Rac, or Cdc42 has been found to block G<sub>1</sub> progression (Jaffe and Hall 2005). RhoA and Rac have been found to lead to cyclin D1 expression, which then causes cell cycle progression because Cdks are then activated by binding to cyclin D1 (Jaffe and Hall 2005; Villalonga and Ridley 2006). During the M phase, the actin cytoskeleton and microtubules are influenced (Jaffe and Hall 2005; Villalonga and Ridley 2006). The Cdc42 effector, mDia3, has been found to regulate attachment of microtubules to the kinetochore, ensuring proper chromosome alignment during metaphase (Villalonga and Ridley 2006). As well, Rho-associated kinase (ROCK) has been shown to control actin-myosin filaments that are required for correct positioning of centrosomes (Jaffe and Hall 2005). Due to the control of the actin cytoskeleton and microtubules by Rho GTPases, cell migration and cell-to-cell interactions are controlled by Rho (Jaffe and Hall 2005). Rho GTPases also regulate gene expression through signal transduction pathways (Jaffe and Hall 2005). The serum response element (SRE) is found in many promoters, including actin (Jaffe and Hall 2005). The SRE interacts with

two transcription factors: the ternary complex factor (TCF), which is regulated by the Ras/ mitogen-activated protein kinase (MAPK) pathway, and the serum response factor (SRF), which is regulated by Rho and requires the co-activator MAL (Jaffe and Hall 2005). After Rho activation, MAL translocates from the cytoplasm to the nucleus (Jaffe and Hall 2005). Additionally, actin cytoskeleton modifications, mediated by Rho, promote the translocation of MAL (Jaffe and Hall 2005). Rho proteins can also activate gene transcription through mechanisms that do not involve the actin cytoskeleton (Jaffe and Hall 2005). For example, Rho, Rac, and Cdc42 can activate the c-Jun N-terminal kinase (JNK) and p38 MAPK pathways (Jaffe and Hall 2005). All three have also been reported to induce the transcriptional activity of nuclear factor- $\kappa$ B (NF- $\kappa$ B) (Perona, Montaner et al. 1997). As well, many Rho GTPases have been found to play a role in apoptosis (Jimenez, Arends et al. 1995). Apoptosis induced by Rho GTPases has been found to be independent of p53, but dependent on B-cell lymphoma gene-2 (Bcl-2) expression and correlates with ceramide generation (Esteve, del Peso et al. 1995).

The most thoroughly studied effector molecules of Rho are the ROCKs (Schmandke and Strittmatter 2007). ROCKs are also known as Rho-associated coiled-coil protein kinases (Tanaka, Nishimura et al. 2006). They are downstream targets of RhoA (Schmandke and Strittmatter 2007). There are two protein isoforms: ROCKI (ROK $\beta$ ) and ROCKII (ROK $\alpha$ ) (Schmandke and Strittmatter 2007). Both ROCKs are serine/threonine kinases with three domains: a RhoA-binding domain (RBD) within the coiled-coil region, a kinase domain, and a cysteine-rich domain with a pleckstrin homology (PH) domain involved in protein-protein interactions (Schmandke and

Strittmatter 2007). The ROCKs are activated by RhoA binding to the RBD (Schmandke and Strittmatter 2007). The second messengers, arachidonic acid and sphingosylphosphorylcholine also activate the ROCKs (Schmandke and Strittmatter 2007). ROCKI can also be activated by caspase-3 through cleaving of ROCKI's autoinhibitory C-terminus (Schmandke and Strittmatter 2007). The ROCKs play roles in cell adhesion, cytokinesis, and gene expression through the alteration of actin dynamics (Tanaka, Nishimura et al. 2006). As well, it has been found that ROCKs can phosphorylate the myosin-binding subunit of myosin phosphatase, inhibiting phosphatase activity (Totsukawa, Yamakita et al. 2000). This leads to an increase in phosphorylation of the myosin light chain of myosin II (Totsukawa, Yamakita et al. 2000). Myosin II has been suggested to induce RhoA mediated stress fibre and focal adhesion assembly; therefore, this may be a feedback mechanism (Totsukawa, Yamakita et al. 2000). ROCKs are the downstream effectors of RhoA, and they lead to an increase in myosin II activity, which in turn induces RhoA.

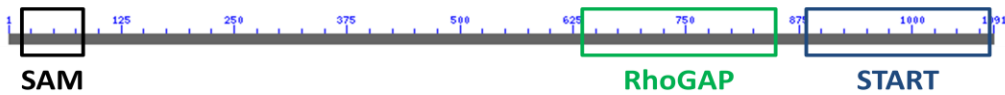
### **1.3 Deleted in liver cancer-1 (Dlc-1), -2 (Dlc-2), and -3 (Dlc-3)**

The human Dlc-1, Dlc-2, and Dlc-3 genes are paralogous tumor suppressor genes with three domains: the RhoGAP domain; the steroidogenic acute regulatory protein (StAR)-related lipid transfer (START) domain; and the sterile alpha motif (SAM) domain, as shown in Figure 2 (Kawai, Kiyota et al. 2007; Kawai, Kitamura et al. 2009; Kawai, Seike et al. 2009). The START domain is a domain of approximately 210 amino acid residues that binds lipids, such as cholesterol (Ponting and Aravind 1999; Christenson and Strauss 2001; Alpy and Tomasetto 2005). It can be regarded as a lipid-exchange or lipid-sensing domain, and acts as a shield to protect hydrophobic lipids from the hydrophilic cytoplasm (Alpy and Tomasetto 2005). In humans, START domains are found in fifteen distinct proteins that are organized into five families (Alpy and Tomasetto 2005). The two families that pertain to this project are the RhoGAP START group, which contains Dlc-1, Dlc-2, and Dlc-3, and the STARD2/phosphatidylcholine (PC) transfer protein (PCTP) group that contains the ceramide transfer protein (CERT) (Alpy and Tomasetto 2005).

The sterile alpha motif (SAM) domain is involved in protein-protein interactions (Qiao and Bowie 2005). SAM domains can bind other SAM domains, allowing proteins to homo- or hetero-oligomerize (Qiao and Bowie 2005). As well, SAM domains have been found to bind to non-SAM domain proteins, such as kinases, and to RNA (Qiao and Bowie 2005). The SAM domain of Dlc-2 (SAM2) was found to have a different four-helix structure, rather than the typical five-helix structure as determined by nuclear

magnetic resonance (NMR) (Kwan and Donaldson 2007; Li, Fung et al. 2007). This may allow the Dlc-2 SAM domain to interact with different ligands compared to proteins with typical SAM domains (Kwan and Donaldson 2007). As well, this special SAM domain allows Dlc-2 to exist as a monomer – the typical SAM domain requires binding (Li, Fung et al. 2007). This unique SAM2 domain exhibits membrane binding properties as well (Li, Fung et al. 2007). The Dlc-1 SAM domain also has a non-typical SAM domain structure with four helices (Zhong, Zhang et al. 2009). The Dlc-1 SAM domain, but not the Dlc-2 SAM domain, has been found to bind to the eukaryotic elongation factor 1A1 (EF1A1) (Zhong, Zhang et al. 2009). This binding facilitated EF1A1 distribution to the membrane periphery and ruffles after growth factor stimulation (Zhong, Zhang et al. 2009). This suggests a possible mechanism for cell migration modulation by Dlc-1 that is independent of Dlc-1's RhoGAP domain (Zhong, Zhang et al. 2009).

**Dlc-1**



**Dlc-2**

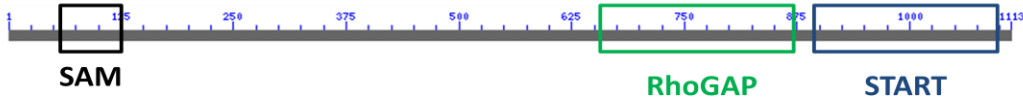


Figure 2: Dlc-1 and Dlc-2 protein domains

Adapted from: Altschul, Madden et al. 1997

### 1.3.1 Dlc-1

The human Dlc-1 gene is located on chromosome 8p21-22 (Yuan, Zhou et al. 2003). The DLC-1 protein interacts specifically with RhoA, RhoB, RhoC, and Cdc42 (Healy, Hodgson et al. 2008). The Dlc-1 gene, unlike Dlc-2 and Dlc-3, has been found to have an additional region – the polybasic region (PBR) (Erlmann, Schmid et al. 2009). DLC-1 has been found to bind phosphatidylinositol-4,5-bisphosphate (PI(4,5)P<sub>2</sub>) through the PBR (Erlmann, Schmid et al. 2009). When the PBR is lacking, DLC-1 does not signal to Rho proteins as efficiently (Erlmann, Schmid et al. 2009). Therefore, DLC-1 is regulated by this lipid, so it may be more active when bound to membranes containing PI(4,5)P<sub>2</sub> (Erlmann, Schmid et al. 2009). In humans, the Dlc-1 gene has three transcripts; the major transcript, Dlc-1 $\alpha$ , is 6.3 kb and encodes a 123 kDa protein (Durkin, Yuan et al. 2007; Ko, Yeung et al. 2010). In humans, there are also isoforms Dlc-1 $\beta$  and Dlc-1 $\gamma$  (Ko, Yeung et al. 2010). Dlc-1 $\alpha$  and Dlc-1 $\beta$  are structurally similar, and both contain the SAM, START, and RhoGAP domains (Ko, Yeung et al. 2010). The Dlc-1 $\gamma$  isoform is the smallest human isoform, and does not contain the START or RhoGAP domains (Ko, Yeung et al. 2010). In mice, the Dlc-1 gene has four transcriptional isomers under the influence of three alternative promoters: isoform 1 is a 6.2 kb transcript that encodes a 127 kDa protein, isoform 2 is a 6.1 kb transcript that encodes a 123 kDa protein, isoform 3 is a 7.6 kb transcript, and isoform 4 is a 2.1 kb transcript (Sabbir, Wigle et al. 2010).

DLC-1 has been found to directly interact with tensin2, which is a focal adhesion protein (Yam, Ko et al. 2006). Tensin2 plays a role in cytoskeleton organization and signal transduction, and has been found to be highly expressed in healthy human liver (Yam, Ko et al. 2006). It was found that both DLC-1 and tensin2 interact with caveolin-1, which is a component of caveolae (Yam, Ko et al. 2006). When tensin2 was transfected into hepatocellular carcinoma cell lines with low tensin2 expression, there was induction of apoptosis and inhibition of growth (Yam, Ko et al. 2006). It has been found that DLC-1 binds to tensin2 through a focal adhesion-targeting (FAT) region on the N-terminal half of the protein (Kawai, Kitamura et al. 2009). Expression of only the FAT domain of DLC-1 in HeLa cells acted as a dominant negative, causing dissociation of DLC-1 from focal adhesions (Kawai, Iwamae et al. 2009). DLC-1 also interacts with the C-terminal tensin-like protein (cten), which is another focal adhesion protein (Liao, Si et al. 2007). DLC-1 mutants can disrupt the interaction between DLC-1 and cten, causing DLC-1 to no longer locate to focal adhesions (Liao, Si et al. 2007). This has been found to disrupt DLC-1's tumor suppressor activity (Liao, Si et al. 2007).

When a recombinant adenovirus encoding wild-type Dlc-1 was used to restore Dlc-1 in the SNU-368 carcinoma cell line, there was an inhibition of cell proliferation (Kim, Lee et al. 2007). Dlc-1 over-expression in the cell line caused disassembly of stress fibres, inhibition of cell migration, and dephosphorylation of focal adhesion proteins (Kim, Lee et al. 2007). It has been found that the restoration of Dlc-1 in M4A4 cells, a metastatic breast tumor cell line, resulted in inhibition of migration and invasion to levels comparable to the non-metastatic NM2C5 cell line (Goodison, Yuan et al.

2005). This suggests that Dlc-1 can act as a metastasis-suppressor gene (Goodison, Yuan et al. 2005). Dlc-1 is found to be down-regulated in breast, colon, prostate, renal, uterine, and rectal cancer cell lines (Yuan, Zhou et al. 2003; Ullmannova and Popescu 2006) and can inhibit the growth and tumorigenicity in breast, liver, and prostate cancer cell lines (Yuan, Zhou et al. 2003). The RhoGAP activity of Dlc-1 has been shown to be essential for Dlc-1's tumor suppressor function; therefore, the cancer suppression of Dlc-1 is occurring because the Dlc-1 RhoGAP is negatively regulating the activity of Rho proteins (Wong, Yam et al. 2005).

### **1.3.2 Dlc-2**

The human Dlc-2 gene, also known as StAR-related lipid transfer protein 13 (StARD13), is located on chromosome 13q12.3 (Ching, Wong et al. 2003). The RhoGAP activity of DLC-2 is specific for RhoA and Cdc42, but has more affinity for RhoA (Ching, Wong et al. 2003; Nagaraja and Kandpal 2004). DLC-2 has four isoforms in humans: DLC-2 $\alpha$ , DLC-2 $\beta$ , DLC-2 $\gamma$ , and DLC-2 $\delta$ . Only DLC-2 $\alpha$ , DLC-2 $\beta$ , and DLC-2 $\gamma$  contain a RhoGAP domain (Leung, Ching et al. 2005). Over-expression of these isoforms in mouse fibroblasts induced stress fibre formation and produced a rounded morphology rather than a spindle morphology, as was present in the non-transfected cells (Leung, Ching et al. 2005). This may be because DLC-2 inhibits cytoskeletal reorganization mediated by Rho (Ching, Wong et al. 2003). DLC-2 has been shown to localize to focal adhesions through interactions with tensin2 by a FAT region on the N-terminal half of the protein (Kawai, Seike et al. 2009). DLC-2 has also been found to

locate to the mitochondria through its START domain (Ng, Chan et al. 2006). Dlc-2 is found to be commonly deleted in hepatocellular carcinomas (Ching, Wong et al. 2003) and to be down-regulated in lung, ovarian, renal, breast, uterine, gastric, colon, rectal, and glioblastoma tumors (Ullmannova and Popescu 2006; de Tayrac, Etcheverry et al. 2009). The transfection of the Dlc-2 RhoGAP caused growth suppression in the MCF7 breast carcinoma cell line (Nagaraja and Kandpal 2004; Popescu and Durkin 2004). Also, Dlc-2 counteracts Ras-mediated cellular transformation (Ching, Wong et al. 2003). In summary, Dlc-2 acts as a tumor suppressor by suppressing RhoA's effects on cytoskeletal reorganizations, cell growth, cell migration, and cell transformation (Leung, Ching et al. 2005).

### **1.3.3 Dlc-3**

The human Dlc-3 gene, also known as StAR-related lipid transfer protein 8 (StARD8) or KIAA0189, is located on chromosome Xq13 (Durkin, Ullmannova et al. 2007). DLC-3 downregulates RhoA and Cdc42 activity (Kawai, Kiyota et al. 2007). DLC-3 has two isoforms: DLC-3 $\alpha$  and DLC-3 $\beta$  (Kawai, Kiyota et al. 2007). The Dlc-3 $\alpha$  gene encodes a protein that is highly similar to DLC-1 and DLC-2 with RhoGAP, START, and SAM domains (Kawai, Kiyota et al. 2007). The Dlc-3 $\beta$  gene encodes a protein that has the RhoGAP and START domains, but lacks the SAM domain (Kawai, Kiyota et al. 2007). Ectopic expression of Dlc-3 in HeLa cells decreased stress fibers, but mutated Dlc-3 had no effect on cellular morphology (Kawai, Kiyota et al. 2007). DLC-3 was found to bind to tensin1 at focal adhesions (Kawai, Kiyota et al. 2007). Due to the

fact that DLC-1, DLC-2, and DLC-3 are all found to localize to focal adhesions, it follows that the DLC proteins may need to be located to focal adhesions to perform their tumor suppressor activity (Kawai, Kiyota et al. 2007; Kawai, Kitamura et al. 2009; Kawai, Seike et al. 2009). Finally, Dlc-3 message levels have been found to be down-regulated in kidney, lung, ovarian, uterine, and breast cancer samples (Durkin, Ullmannova et al. 2007).

#### **1.4 Ceramide**

Ceramide is the simplest of the sphingolipids (Futerman and Hannun 2004). It consists of a sphingosine and a fatty acid (Hannun and Obeid 2008), as shown in Figure 3. It can act as a cell signaling molecule and as a precursor to more complex sphingolipids (Futerman and Hannun 2004). Ceramide can function as a second messenger, and has been known to regulate differentiation, growth suppression, cell senescence, and apoptosis (Hannun, Obeid et al. 1993; Siskind 2005). Accumulation of intracellular ceramide causes cells to be driven towards a cytostatic state, inhibiting cell growth (Hannun, Obeid et al. 1993). At higher intracellular concentrations of ceramide, cells initiated apoptosis (Hannun, Obeid et al. 1993). Tumor necrosis factor- $\alpha$  (TNF- $\alpha$ ), Fas ligands,  $\gamma$ -interferon, interleukin-1, nerve growth factor (NGF), nitric oxide (NO), dexamethasone, cytosine arabinoside, daunorubicin, vincristine, heat, radiation, human immunodeficiency virus (HIV) infection, and cell senescence have been found to induce ceramide formation (Birbes, El Bawab et al. 2002).

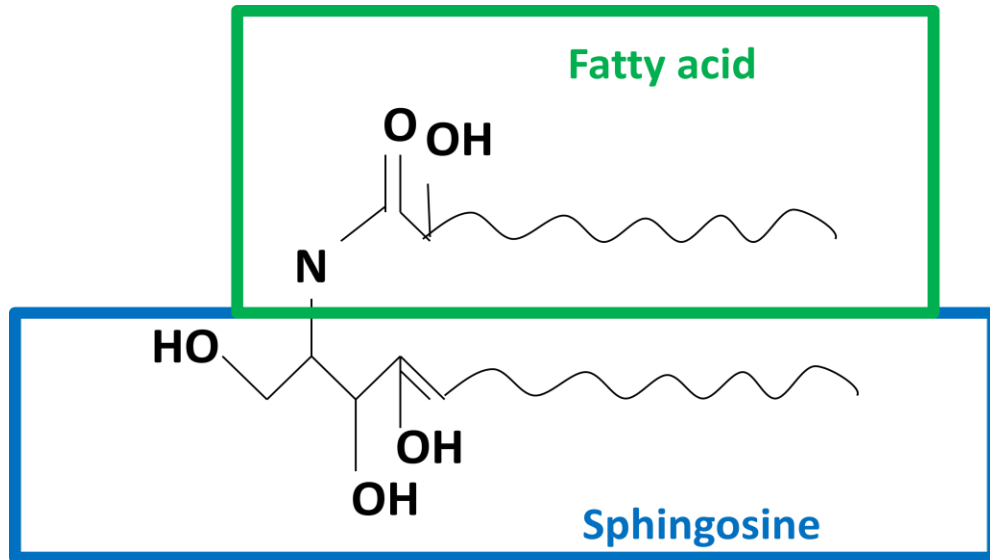


Figure 3: Ceramide

Adapted from: Hannun and Obeid 2008

Ceramide is important to cellular signaling (Hannun, Obeid et al. 1993). Ceramide can activate the serine/threonine phosphatases protein phosphatase 1 (PP1) and protein phosphatase 2A (PP2A) (Birbes, El Bawab et al. 2002). PP1 activation by ceramide results in dephosphorylation of the serine/arginine-rich (SR) proteins that regulate messenger RNA (mRNA) splicing (Birbes, El Bawab et al. 2002). Ceramide-activated protein phosphatase (CAPP) of the PP2A family can mediate the dephosphorylation of the anti-apoptotic protein Bcl-2 (Birbes, El Bawab et al. 2002). CAPP is specifically activated by ceramide (Hannun, Obeid et al. 1993). Protein phosphorylation is a mechanism of signal-transduction, so ceramide is indeed a second messenger (Hannun, Obeid et al. 1993). Ceramide also activates the ceramide-activated protein kinase (CAPK) (Birbes, El Bawab et al. 2002). CAPK is a membrane-bound, proline-directed serine/threonine kinase that phosphorylates Raf-1 (Birbes, El Bawab et al. 2002). Raf-1 then phosphorylates the MAPK/ERK kinase (MEK), leading to activation of the MAPK cascade (Birbes, El Bawab et al. 2002). Ceramide activates protein kinase C  $\delta$  (PKC $\delta$ ), which is involved in NF- $\kappa$ B activation (Birbes, El Bawab et al. 2002). Ceramide also affects cell cycle regulation through dephosphorylation of retinoblastoma protein (Rb) through the PP1 phosphatase (Birbes, El Bawab et al. 2002). Ceramide down-regulates the transcription factor c-myc, and activates the transcription factor c-jun (Birbes, El Bawab et al. 2002). Ceramide has also been found to regulate stress-activated protein kinases (SAPK), mitogen-activated protein kinases p42/44, phospholipase A<sub>2</sub> (PLA<sub>2</sub>), protein kinase B, and phospholipase D (Gomez-Munoz 2006).

Ceramide and other sphingolipids are important to the formation and stability of “lipid rafts,” which are segregated lipid microdomains on the lateral plane of the lipid bilayer (Futerman and Hannun 2004; Zhang, Li et al. 2009). These lipid rafts are enriched in sphingolipids and cholesterol (Futerman and Hannun 2004; Zhang, Li et al. 2009). Plasma membrane rafts have been found to act as signaling platforms (Futerman and Hannun 2004). Ceramide is formed in cellular membranes by the *de novo* pathway of ceramide synthesis or by acid sphingomyelinases (Zhang, Li et al. 2009). The release of ceramide in membranes causes the spontaneous association of other ceramide molecules to bind to the released ceramide molecules, causing small ceramide-enriched microdomains (Zhang, Li et al. 2009). It has been shown in artificial membranes that the accumulation of ceramide then displaces cholesterol from the raft (Zhang, Li et al. 2009). More ceramide then accumulates to form ceramide-enriched macrodomains and membrane platforms (Zhang, Li et al. 2009). Therefore, ceramide can change the biophysical characteristics of membranes (Zhang, Li et al. 2009). Ceramide-enriched membrane platforms have been shown to trap and cluster receptor molecules, allowing for increased amplification of cellular signals (Zhang, Li et al. 2009). Also, the receptor aggregation allows for a more stable interaction between the receptor and its ligand (Zhang, Li et al. 2009).

Ceramide is a neutral lipid, so it can “flip-flop” across membranes (Hannun and Obeid 2008). Ceramide has a minimal hydrophilic region (two hydroxide [–OH] groups) when compared to more complex sphingolipids (Futerman and Hannun 2004). Therefore, natural ceramides are very hydrophobic with low solubility in aqueous solutions (Hannun, Obeid et al. 1993). This made it very difficult to study the effects of

ceramides on cells in culture (Hannun, Obeid et al. 1993). This problem was overcome by the development of more soluble, cell-permeable analogs of ceramide (Hannun, Obeid et al. 1993). These analogs contained either a shorter sphingosine backbone or a shorter fatty acid (acyl) group (Hannun, Obeid et al. 1993). The ceramide analog used in this project was C<sub>2</sub>-ceramide (N-acetylsphingosine). At very high concentrations, C<sub>2</sub>-ceramide becomes cytotoxic to cells (Hannun, Obeid et al. 1993). C<sub>2</sub>-ceramide was also found to inhibit cell growth in a dose-dependent manner in HL-60 cells, U937 monocytic leukemia cells, human T cells, B cells, human glioma cells, and yeast cells (Hannun, Obeid et al. 1993).

## **1.5 Sphingolipid Metabolism**

Ceramide is the central molecule, or metabolic hub, in sphingolipid metabolism (Birbes, El Bawab et al. 2002; Futerman and Hannun 2004; Hannun and Obeid 2008). Ceramides act as sphingolipid building blocks (sphingoid bases), and are the hydrophobic backbones of all complex sphingolipids (Tomassini and Testi 2002; Siskind 2005). The *de novo* synthesis of ceramide occurs in the endoplasmic reticulum (ER) or the mitochondria; synthesis of sphingomyelin and other complex sphingolipids and glycosphingolipids occurs after ceramide has been shuttled to the Golgi apparatus (Golgi) from the ER (Futerman and Hannun 2004; Siskind 2005). Ceramide can also be produced by sphingomyelin hydrolysis and through a salvage pathway (Birbes, El Bawab et al. 2002; Siskind 2005; Kitatani, Idkowiak-Baldys et al. 2008). The outline of sphingolipid metabolism can be seen in Figure 4.

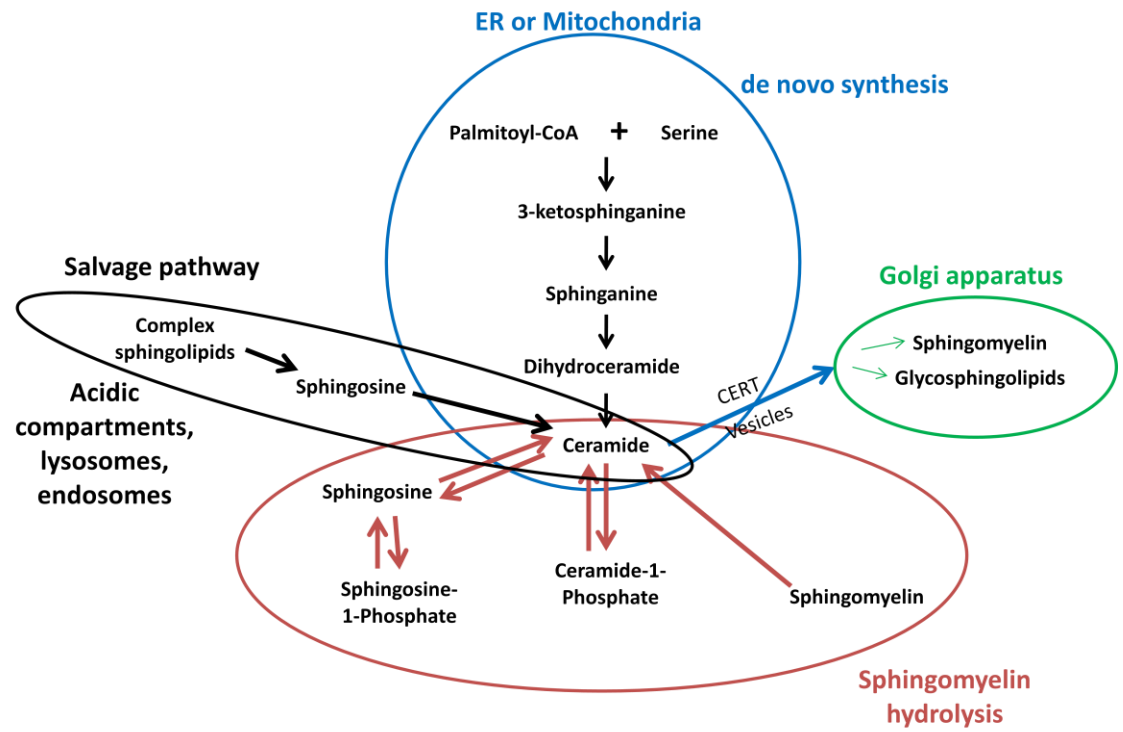


Figure 4: Sphingolipid Metabolism

Adapted from: Hannun and Obeid 2008

The *de novo* biosynthesis of ceramide begins with palmitoyl-coenzyme A (CoA) being condensed with serine by serine palmitoyl transferase to form 3-ketosphinganine (Grant and Spiegel 2002; Siskind 2005). This condensation is the entry point of sphingolipid biosynthesis (Hannun and Obeid 2008). 3-ketosphinganine is then reduced to form sphinganine (Grant and Spiegel 2002; Siskind 2005). Ceramide synthase then N-acylates the sphinganine to produce dihydroceramide (Birbes, El Bawab et al. 2002; Grant and Spiegel 2002). Dihydroceramide is then desaturated to produce ceramide (a *trans* double bond is introduced at the 4-5- position) (Grant and Spiegel 2002; Siskind 2005).

Ceramide that is synthesized in the ER through the *de novo* pathway is translocated to the Golgi for further processing in mammalian cells (Hanada, Kumagai et al. 2003). There are two pathways for ceramide transport from the ER to the Golgi (Hanada, Kumagai et al. 2003). There is an adenosine triphosphate (ATP)- and cytosol-dependent major pathway (non-vesicular), and an ATP- or cytosol-independent minor pathway (vesicular) (Hanada, Kumagai et al. 2003; Futerman and Hannun 2004). It was shown in LY-A Chinese hamster ovary (CHO) cells, where the major pathway is impaired, that ceramide transport was not impaired because the minor pathway was still functional (Hanada, Kumagai et al. 2003). It was shown that the major pathway involves CERT, and this protein was defective in the LY-A cells (Hanada, Kumagai et al. 2003). CERT can mediate transfer of various ceramides (C<sub>14</sub>-, C<sub>16</sub>-, C<sub>18</sub>-, C<sub>20</sub>-, C<sub>16</sub>-dihydroceramide, and C<sub>16</sub>-phytoceramide) (Kumagai, Yasuda et al. 2005). CERT is a 68 kDa cytoplasmic protein that mediates the ATP-dependent major pathway of

ceramide transport in a non-vesicular manner (Hanada, Kumagai et al. 2003). It has a phosphoinositide-binding PH domain that recognizes phosphatidylinositol-4-monophosphate (PtdIns4P), allowing CERT to be targeted to the Golgi (Hanada, Kumagai et al. 2003). CERT also contains a START domain and a middle region with coiled-coil motifs (Hanada, Kumagai et al. 2003). CERT was found to interact with ER membranes and extract ceramide specifically (Hanada, Kumagai et al. 2003). CERT was dependent on its START domain to transport ceramide to the Golgi (Hanada, Kumagai et al. 2003). The crystal structure of the CERT START domain shows that ceramides with different fatty acyl chain lengths can be buried in a long amphiphilic cavity (Kudo, Kumagai et al. 2008). There is a structural basis for the fact that START can distinguish ceramide from other lipids (Kudo, Kumagai et al. 2008).

Once ceramide is formed through *de novo* synthesis, it is metabolized in the Golgi (Siskind 2005). Ceramide can be glycosylated to form glycosphingolipids (Siskind 2005). It can also form sphingomyelin by sphingomyelin synthase (Siskind 2005). Sphingomyelin synthase transfers a phosphocholine head group from phosphatidylcholine to ceramide to generate sphingomyelin and diacylglycerol (Birbes, El Bawab et al. 2002; Siskind 2005).

Ceramide can also be generated by the hydrolysis of sphingomyelin (Birbes, El Bawab et al. 2002; Siskind 2005). Sphingomyelinases are distinguished according to their pH optimum (Birbes, El Bawab et al. 2002). There are at least eight sphingomyelinases (Birbes, El Bawab et al. 2002). Acid sphingomyelinases have a pH

optimum of 4.5-5, and are localized mainly in lysosomes (Siskind 2005). They can also be found in the plasma membrane and can be secreted (Siskind 2005). The deficiency of acid sphingomyelinases causes Niemann-Pick disease, which is a lysosomal storage disorder (Birbes, El Bawab et al. 2002). There are also many neutral sphingomyelinases that are localized to the plasma membrane, the cytosol, the endoplasmic reticulum, and nuclear membranes (Birbes, El Bawab et al. 2002). Neutral sphingomyelinases can be classified as magnesium ( $Mg^{2+}$ )/manganese ( $Mn^{2+}$ )-dependent or –independent (Siskind 2005). There are also alkaline sphingomyelinases (Birbes, El Bawab et al. 2002; Siskind 2005). Alkaline sphingomyelinases have been found to be activated by bile salts and are found in intestinal cells (Siskind 2005). Sphingomyelinases are activated by inflammatory cytokines, growth factors, G-protein-coupled receptors, and cell stress (Nixon 2009). Activation of sphingomyelinases leads to the breakdown of sphingomyelin to ceramide (Nixon 2009).

Ceramide can be phosphorylated by ceramide kinase to form ceramide-1-phosphate (C1P) (Nixon 2009). C1P can then be recycled by C1P phosphatase to form ceramide again (Bartke and Hannun 2009). Ceramide can also be degraded by ceramidases to produce sphingosine (Nixon 2009). Sphingosine can be phosphorylated in the cytosol or ER by sphingosine kinases to produce sphingosine-1-phosphate (S1P) (Siskind 2005; Nixon 2009). There are two known sphingosine kinases (SKs) in mammalian cells: SK1 and SK2 (Nixon 2009). S1P can then be dephosphorylated back to sphingosine by sphingosine phosphatase or S1P lyase (Nixon 2009). This is the exit point of sphingolipid metabolism, as S1P lyase breaks down S1P into the non-

sphingolipid molecules, ethanolamine phosphate and hexadecenal (Hannun and Obeid 2008). Sphingomyelin can be re-synthesized from sphingosine by ceramide synthase (to make ceramide) and by sphingomyelin synthase (ceramide to sphingomyelin) (Nixon 2009). Ceramide can also be glycosylated by glucosyl or galactosyl ceramide synthases (Bartke and Hannun 2009). Ceramide can also be formed by the breakdown of glycosphingolipids to produce glucosylceramide and galactosylceramide by hydrolases (Bartke and Hannun 2009). These are then hydrolyzed by specific  $\beta$ -glucosidases and galactosidases to release ceramide (Bartke and Hannun 2009).

Ceramide breakdown is due to the action of ceramidases (Birbes, El Bawab et al. 2002). Ceramidases liberate the fatty acid from the sphingoid base of ceramide (Birbes, El Bawab et al. 2002). There are acid, neutral/alkaline, and alkaline ceramidases (Birbes, El Bawab et al. 2002). The acid ceramidase is located lysosomally (Birbes, El Bawab et al. 2002). The neutral/alkaline ceramidases are localized to mitochondria, the nuclear membrane, and the ER (Birbes, El Bawab et al. 2002; Siskind 2005). The alkaline ceramidases are found in the Golgi and ER (Birbes, El Bawab et al. 2002). The neutral/alkaline ceramidases also catalyze the reverse reaction to generate ceramide from sphingosine and fatty acids (Siskind 2005). Ceramidases also establish a balance between the ceramide/sphingosine and S1P signaling pathways (Birbes, El Bawab et al. 2002). The sphingosine released by ceramidases can be reincorporated into ceramide by ceramide synthase or phosphorylated to S1P by sphingosine kinase (Birbes, El Bawab et al. 2002). Farber Disease, also called lipogranulomatosis, is a disorder of ceramide metabolism due to deficient activity of lysosomal ceramidase (Levade, Tempesta et al.

1993). It is a lipid storage disorder, and results in accumulation of ceramide in tissues, causing swelling of joints and subcutaneous nodules due to impaired ceramide degradation (Levade, Tempesta et al. 1993).

The salvage pathway of ceramide production involves the reacylation of sphingosine, produced by the breakdown of complex sphingolipids, into ceramide (Kitatani, Idkowiak-Baldys et al. 2008). Degradation of sphingolipids and glycosphingolipids occurs in acidic subcellular compartments, the late endosomes, and lysosomes (Kitatani, Idkowiak-Baldys et al. 2008). Acidic exohydrolases cause the release of monosaccharide units from glycosphingolipids, leading to ceramide (Kitatani, Idkowiak-Baldys et al. 2008). Acid sphingomyelinase degrades sphingomyelin to produce ceramide (Kitatani, Idkowiak-Baldys et al. 2008). Ceramide can then be hydrolyzed by acid ceramidase to form sphingosine and a free fatty acid that can leave the lysosome (Kitatani, Idkowiak-Baldys et al. 2008). These metabolites are then re-incorporated in sphingolipid and ceramide biosynthesis to produce ceramide and S1P (Kitatani, Idkowiak-Baldys et al. 2008). This salvage pathway reuses the long fatty acids released to reform ceramide via ceramide synthase (Kitatani, Idkowiak-Baldys et al. 2008). This pathway seems to be involved with PKC $\delta$ , as PKC $\delta$  has been shown to activate acid sphingomyelinase (Kitatani, Idkowiak-Baldys et al. 2008).

## 1.6 Other Sphingolipids

Sphingomyelin can be found in the nuclear envelope and intranuclear sites (Ledeen and Wu 2008). Sphingomyelin turnover occurs in response to  $1\alpha,25$ -dihydroxyvitamin D<sub>3</sub>, TNF- $\alpha$ , and  $\gamma$ -interferon (Hannun, Obeid et al. 1993). Nuclear sphingomyelinases can break down sphingomyelin in the nucleus to produce ceramide, which then triggers apoptosis and other metabolic changes (Ledeen and Wu 2008).

S1P is a more soluble sphingolipid, and generally acts in as an antagonist to ceramide (Futerman and Hannun 2004; Hannun and Obeid 2008; Bartke and Hannun 2009). S1P is a tumor-promoting lipid (Bartke and Hannun 2009). It is involved in proliferation, cell growth, cell survival, cell migration, inflammation, angiogenesis, vasculogenesis, and resistance to apoptotic cell death (Gomez-Munoz 2006; Bartke and Hannun 2009). It has been found to be up-regulated by the activation of G-protein-coupled receptors, growth factor receptors, and cytokine receptors (Hannun and Obeid 2008; Nixon 2009).

C1P is localized to the cell cytoplasm or perinuclear regions (Nixon 2009). C1P regulates cell proliferation and apoptosis by promoting cell survival (Gomez-Munoz 2006). As well, it has been found to be involved in phagocytosis and inflammation (Gomez-Munoz 2006). It has been found to interact with PLA<sub>2</sub> (Nixon 2009). C1P was found to stimulate deoxyribonucleic acid (DNA) synthesis and cell division in rat

fibroblasts (Gomez-Munoz 2006). As well, C1P stimulated cell proliferation and inhibited apoptosis in birds (Gomez-Munoz 2006). C1P blocks apoptosis by inhibiting acid sphingomyelinase activity (and thus ceramide accumulation), blocking DNA fragmentation, and blocking the stimulation of the caspase-9/caspase-3 pathway (Gomez-Munoz 2006). C1P can stimulate phosphatidylinositol 3-kinase (PI3-kinase), which leads to the activation of NF- $\kappa$ B and the expression of anti-apoptotic genes (Gomez-Munoz 2006). PI3-kinase activation also generates phosphatidylinositol (3,4,5)-triphosphate (PIP3) which can also inhibit acid sphingomyelinases (Gomez-Munoz 2006). In summary, C1P acts in a manner opposite to ceramide, inhibiting cell death and promoting cell survival (Gomez-Munoz 2006).

Sphingolipids were named by J.L.W. Thudichum in 1884 after the sphinx due to “the riddle of their function” (Futerman and Hannun 2004). Ceramide and sphingosine have been reported to act as tumor suppressor lipids (Bartke and Hannun 2009). They generally inhibit proliferation and promote apoptosis, while S1P and C1P have been found to be cell proliferation stimulators (Futerman and Hannun 2004; Gomez-Munoz 2006). The balance between relative and absolute levels of ceramide and other sphingolipid metabolites regulate differentiation, cell cycle arrest, cellular senescence, and apoptosis (Birbes, El Bawab et al. 2002). The formation and degradation of ceramide, sphingosine, C1P, and S1P are interconnected and interdependent (Bartke and Hannun 2009). For example, ceramide and S1P form a sphingolipid “rheostat” that regulates pro- and anti-apoptotic pathways (Nixon 2009). An increase in ceramide with a decrease in S1P results in the activation of apoptosis; a decrease in ceramide with an

increase in S1P results in the stimulation of ant-apoptotic pathways (Nixon 2009). The concentrations of ceramide, sphingosine, and S1P differ by about an order of magnitude with ceramide the most abundant and S1P the least (Bartke and Hannun 2009).

Therefore, a small change in ceramide can drastically increase the levels of sphingosine or S1P (Hannun and Obeid 2008; Bartke and Hannun 2009). Hence, it is important to note that the effects of one lipid may in reality be due to a combination of all the interconnected sphingolipids (Hannun and Obeid 2008).

## **1.7 Basics of Apoptosis**

Apoptosis, or programmed cell death, is an active process that leads to cell death (Cho and Choi 2002). Apoptosis occurs in normal physiological processes such as development and tissue homeostasis (Kam and Ferch 2000; Schug and Gottlieb 2009). Deregulation of apoptosis is linked to many diseases and disorders, such as cancer, cardiovascular diseases, and neurodegenerative diseases (Kam and Ferch 2000; Vermeulen, Van Bockstaele et al. 2005). There are various changes that occur as a result of apoptotic signaling pathways: shrinkage of the cytoplasm, membrane blebbing, nuclear chromatin compaction, chromosomal DNA fragmentation, exposure of phosphatidylserine (PS) at the external surface of the cell, reactive oxygen species (ROS) formation, mitochondrial membrane permeabilization, and the formation of apoptotic bodies which are then engulfed by phagocytes (Kam and Ferch 2000; Cho and Choi 2002; Vermeulen, Van Bockstaele et al. 2005; Schug and Gottlieb 2009). There are two signaling pathways that lead to apoptosis (Cho and Choi 2002; Schug and Gottlieb 2009).

The intrinsic pathway is activated from inside the cell by the pro-apoptotic Bcl-2 protein family (Cho and Choi 2002; Schug and Gottlieb 2009). The extrinsic pathway is activated from outside the cell by pro-apoptotic ligands that cause clustering of death receptors at the cell surface, such as Fas (Cho and Choi 2002; Vermeulen, Van Bockstaele et al. 2005; Schug and Gottlieb 2009). There are two stages of apoptosis: the initiation phase and the execution phase (Kam and Ferch 2000). The initiation phase is under the control of regulatory genes, such as p53 and the Bcl-2 family (Kam and Ferch 2000). The execution phase of apoptosis is under the control of caspases, which are aspartate-specific cysteine proteases (Kam and Ferch 2000; Vermeulen, Van Bockstaele et al. 2005). Caspases are synthesized in normal cells as proenzymes, and they are then cleaved to be activated (Vermeulen, Van Bockstaele et al. 2005). There are two types of caspases relevant to apoptosis: the initiator caspases (caspases-2, -8, -9, and -10) and the effector caspases (caspases-3, -6, and -7), which are activated by the initiator caspases (Cho and Choi 2002; Vermeulen, Van Bockstaele et al. 2005; Schug and Gottlieb 2009).

Many apoptotic signals merge at the mitochondria, so the mitochondria act as “gatekeepers” of the intrinsic pathway of apoptosis (Riedl and Salvesen 2007; Smith, Ng et al. 2008). The critical event regarding mitochondrial apoptosis is outer mitochondrial membrane (OMM) permeabilization (Schug and Gottlieb 2009). This leads to the release of the apoptosis-inducing factor (AIF) and cytochrome *c* (Vermeulen, Van Bockstaele et al. 2005; Schug and Gottlieb 2009). The AIF translocates to the nucleus upon apoptosis induction, and initiates chromatin condensation and fragmentation (Vermeulen, Van Bockstaele et al. 2005; Schug and Gottlieb 2009). Cytochrome *c* is bound to the outer

surface of the inner mitochondrial membrane (IMM) by its association with CL (Ott, Zhivotovsky et al. 2007; Schug and Gottlieb 2009). Cytochrome *c* release is biphasic – first the loosely bound pool is released, and then the tightly-bound pool is released upon cristae remodelling (Garrido, Galluzzi et al. 2006). OMM permeabilization is a decisive event in cytochrome *c* release and is the “point of no return” of the mitochondrial apoptotic pathway (Garrido, Galluzzi et al. 2006). During the initial loss of cytochrome *c*, the electron transport chain (ETC) is disrupted, which generates ROS (Garrido, Galluzzi et al. 2006). This then leads to CL peroxidation, which is also catalyzed by cytochrome *c* (Garrido, Galluzzi et al. 2006). Peroxidized CL has less affinity for cytochrome *c*, which then dissociates in the second part of cytochrome *c* release (Garrido, Galluzzi et al. 2006). Once in the cytosol, cytochrome *c* mediates the formation of the apoptosome in the presence of ATP to further the process of apoptosis (Garrido, Galluzzi et al. 2006; Riedl and Salvesen 2007). In the apoptosome, cytosolic apoptotic protease activating factor-1 (APAF-1) binds to the released cytochrome *c* at its WD40 region (Riedl and Salvesen 2007). The cytochrome *c*-bound APAF-1 then oligomerizes in an ATP-dependent manner into a wheel-shaped heptamer with its seven caspase-recruitment domains (CARDs) at the center of the wheel (Riedl and Salvesen 2007). The APAF-1 heptamer apoptosome then recruits procaspase-9, allowing dimerization and activation of caspase-9 and the following apoptotic caspase cascade (activation of caspases-3 and -7) (Riedl and Salvesen 2007).

## 1.8 Ceramide and Apoptosis

There is abundant evidence that ceramide is involved in apoptosis. Ceramide accumulation by *de novo* synthesis or the hydrolysis of sphingomyelin activates cytochrome *c* release, caspase activation, and thus apoptosis (Grant and Spiegel 2002). Various stress stimuli and anti-cancer drugs generate ceramide through the sphingomyelin hydrolysis pathway (Grant and Spiegel 2002). Both the neutral and acidic sphingomyelinases have been implicated in apoptosis induction (Grant and Spiegel 2002). Sphingomyelinase knockout mice are resistant to ionizing radiation (Birbes, El Bawab et al. 2002). Overexpression of bacterial sphingomyelinases that generates ceramide from intracellular pools of sphingomyelin, but not the extracellular sphingomyelin pools led to apoptosis (Birbes, El Bawab et al. 2002).

Apoptosis induced by ultraviolet radiation (UV) and TNF- $\alpha$  treatment has been shown to occur by an increase in mitochondrial ceramide levels (Siskind 2005). The increase in mitochondrial ceramide precedes cytochrome *c* release and the mitochondrial phase of apoptosis (Siskind 2005). Ceramide accumulation in the mitochondria leads to several apoptotic changes: an increase in ROS generation, an alteration of calcium ( $\text{Ca}^{2+}$ ) homeostasis, a collapse in IMM potential, inhibition or activation of ETC components, depletion of ATP, and release of intermembrane space proteins (Siskind 2005). Apoptosis can be blocked by inhibiting ceramide generation in mitochondria (Siskind 2005). As well, defective ceramide generation has been linked to a resistance to radiation-induced apoptosis (Siskind 2005). Mitochondria contain ceramide synthase,

which is a ceramide synthesis enzyme, and ceramidase, which is a ceramide hydrolysis enzyme (Siskind 2005). Ceramide-induced apoptosis is specific, as dihydroceramide does not induce apoptosis (the only difference between ceramide and dihydroceramide is the lack of a double bond in dihydroceramide) (Siskind 2005). The conversion of dihydroceramide to ceramide in the mitochondria is a way to rapidly generate ceramide and induce apoptosis (Siskind 2005). In mitochondria of healthy rat livers, there is much more dihydroceramide (non-apoptotic) compared to ceramide (pro-apoptotic) (Richter and Ghafourifar 1999; Siskind 2005). This causes a reduction in mitochondrial oxygen consumption, mitochondrial transmembrane potential, and  $\text{Ca}^{2+}$  retention (Richter and Ghafourifar 1999). This interaction between ceramide and cytochrome *c* mediates ceramide's apoptogenic properties (Richter and Ghafourifar 1999). The conversion between ceramide and dihydroceramide controls the life and death of cells, as healthy mitochondria contain a higher percentage of dihydroceramide in the OMM than ceramide (Siskind 2005).

Apoptosis has been induced in cancer cell lines by the addition of ceramide metabolism inhibitors, and by the addition of cell-permeable ceramide analogues (Siskind 2005). Cell-permeable ceramide analogues have been shown to induce cytochrome *c* release (Siskind 2005). The addition of  $\text{C}_2$ -ceramide to human lymphoid and mononuclear cells resulted in DNA fragmentation, with the characteristic ladder of apoptosis, and led to apoptosis (Hannun, Obeid et al. 1993). The addition of  $\text{C}_2$ -ceramide to HL-60 cells results in down-regulation of *c-myc* mRNA by inducing a block to transcription elongation (Hannun, Obeid et al. 1993). Tumor cells that were treated with

B13, which is a ceramidase inhibitor, had increased endogenous ceramide levels, which resulted in activation of the apoptotic cascade (Birbes, El Bawab et al. 2002). Also, CAPP can mediate the dephosphorylation of Bcl-2 (Birbes, El Bawab et al. 2002). It has been found that fumonisin B1, which is a ceramide synthase inhibitor and inhibitor of the *de novo* pathway of ceramide synthesis, can block ceramide generation and apoptosis in response to retinoic acid, etoposide, and daunorubicin (Birbes, El Bawab et al. 2002). As well, ceramide can activate cathepsin D (Hannun and Obeid 2008). Cathepsin D may be a target of lysosomally-generated ceramide and may couple the action of lysosomal acid sphingomyelinases to the mitochondrial pathway of apoptosis (Hannun and Obeid 2008).

Induction of apoptosis by cytotoxic drugs causes the translocation of PKC $\delta$  to the mitochondria (Grant and Spiegel 2002). This then leads to cytochrome *c* release, caspase activation, and apoptosis (Grant and Spiegel 2002). Ceramide generation may be either a cause or a consequence of PKC $\delta$  activation (Grant and Spiegel 2002). The accumulation of ceramide and the translocation of PKC $\delta$  seem to cooperate to amplify apoptotic signals (Grant and Spiegel 2002). In LNCaP prostate cancer cells (these cells express PKC $\delta$ ), cytotoxic drugs induce a biphasic increase in ceramide synthesis (Sumitomo, Ohba et al. 2002). The initial, transient increase is due to the *de novo* pathway of ceramide synthesis; the second, sustained increase is due to activation of neutral sphingomyelinases and sphingomyelin hydrolysis (Sumitomo, Ohba et al. 2002). This second increase seems to be dependent upon caspase-9 activation, which is a consequence of PKC $\delta$  translocation to the mitochondria (Sumitomo, Ohba et al. 2002).

Ceramide-induced apoptosis may also be due to the fact that ceramide can form protein-permeable channels in mitochondrial membranes (Siskind 2005). Ceramide is found in the OMM at a three-fold higher concentration than the IMM (Siskind 2005). OMM permeability is regulated by mitochondrial ceramide levels, and ceramide increases OMM permeability through its ability to form the large protein-permeable channels (Siskind 2005). Short cell-permeable ceramide analogues and natural long-chain ceramides have been found to form large channels in planar phospholipid membranes (Siskind 2005). Therefore, it seems that ceramide does not directly induce a cytochrome *c* release mechanism, but raises the OMM permeability to allow all small proteins to leave the mitochondria (Siskind 2005). Ceramides differ from most lipids because they have several hydrogen-bond donating and accepting groups (the two –OH groups, the amide nitrogen, and the carbonyl oxygen), which may be why ceramides can form channels in membranes (Siskind 2005). Other sphingosines can also form channels, but these channels only allow metabolites, and not proteins, to pass through membranes (Siskind 2005). These channels may play a protective role in the OMM because they allow things other than mitochondrial proteins to pass through the membranes (Siskind 2005). The conversions between ceramide and sphingosine can control what goes in and out of the mitochondria, and thus control apoptosis (Siskind 2005). The levels of ceramide and sphingosine can control OMM permeability and regulate the life and death of a cell (Siskind 2005).

## 1.9 Phosphatidylglycerolphosphate (PGP) Synthase

PGP synthase is the enzyme responsible for catalyzing the committed step of CL synthesis (Kuchler, Daum et al. 1986; Kawasaki, Kuge et al. 2001). PGP synthase is localized to the IMM fraction in *Saccharomyces cerevisiae* and other eukaryotes (Kuchler, Daum et al. 1986). A mutant CHO cell line was developed that contained a temperature-sensitive PGP synthase enzyme (Ohtsuka, Nishijima et al. 1993). This cell line showed morphological and functional mitochondrial abnormalities (Ohtsuka, Nishijima et al. 1993). This mutant was defective in the synthesis of phosphatidylglycerol (PG) and CL (Ohtsuka, Nishijima et al. 1993). As well, this cell line was temperature-sensitive for cell growth (Ohtsuka, Nishijima et al. 1993). It was also shown that PG is the major metabolic precursor of CL (Ohtsuka, Nishijima et al. 1993). When a temperature-resistant revertant of the mutant PGP synthase cell line was developed, the ability to synthesize PG and CL was restored to nearly the same level as in non-mutant cells (Ohtsuka, Nishijima et al. 1993). Cell growth was also restored (Ohtsuka, Nishijima et al. 1993). Therefore, PGP synthase is essential for the cell growth of CHO-K1 cells (Ohtsuka, Nishijima et al. 1993). When the PGP synthase mutant CHO cell line developed by Ohtsuka et al. was transfected with PGP synthase complementary DNA (cDNA), the previously morphologically abnormal mitochondria returned to normal (Kawasaki, Kuge et al. 1999). Also, normal PG and CL synthesis was restored (Kawasaki, Kuge et al. 1999). These results suggest that the abnormalities associated with the mutant CHO cell line are due to the reduced ability of the cell line to make PG and/or CL (Kawasaki, Kuge et al. 1999). PGP synthase is repressed by inositol, which is

a carbohydrate and phospholipid precursor, through the phosphorylation of the PGP synthase enzyme rather than degradation (Greenberg, Hubbell et al. 1988; He and Greenberg 2004). PGP synthase activity is increased by thyroxin, which is a thyroid hormone (Chicco and Sparagna 2007). As well, it has been found that N-acetylsphingosine (C<sub>2</sub>-ceramide) stimulates PGP synthase enzyme activity in H9c2 cardiac cells (Xu, Kelly et al. 1999). This has been found to increase PG and CL biosynthesis (Xu, Kelly et al. 1999). It was found that addition of TNF- $\alpha$ , which causes the production of intracellular ceramide, also increased PGP synthase activity in H9c2 cells (Xu, Kelly et al. 1999). Therefore, PG and CL metabolism seems to be regulated by intracellular ceramide signaling (Xu, Kelly et al. 1999).

### **1.10 Cardiolipin**

CL was isolated from beef heart in 1942 by Mary Pangborn, hence the name “cardio”- lipin (Pangborn 1942). CL is a dimeric phospholipid that consists of four acyl chains, three glycerols, and two phosphate groups per molecule (Schlame, Rua et al. 2000; Gonzalvez and Gottlieb 2007). The structure of CL can be seen in Figure 5. The acyl chain compositions of CL varies between organisms, tissues, and cell types (Houtkooper and Vaz 2008). The CL in *Saccharomyces cerevisiae* contains equal amounts of C<sub>18</sub> and C<sub>16</sub> fatty acids (Schlame, Rua et al. 2000). Higher eukaryotic CLs contain mainly C<sub>18</sub> fatty acid chains (Schlame, Rua et al. 2000). The fatty acid strands of CL have high levels of polyunsaturated fatty acids and low levels of saturated fatty acids (Hatch 1996). In *Saccharomyces cerevisiae*, CL contains mainly mono-unsaturated acyl

chains; in contrast, human CL contains mainly di-unsaturated acyl chains (Houtkooper and Vaz 2008). In bivalves and sea urchin sperm, CL contains mainly longer poly-unsaturated acyl chains (Houtkooper and Vaz 2008). These different compositions may be due to adaptation for different environmental conditions (Houtkooper and Vaz 2008). However, the symmetrical distribution of the CL acyl chains is maintained throughout different organisms (Houtkooper and Vaz 2008). This may be to promote the structured organization of the mitochondrial membrane (Houtkooper and Vaz 2008).

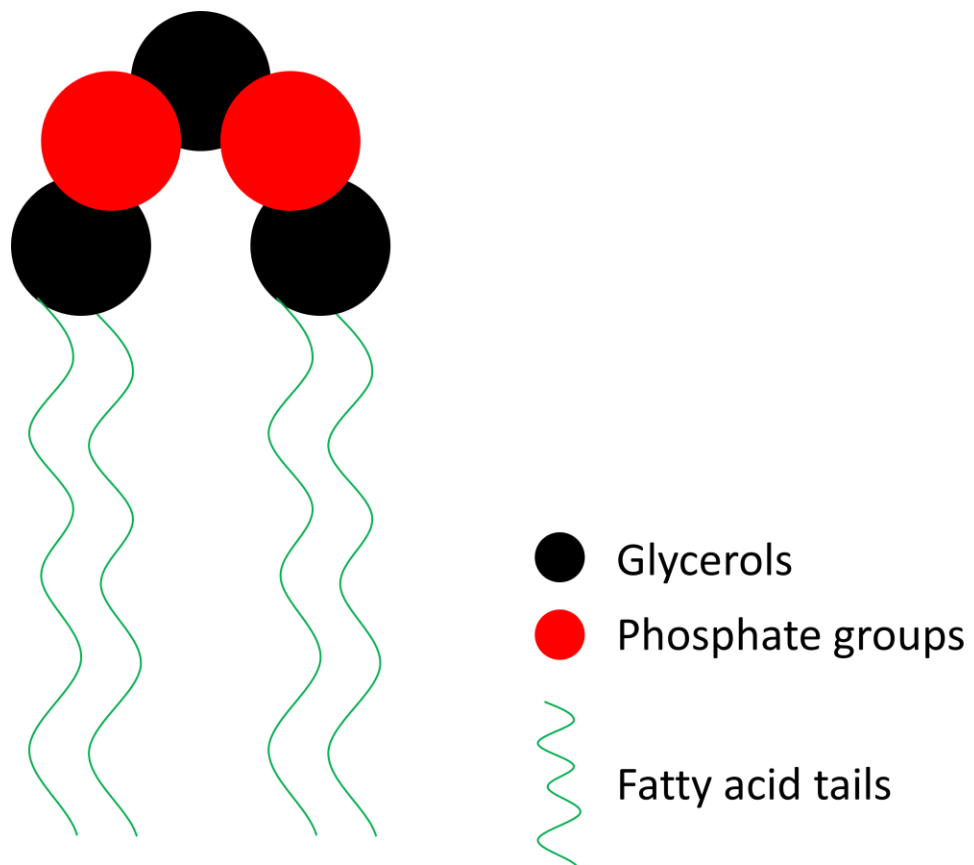


Figure 5: Cardiolipin Structure

Adapted from: Gonzalvez and Gottlieb 2007

## 1.11 Cardiolipin Localization and Synthesis

CL is localized in the IMM, at contact sites between the IMM and OMM, and small amounts are found in the OMM (Schlame, Rua et al. 2000; McMillin and Dowhan 2002; Gonzalvez and Gottlieb 2007; Houtkooper and Vaz 2008). CL is synthesized *de novo* in mitochondria in mammalian cells (Hauff and Hatch 2006). The synthesis of CL occurs on the inner leaflet of the IMM (Hauff and Hatch 2006). CL synthesis can be seen in Figure 6. The first step of CL synthesis is the condensation of phosphatidic acid (PA) and cytidine-5'-triphosphate (CTP) to form cytidine-diphosphate-1,2-diacyl-*sn*-glycerol (CDP-DG) by CDP-DG synthetase (Hauff and Hatch 2006). The second committed step of CL synthesis, is the addition of glycerol-3-phosphate (G3P) to CDP-DG to form PGP by PGP synthase (Hauff and Hatch 2006). The phosphate group of PGP is then rapidly removed by PGP phosphatase to produce PG (Hauff and Hatch 2006). The final step of CL synthesis is the condensation of PG with a second CDP-DG molecule to form CL by CL synthase (Hauff and Hatch 2006). CL that is newly synthesized is rapidly remodelled in mammalian cells, and becomes enriched in linoleic acid (Hauff and Hatch 2006). PLA<sub>2</sub> catalyzes the removal of acyl chains from CL, resulting in monolysocardiolipin (MLCL) (Hauff and Hatch 2006). The MLCL is then reacylated by MLCL acyltransferase (MLCLAT) in a CoA-dependent deacylation-reacylation cycle (Hauff and Hatch 2006; Houtkooper and Vaz 2008). The CoA-dependent cycle is called Lands cycle (Houtkooper and Vaz 2008). CL is also remodelled by a CoA-independent transacylation between phospholipids (Houtkooper and Vaz 2008). In CoA-independent transacylation, phospholipids such as PC or PA act as acyl donors to CL (Houtkooper and Vaz 2008).

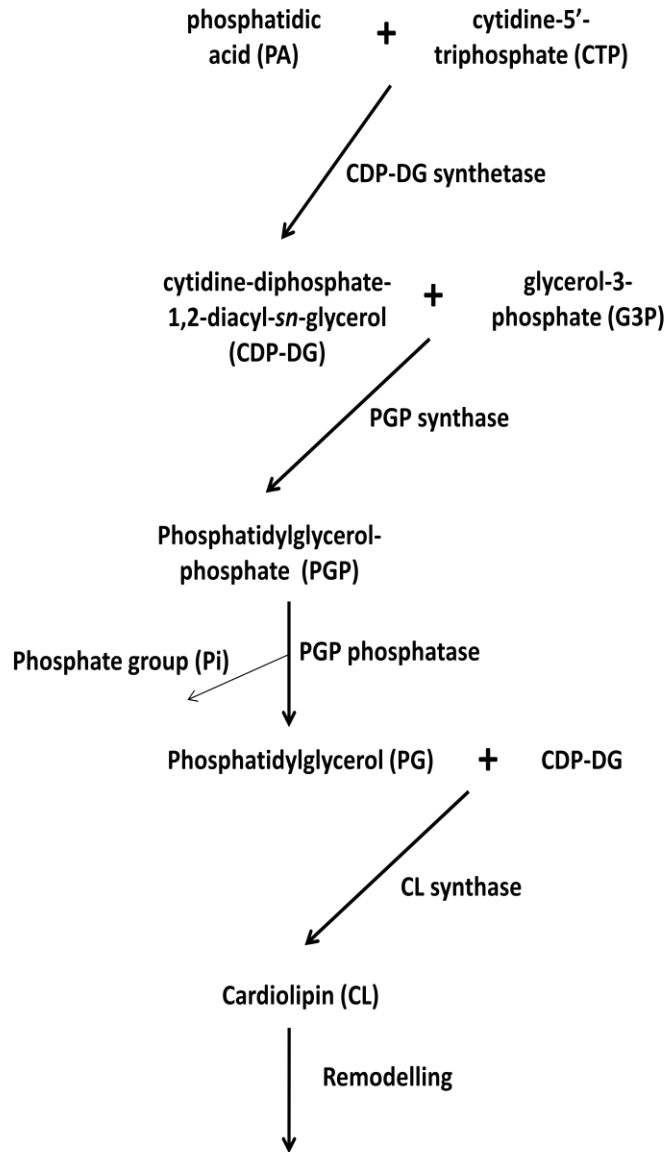


Figure 6: Cardiolipin Metabolism

Adapted from: Hatch 1996

## 1.12 Cardiolipin Functions

CL is directly required for the maintenance of mitochondrial structure (Gonzalvez and Gottlieb 2007). CL is also associated with several key mitochondrial enzymes, such as: carnitine palmitoyltransferase, creatine phosphokinase, pyruvate translocator, tricarboxylate carrier, mitochondrial glycerol-3-phosphate dehydrogenase (GAPDH),  $\beta_2$ -glycoprotein I, CL-activated protein kinase, protease-activated protein kinase, RNA polymerase, topoisomerase I, adenosine monophosphate (AMP) deaminase, and glycerophosphate acyltransferase (Hatch 1996; Schlame, Rua et al. 2000; Houtkooper and Vaz 2008). CL is required by complexes of oxidative phosphorylation, or the ETC, including: complex I (nicotinamide adenine dinucleotide [NADH]:ubiquinone oxidoreductase), complex III (ubihydroquinone:cytochrome *c* oxidoreductase), complex IV (cytochrome *c* oxidase), and complex V (ATP synthase) (Schlame, Rua et al. 2000; Gonzalvez and Gottlieb 2007). CL acts like the glue that holds the ETC together (Hauff and Hatch 2006). CL is associated with cytochrome *c* itself, which acts as an electron shuttle between complexes III and IV of the ETC (Garrido, Galluzzi et al. 2006). There are loosely and tightly bound pools of cytochrome *c* in the mitochondria (Garrido, Galluzzi et al. 2006). The loosely bound cytochrome *c* is involved in electron transport, inhibition of ROS formation, and prevents oxidative stress (Garrido, Galluzzi et al. 2006). It is loosely attached to the IMM by electrostatic interactions with the IMM phospholipids, including CL (Garrido, Galluzzi et al. 2006). The tightly bound pool of cytochrome *c* is bound to CL, and has peroxidase activity (Garrido, Galluzzi et al. 2006; Gonzalvez and Gottlieb 2007). The cytochrome *c* peroxidase function requires physical

contact with CL to cause CL peroxidation (Kagan, Bayir et al. 2009). CL also has an important role in apoptosis (Degli Esposti 2004; Garrido, Galluzzi et al. 2006; Gonzalvez and Gottlieb 2007).

### **1.13 Cardiolipin and Apoptosis**

Under apoptotic conditions, CL is redistributed between the IMM and OMM (Gonzalvez and Gottlieb 2007). CL is exposed on the OMM after death receptor stimulation, during ROS production, and before mitochondria depolarization and permeabilization (Gonzalvez and Gottlieb 2007). This may occur due to peroxidation of CL by ROS, which may allow CL to bind the active form of BH3 interacting domain death agonist (Bid), tBid (Gonzalvez and Gottlieb 2007). CL is particularly susceptible to oxidation by ROS due to its high level of unsaturated fatty acids and because CL interacts with cytochrome *c*, which has peroxidase activity, and complexes of the ETC, which are sources of ROS (Chicco and Sparagna 2007; Paradies, Petrosillo et al. 2009). The mitochondria-mediated ROS also promotes detachment of cytochrome *c* from CL due to the peroxidation (Paradies, Petrosillo et al. 2009). It has been found that under apoptotic conditions, binding of  $\text{Ca}^{2+}$ , which is used for stimulating oxidative phosphorylation under normal conditions, to CL changes the membrane topography in a manner that favors CL peroxidation (Paradies, Petrosillo et al. 2009). Furthermore, it was also found that after Fas stimulation, CL relocates from mitochondria to other intracellular organelles and the cell membrane (Sorice, Circella et al. 2004).

CL is required for the processing of caspase-8, a pro-apoptosis initiator caspase, on mitochondria after Fas activation in HeLa cells (Gonzalvez, Schug et al. 2008). CL acts as an anchor and activating platform for caspase-8 (Gonzalvez, Schug et al. 2008). Bid is a pro-apoptotic protein of the Bcl-2 family (Vermeulen, Van Bockstaele et al. 2005). N-terminal cleavage of Bid by caspase-8 in response to the activation of death receptors during apoptosis produces tBid, the active C-terminus of Bid (Vermeulen, Van Bockstaele et al. 2005). After Bid is cleaved by caspase-8, tBid rapidly moves to mitochondria and promotes the release of cytochrome *c* (Garrido, Galluzzi et al. 2006; Gonzalvez and Gottlieb 2007; Scorrano 2008). The  $\alpha$ H6 helix of tBid is required to bind CL, to localize tBid to the mitochondria, and for its pro-apoptotic activity (Gonzalvez, Pariselli et al. 2010). tBid seems to act as a bifunctional molecule (Gonzalvez, Pariselli et al. 2010). Initially, it binds to CL and destabilizes mitochondrial structure and function (Gonzalvez, Pariselli et al. 2010). tBid then promotes the activation and oligomerization of Bcl-2-associated X protein (Bax), another pro-apoptotic Bcl-2 protein, leading to OMM permeabilization, cytochrome *c* release, and execution of apoptosis (Vermeulen, Van Bockstaele et al. 2005; Gonzalvez, Pariselli et al. 2010). CL acts as a docking platform for tBid at contact sites between the IMM and OMM, where tBid can then interact with Bax on the OMM (Gonzalvez, Schug et al. 2008). Cells derived from a Barth syndrome patient, which is a syndrome that has immature CL, were resistant to Fas-induced apoptosis (the extrinsic apoptosis pathway) (Gonzalvez, Schug et al. 2008). This may be due to the fact that cytochrome *c* release was impaired in these cells due to defects in OMM permeabilization or other upstream events (Gonzalvez, Schug et al. 2008). However, transient transfection with a tBid-expressing vector was still able to

induce OMM permeabilization and the subsequent apoptosis cascade (Gonzalvez, Schug et al. 2008). Therefore, the immature CL was still able to interact with tBid (Gonzalvez, Schug et al. 2008). In the Barth syndrome-derived cells, there was less activated caspase-8, which would then cleave Bid to form tBid (Gonzalvez, Schug et al. 2008). However, there were equal amounts of procaspase-8 in the HeLa and Barth syndrome cells after Fas activation, so the defect in the extrinsic apoptotic pathway is at the docking and activation of caspase-8 on the mitochondria (Gonzalvez, Schug et al. 2008). This suggests that mature CL is required for caspase-8 activation (Gonzalvez, Schug et al. 2008). In summary, in the Barth syndrome cells, there were defects in the localization, oligomerization, and cleavage of caspase-8 on the mitochondria after Fas activation (Gonzalvez, Schug et al. 2008). This is highly indicative that CL provides the activating platform for caspase-8 on the mitochondria after Fas activation (Gonzalvez, Schug et al. 2008).

#### **1.14 Cardiolipin and Disease**

It has been hypothesized that a loss of CL contributes to age-related decline in mitochondrial function in many tissues, such as the heart and the brain (McMillin and Dowhan 2002; Chicco and Sparagna 2007). This loss of CL may play a factor in heart failure and neurodegenerative diseases, such as Parkinson's and Alzheimer's (Chicco and Sparagna 2007). Following heart ischemia and reperfusion, there is a loss of CL that precedes and exceeds the losses of other phospholipids. This may be linked to ROS production and causes impaired ETC function (Chicco and Sparagna 2007).

Thyroid hormone is a regulator of mitochondrial biogenesis, respiratory function, and lipid metabolism. CL synthesis is induced by thyroid hormone because PGP synthase and CL synthase activities are increased by thyroxin. Thyroxin also promotes CL remodelling by increasing MLCLAT activity. Therefore, hyperthyroidism increases CL levels, but hypothyroidism decreases CL levels (Chicco and Sparagna 2007).

Barth syndrome, which is an X-linked cardiomyopathy, has abnormal mitochondria and has been linked to a disorder in CL metabolism (McMillin and Dowhan 2002). Barth syndrome includes dilated cardiomyopathy, neutropenia, failure to thrive, abnormal mitochondria, and 3-methylglutaconic aciduria (Gonzalez 2005). Barth syndrome patients have abnormal cristae ultrastructure in their mitochondria (Claypool, Boontheung et al. 2008). The gene deleted in Barth syndrome is the TAZ gene, which produces tafazzins that act as acyltransferases in the remodelling of CL (Gonzalez 2005). Over ninety mutations in the TAZ gene have been described including frameshifts, non-sense, splice-site, and missense mutations (Hauff and Hatch 2006).

## 1.15 Previous Laboratory Work

Retroviral promoter trap mutagenesis was used in CHO-K1 cells to identify genes involved in drug-induced apoptosis. The CHO-K1 cell line was used because one mutational event is usually sufficient to result in the loss of gene function (Hubbard, Walls et al. 1994). This is because CHO-K1 cells are functionally hemizygous at 20% of the gene loci (Hubbard, Walls et al. 1994). As well, the cells have a constant diploid chromosome number of twenty-two (Hubbard, Walls et al. 1994). The U3NeoSV1 promoter trap retrovirus vector (obtained from Dr. Earl Ruley of Vanderbilt University) was used to create etoposide-resistant CHO clones. This construct can be seen in Figure 7. This construct contains *Bam*HI and *Eco*RI restriction sites to allow for cloning of the 5' and 3' flanking sequence (Hicks, Shi et al. 1995). It contains a pBR322 origin of replication (Ori) and an ampicillin resistance gene (Amp<sup>R</sup>) (Hicks, Shi et al. 1995). As well, the vector contains a promoter-less neomycin (G418) selection cassette in the U3 long terminal repeat (LTR) region (Hicks, Shi et al. 1995). The vector integrated randomly within CHO-K1 genome (Hicks, Shi et al. 1995). Inactivation of target genes resulted when the virus integrated within 500 nucleotides of a cellular promoter or was spliced from a nearby exon into the 3' splice acceptor site in the neomycin gene (Hicks, Shi et al. 1995). These integrations allowed the expression of the neomycin gene, and clones were selected using G418 (Hicks, Shi et al. 1995).

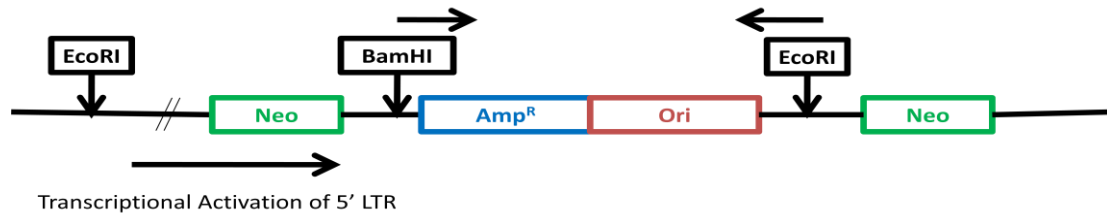
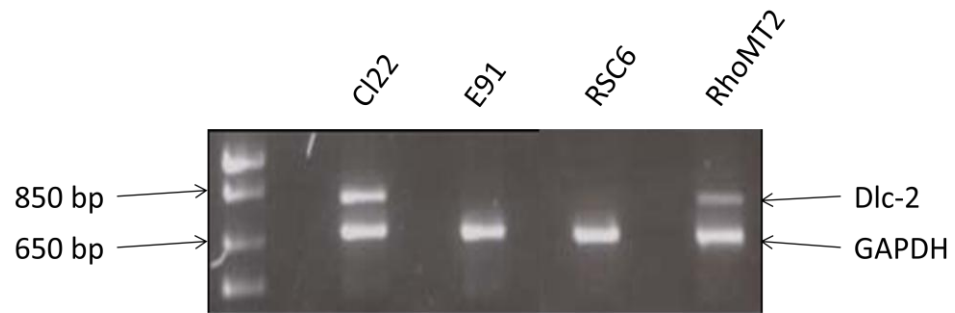


Figure 7: U3NeoSV1 Viral Vector

Adapted from: Hicks, Shi et al. 1995; Hicks Shi et al. 1997

The CHO-K1 clone twenty-two (C122) cell line was developed as a control cell line (Hatch, Gu et al. 2008). This cell line contained a transfected ecotropic retrovirus receptor gene, and was sensitive to etoposide-induced apoptosis (Hatch, Gu et al. 2008). The E91 cell line was isolated from a pool of U3NeoSV1-infected CHO-K1 clones that were resistant to etoposide (Hatch, Gu et al. 2008). This cell line was also observed to be resistant to ceramide-induced apoptosis, and it had a defect in ceramide-induced PGP synthase enzyme induction (Hatch, Gu et al. 2008). In this cell line, the retrovirus had integrated into intron one-two of the Dlc-2 gene (Hatch, Gu et al. 2008). The RSC6 cell line was created by Yuan Gu using the pSUPER (OligoEngine) vector-mediated short hairpin RNA interference (shRNAi) (Hatch, Gu et al. 2008). This cell line contained the Dlc-2 mRNA transcript knocked down by the shRNAi (Hatch, Gu et al. 2008). The final cell line used in this project was the RhoMT2 cell line, which served as a control line for the RSC6 cell line. The RhoMT2 line was also created by Yuan Gu using the pSUPER vector (Hatch, Gu et al. 2008). This line contained the Dlc-2 mRNA sequence mutated at three positions, and did not knock down the gene transcript (Hatch, Gu et al. 2008). Multiplex reverse transcription-polymerase chain reaction (RT-PCR) was conducted by Yuan Gu using primers for Dlc-2 and GAPDH cDNAs to show the knock down in gene expression of Dlc-2 in the CHO cell lines used in this project. This can be seen in Figure 8.



Data from Yuan Gu

Figure 8: Multiplex RT-PCR of CHO-K1 cell lines

Adapted from: Hatch, Gu et al. 2008

## 1.16 Antibody Production Using Phage Display

Bacteriophage (phage) are viruses that can infect prokaryotes (Bratkovic 2010). Phage are convenient to use in the laboratory due to their genetic and structural simplicity and because they can be easily grown in bacterial hosts (Bratkovic 2010). Phage display is the process of displaying foreign (poly)peptides on the surface of the phage molecules (Bratkovic 2010). This occurs by splicing a gene that encodes for such a peptide into a gene that encodes a capsid protein (Bratkovic 2010). The capsid then acts as an anchor for the displayed peptide, but should not affect its structure (Bratkovic 2010). Peptide linkers are used to attach the displayed peptide to the replicating phage (Bratkovic 2010). Recombinant DNA technology has been used to collect billions of peptides, protein variants, gene fragments, or cDNA-encoded proteins to be linked to the phage creating phage-displayed libraries (Bratkovic 2010). The basic steps of phage display selection are as follows: the phage library is incubated with an immobilized target, non-binding phage are washed away, binding phage are eluted and amplified in bacteria (Bratkovic 2010). This selection, or panning, process allows for amplification of only the phage that bind to the target (Bratkovic 2010).

The phage libraries used in this project are the human single-fold single chain variable fragment (scFv) Tomlinson I and J libraries (Winter 2002). The scFv fragments are a single polypeptide with the variable regions of the heavy and light chains of immunoglobulin (VH and VL) attached by a flexible glycine-serine linker (Winter 2002). These libraries consist of over 100 million different scFv fragments cloned into a

phagemid vector with ampicillin resistance (Winter 2002). The size of the Tomlinson I library is  $1.47 \times 10^8$  phagemid clones in T-phage resistant (TG1) *Escherichia coli* (*E. coli*) (with 96% of the clones containing functional antibody inserts), and the Tomlinson J library is  $1.37 \times 10^8$  (with 88% of the clones containing functional antibody inserts) (Winter 2002). The antibodies are displayed on the minor coat protein pIII of filamentous phage, cloned in an ampicillin resistant phagemid vector (Winter 2002). The Tomlinson I and J libraries were successfully used to develop phage antibodies against palytoxin, a dangerous marine toxin (Garet, Cabado et al. 2010). These phage antibodies can then be used to detect the toxins in shellfish (Garet, Cabado et al. 2010). The libraries were also used to successfully develop phage antibodies against the surface glycoprotein S16 of *Cryptosporidium parvum* (*C. parvum*) (Boulter-Bitzer, Lee et al. 2010). *C. parvum* can cause a diarrheal infection when contaminated water or food is ingested or direct contact with infected humans, animals, or contaminated surfaces occurs (Boulter-Bitzer, Lee et al. 2010). The development of a phage antibody that can detect *C. parvum* has the potential for use in pathogen detection and immunotherapy (Boulter-Bitzer, Lee et al. 2010). Therefore, there is evidence that phage display has been used successfully to produce phage antibodies.

### **1.17 Project Rationale**

The purpose of this project is to determine how Dlc-2 and Rho signaling modulate the ceramide induction of PGP synthase. The specific aims of this project are:

- To determine if there is transcriptional control of the PGP synthase gene occurring by ceramide and Dlc-2,
- To determine if there is post-transcriptional control of PGP synthase mRNA stability, and
- To determine if there is translational or post-translational protein control occurring by Dlc-2 and ceramide on the PGP synthase enzyme itself.

## 1.18 Hypotheses

It has already been found that ceramide causes induction of PGP synthase enzyme activity in CHO cell lines with functional Dlc-2, and that this induction is lost when Dlc-2 is not functional (Hatch, Gu et al. 2008). In regards to the first aim of this project, we hypothesized that the induction of PGP synthase is due to the transcriptional control of the PGP synthase gene by Rho proteins upon ceramide stimulation, and that these proteins are mediated by Dlc-2. One possibility is that when Dlc-2 is functioning properly, it will inactivate Rho proteins, allowing induction of PGP synthase. The active Rho proteins may be causing binding of repressors at the PGP synthase promoter. When Dlc-2 causes the inactivation of the Rho proteins, PGP synthase transcription may be activated. Alternatively, the Rho proteins may stimulate PGP synthase transcription when they are inactive, but not in their active conformation.

With respect to the second aim, we hypothesized that Rho proteins are affecting PGP synthase mRNA stability. Inactive Rho proteins (due to the proper function of Dlc-2, and stimulated by ceramide) may enhance PGP synthase mRNA stability. Alternatively, active Rho proteins may actively decrease PGP synthase mRNA stability upon ceramide stimulation. Therefore, when properly functioning Dlc-2 causes the inactivation of Rho proteins, the PGP synthase mRNA may be more stable.

Finally, with respect to the third aim, we hypothesize that PGP synthase protein induction after ceramide stimulation is prevented by Rho protein activity, mediated by the RhoGAP domain of Dlc-2. Active Rho proteins may be causing degradation of PGP synthase protein. When Dlc-2 inactivates Rho proteins, this may prevent the degradation of the PGP synthase protein. This may be occurring through post-translational modifications.

As well, we hypothesize that the START domain of Dlc-2 may be a target of ceramide, as ceramide binds to the START domain of CERT (Hanada, Kumagai et al. 2003; Futerman and Hannun 2004; Kudo, Kumagai et al. 2008). This may be a manner by which ceramide mediates Dlc-2 activity. The addition of ceramide may increase Dlc-2's ability to inactivate Rho proteins, causing an increased response in PGP synthase.

## **CHAPTER 2 – MATERIALS AND METHODS**

### **2.1 Transcriptional and Post-Transcriptional Control Experiments**

To determine if ceramide and Dlc-2 are affecting the gene expression of PGP synthase, the following experiments were conducted.

#### **2.1.1 Cell Culture Conditions**

All cell culture was performed in a NuAire Biosafety Cabinet. CHO-K1 cell lines Cl22, E91, RSC6, and RhoMT2 were grown in a humidified incubator with 5% carbon dioxide (CO<sub>2</sub>) at 37°C. They were grown in  $\alpha$ -Minimum Essential Medium ( $\alpha$ -MEM) (GIBCO) supplemented with 60 mg/L penicillin G sodium salt (Sigma-Aldrich), 2.2 g/L sodium bicarbonate (NaHCO<sub>2</sub> from Sigma-Aldrich), and 100 mg/L streptomycin sulphate (Sigma-Aldrich). The  $\alpha$ -MEM was filtered through a 0.22  $\mu$ m pore-sized Stericap PLUS Filter Unit (Millipore) before use in cell culture. Cl22, E91, RSC6, and RhoMT2 cells were grown in  $\alpha$ -MEM supplemented with 10% fetal bovine serum (FBS from Sigma-Aldrich) to confluency in 100-mm cell culture plates (Nunc or Greiner Bio-One). During growth, the cells were washed with phosphate buffered saline (PBS: 0.2 g/L potassium chloride [KCl from Fisher Scientific], 8 g/L sodium chloride [NaCl from Fisher Scientific], 1.1 g/L sodium phosphate dibasic [Na<sub>2</sub>HPO<sub>4</sub> from Fisher Scientific], 0.24 g/L potassium phosphate monobasic [KH<sub>2</sub>PO<sub>4</sub> from Mallinckrodt], pH 7.4) and the  $\alpha$ -MEM was changed every 2 – 3 days. The RSC6 cell line was grown in

$\alpha$ -MEM supplemented with 10% FBS and 0.5 g/L Geneticin (Invitrogen) for selection, and the Geneticin was removed prior to cell treatments. When the cells reached confluency (as determined by looking at them under an Olympus Tokyo CK microscope at ten times magnification), they were washed with PBS, treated with 1 mL Trypsin (0.05% [1X] with ethylenediaminetetraacetic acid [EDTA] 4Na, liquid from GIBCO) for 5 minutes in humidified incubator with 5% CO<sub>2</sub> at 37°C, and then split into two plates. Cells were grown and split until a sufficient number of plates were produced for separate treatments.

### **2.1.2 Cell Treatments**

Cells were grown to 70-80% confluency, and were then starved for 12 hours in  $\alpha$ -MEM with no FBS. For the transcriptional control experiments, cells were treated with 10 mg/L C<sub>2</sub>-ceramide (N-acetyl-D-sphingosine from Sigma-Aldrich) diluted in 100% ethanol (Manitoba Liquor Control Commission) or the same volume of ethanol alone in  $\alpha$ -MEM supplemented with 10% FBS for 1, 2, 3, 4, 5, 6, 8, 12, 16, and 24 hours. For the post-transcriptional control experiments, cells were treated with 10 mg/L C<sub>2</sub>-ceramide, the same volume of ethanol, or nothing for 4 hours and then treated with actinomycin D (AD from Sigma-Aldrich) alone at a concentration of 10 mg/L for 0, 1, 2, 3, 4, 5, and 6 hours. Cells were harvested after treatments by scraping with sterile cell scrapers (Nunc). Cells were then pelleted by centrifugation in an IEC DPR-6000 centrifuge at 1,000 times gravity (xg), and frozen at -20°C in 15-mL centrifuge tubes (Becton Dickinson).

### 2.1.3 RNA Extraction

Total cellular RNA was extracted from CHO cell pellets previously frozen at  $-20^{\circ}\text{C}$  (see section 2.1.2) using the spin protocol for animal cells from the Qiagen RNeasy Mini kit (Qiagen 2006). The cell pellets were placed on ice, and the following protocol was carried out with the cells on ice as much as possible. Six hundred  $\mu\text{L}$  of Buffer RLT (Qiagen lysis buffer) was placed on each pellet. The pellet was mixed with the lysis buffer by pipetting to produce the cell lysate. The lysate was then homogenized by passing it through a 22-gauge needle (Becton Dickinson) fitted to a ribonuclease (RNase)-free, deoxyribonuclease (DNase)-free 1 mL syringe (Becton Dickinson) ten times. Six hundred  $\mu\text{L}$  of 70% ethanol was then placed in each tube and mixed with the lysate by pipetting. Seven hundred  $\mu\text{L}$  of the mixture was placed in an RNeasy spin column, which was inside a 2-mL collection tube. The tube was spun in an Eppendorf 5415C microcentrifuge at maximum speed for 15 seconds. The flow-through was discarded, leaving only the total RNA within the column. The remaining lysate-ethanol mixture was then added to the RNeasy spin column. The column was spun again for 15 seconds, and the flow-through was discarded. Seven hundred  $\mu\text{L}$  of Buffer RWI (Qiagen wash buffer) was added to the spin column. The column was spun at maximum speed for 15 seconds, and the flow-through was discarded. Five hundred  $\mu\text{L}$  of ethanol-supplemented Buffer RWI (Qiagen wash buffer) was then added to the column. The column was spun at maximum speed for 15 seconds, and the flow-through was discarded. Another 500  $\mu\text{L}$  of Buffer RWI was added to the column. The column was spun at maximum speed for 2 minutes, and then both the collection tube and flow-through were

discarded. The column was placed in a new collection tube, and spun at maximum speed for 1 minute. The collection tube and flow-through were discarded again, and the column was placed in a 1.5-mL RNase-free, DNase-free lidded collection tube. Forty  $\mu\text{L}$  of RNase-free, DNase-free double distilled water ( $\text{ddH}_2\text{O}$  from Qiagen) was then added to the column. The column was spun at maximum speed for 1 minute. The flow-through was retained because it was the RNA filled elution. The 40  $\mu\text{L}$  of elution was placed back into the column, and the column was spun again at maximum speed for 1 minute. The more concentrated RNA elution was retained and stored at  $-20^\circ\text{C}$  (Qiagen 2006).

#### **2.1.4 DNase Treatment**

The DNase treatment protocol was conducted on ice. RNA was treated with DNase (Sigma-Aldrich) prior to cDNA synthesis. Five  $\mu\text{L}$  of DNase mixture (15 U/mL DNase, 0.19 mg/mL magnesium chloride [ $\text{MgCl}_2$  from Fisher Scientific]) was mixed with 2  $\mu\text{L}$  of RNA, as acquired by the Qiagen RNeasy Mini kit (see section 2.1.3). The reaction was carried out at  $37^\circ\text{C}$  for 15 minutes followed by deactivation of the DNase enzyme at  $75^\circ\text{C}$  for 10 minutes in an MJ Research PTC-200 Peltier Thermal Cycler.

### 2.1.5 cDNA Synthesis

The cDNA production protocol was conducted on ice. cDNA was produced following DNase treatment (see section 2.1.4). The protocol for SuperScript II Reverse Transcriptase (Invitrogen 2003) was used with 5  $\mu$ L DNase mixture and 2  $\mu$ L RNA. Two  $\mu$ L random primers (Invitrogen) and 4  $\mu$ L deoxyribonucleotide triphosphate (dNTP: 2.5 mM from Invitrogen) were mixed with the 7  $\mu$ L from the DNase reaction. This was centrifuged briefly at maximum speed in an Eppendorf 5415C microcentrifuge, and then incubated at 65°C for 5 minutes in an MJ Research PTC-200 Peltier Thermal Cycler in a 0.65-mL DNase-free, RNase-free microcentrifuge tube (Axygen). Four  $\mu$ L of 5X First-Strand Buffer (Invitrogen) and 2  $\mu$ L dithiothreitol (0.1M DTT from Invitrogen) were added to the tube. This was centrifuged briefly, and incubated at 25°C for 2 minutes in the thermal cycler. One  $\mu$ L of SuperScript II Reverse Transcriptase was then added and the mixture was mixed by pipetting. The cDNA reaction was carried out in the thermal cycler at 25°C for 10 minutes, 42°C for 50 minutes, inactivated at 70°C for 15 minutes, and then left at 8°C until the tubes were removed and stored at -20°C. The cDNA concentration was determined using a GeneQuant pro spectrophotometer from the laboratory of Dr. David Eisenstat (Invitrogen 2003).

### 2.1.6 Real-Time RT-PCR

Real-Time RT-PCR was performed to quantify mRNA levels. Relative gene expression was determined using the  $2^{-\Delta\Delta C_t}$  method (Livak and Schmittgen 2001). GAPDH was used as the housekeeping reference gene. Primers were designed by Yuan Gu using the Primer3 software available free on the internet. The primers were purchased from Eurofins MWG Operon, and had the following sequences: PGP synthase forward, 5'-GAC AAC AAC GTC GTC TTG AGT G -3'; PGP synthase reverse, 5'-GAA GTC TGC AAT CTC AGC ACA G-3'; GAPDH forward, 5'-CGA AGG TGG AAG AGT GGG AG-3'; GAPDH reverse, 5'-TGA AGC AGG CAT CTG AGG G-3'. For each well of a ninety-six-well Real-Time RT-PCR plate (Bio-Rad), 6.25  $\mu$ L of SYBR Green Master Mix (Qiagen), 0.5  $\mu$ L of Primer 1 (forward PGP or GAPDH), 0.5  $\mu$ L of Primer 2 (reverse PGP or GAPDH), 4.25  $\mu$ L of ddH<sub>2</sub>O, and 1  $\mu$ L of serially diluted cDNA was added (Qiagen 2005). The Real-Time RT-PCR reactions were run in triplicate with 1-in-10 and 1-in-100 serial dilutions of cDNA. The plate was then covered with a Microseal adhesive seal (Bio-Rad), and spun in a Beckman Coulter Allegra 25R centrifuge at 300xg for 2 minutes. The reactions were performed using a Bio-Rad Real-Time RT-PCR Detection System iQ5 cycler from the laboratory of Dr. S. Gibson. The Real-Time RT-PCR program was as follows: 95°C for 15 seconds, 55°C for 30 seconds, and 72°C for 30 seconds for 40 cycles (Qiagen 2005). The iQ5 program also included amplification cycle graphs and melting curves to confirm the Real-Time RT-PCR reactions were successful. The reactions were successful when the amplification cycle curves were logarithmic, and the melting curves had one sharp peak per well. After

completion of the Real-Time RT-PCR reaction, agarose gels were used to confirm there was only one PCR product produced per well (see section 2.1.7). Three Real-Time RT-PCR reactions with three batches of treated cells were run for each treatment time. Real-Time RT-PCR data was statistically analyzed using SAS software (Yuan, Reed et al. 2006). Data were compiled in Microsoft Excel, SigmaPlot, and Origin. Origin was used to perform one way analysis of variance (ANOVA) statistical analysis.

### **2.1.7 Agarose Gels**

One percent agarose tris-acetate-EDTA (TAE) gels were made by adding 0.65 g agarose powder (SeaKem) to 65 mL TAE buffer (0.3 g/L EDTA [Sigma-Aldrich], 4.84 g/L tris base [US Biologicals], 5.7% glacial acetic acid [Fisher Scientific], pH 7.6). This was microwaved for 2 minutes on high until the agarose powder was dissolved. The agarose-TAE mixture was allowed to cool for 5 minutes, and then 10 mg/L ethidium bromide (EtBr from Sigma-Aldrich) was added. The mixture was then poured into a gel-casting tray with a comb, and was allowed to set. The tray was then placed in a Bio-Rad Wide Mini-Sub Cell agarose gel electrophoresis cell, and the apparatus was filled with TAE buffer. The gel was then loaded with 10  $\mu$ L sample or ladder (diluted 1-in-10 from Fermentas) mixed with 2  $\mu$ L 6X loading buffer (2.5 mg/mL bromophenol blue sodium salt [Sigma-Aldrich], 300 g/L glycerol [Fisher Scientific]). The gel was run at 80 V for 30 minutes, using a Bio-Rad Model 250/2.5 Power Supply.

## **2.2 Post-Translational Control**

To determine if ceramide and Dlc-2 are affecting the protein levels of PGP synthase, the following experiments were conducted.

### **2.2.1 Cloning of PGP Synthase into *E. coli***

The PGP synthase gene (Open Biosystems catalogue # MHS1011-7509250) was subcloned into the pET28a plasmid (Novagen), which we then renamed pET-1not1. The plasmid was then transformed into pTF16 *E. coli* by Roien Ahmedhi by electroporation.

### **2.2.2 Mini-Preparation**

pTF16 *E. coli*, with the PGP synthase gene, was grown on a 100-mm plate (Fisher Scientific) with lysogeny broth (LB) agar (10 g/L NaCl [Fisher], 10 g/L tryptone [Fisher], 5 g/L yeast extract [Fisher], 15 g/L agar [Fisher], pH 7.0) and 30 µg/mL kanamycin (Sigma-Aldrich) overnight in an incubator at 37°C. A well-isolated colony was selected, and transferred with a sterile loop into a 10-mL culture tube (Becton Dickinson) with 3 mL LB (10 g/L NaCl, 10 g/L tryptone, 5 g/L yeast extract, pH 7.0) and 30 µg/mL kanamycin. The culture was grown overnight at 37°C with shaking at 250 rpm. Half of the culture was transferred into a 1.5-mL microcentrifuge tube. The remaining 1.5 mL of overnight culture was made into two glycerol stocks by mixing 750 µL of culture with 250 µL of glycerol in a 1.5-mL microcentrifuge tube. The two tubes were then frozen at -80°C. The microcentrifuge tube with 1.5 mL of culture was spun at 3,000xg in an

Eppendorf 5415C microcentrifuge for 2 minutes. The supernatant was then removed by aspiration. One hundred  $\mu\text{L}$  of Buffer P1 (7.6 g/L tris base, 4.65 g/L EDTA, 100 mg/L RNase A [Sigma-Aldrich] added just before use, pH 8.0) was added to the bacterial pellet. The pellet was resuspended by mixing. Two hundred  $\mu\text{L}$  Buffer P2 (8 g/L sodium hydroxide [NaOH from Fisher Scientific], 10 g/L sodium dodecyl sulfate [SDS from Pierce]) was added to the tube, and the tube was inverted six times. The tube sat for 2 minutes at room temperature. One hundred fifty  $\mu\text{L}$  Buffer P3 (294.5 g/L potassium acetate [KCH<sub>3</sub>COO from Sigma-Aldrich], 100 g/L glacial acetic acid, pH 5.5) was added, and the tube was inverted six times. The tube then sat for 5 minutes on ice. The tube was spun at maximum speed in the microcentrifuge for 2 minutes. Four hundred  $\mu\text{L}$  of the supernatant, but none of the precipitate, was transferred to a fresh microcentrifuge tube. Eight hundred  $\mu\text{L}$  of 100% ethanol was added to the supernatant. The tube was inverted four times, and centrifuged for 2 minutes at top speed. The supernatant was carefully aspirated, leaving the DNA pellet. The DNA pellet was washed with 1 mL of 70% ethanol, and spun at top speed for 2 minutes. The wash was carefully aspirated, and the DNA pellet was allowed to air dry for 15 minutes until the ethanol evaporated. The DNA pellet was resuspended in 30  $\mu\text{L}$  of sterile ddH<sub>2</sub>O. Five  $\mu\text{L}$  of the DNA was digested with 2  $\mu\text{L}$  *SalI* restriction enzyme [New England Biolabs], 2  $\mu\text{L}$  *NotI* restriction enzyme [New England Biolabs], 3  $\mu\text{L}$  Buffer 3 [New England Biolabs], 1  $\mu\text{L}$  bovine serum albumin [BSA from New England Biolabs], and 7  $\mu\text{L}$  ddH<sub>2</sub>O in a 0.65-mL RNase-free, DNase-free microcentrifuge tube. The reaction ran for 2 hours at 37°C in a thermal cycler. The reaction product was run on an agarose gel to ensure the proper plasmid was in the *E. coli* (See section 2.1.7).

### 2.2.3 Protein Induction

pTF16 *E. coli*, expressing trigger factor to prevent protein aggregation, (Nishihara, Kanemori et al. 2000) with the PGP synthase plasmid, was grown from the glycerol stocks made in the mini-preparation (see section 2.2.2). Sixty mL of bacteria was grown from 2  $\mu$ L of the glycerol stock in LB broth with 30  $\mu$ g/mL kanamycin overnight at 37°C with shaking at 250 rpm in a 250-mL flask. The next day, 20 mL of overnight culture was added to 250 mL of LB broth with 30  $\mu$ g/mL kanamycin and 20  $\mu$ g/mL chloramphenicol (Sigma-Aldrich) in 500-mL flasks. The flasks were grown at 37°C with shaking at 250 rpm until the absorbance at 600 nm (OD600) was 0.8. Ten g/L L-(+)-arabinose (Sigma-Aldrich) was added to all but one of the flasks to induce protein expression. The remaining flask served as a non-induced protein control, as no L-(+)-arabinose was added to this flask. The flasks were then grown at 37°C with shaking at 250 rpm until the OD600 was 1.0. Isopropyl- $\beta$ -D-thiogalactopyranoside (IPTG from Sigma-Aldrich) was then added to the induced flasks, but not to the non-induced control flask, at 0.24 g/L. The flasks were grown for an additional 4 hours at 37°C with shaking at 250 rpm. The flasks were placed on ice for 5 minutes, and a centrifuge bottle for each flask was weighed and labelled. Twenty mL of bacterial culture was set aside from each flask, and was stored at 4°C. The bacteria was collected by centrifugation at 10,000xg for 10 minutes at 4°C in a Beckman J2-MC centrifuge. The supernatants were poured off, and all liquid was removed by inverting the bottles for 1 minute. The centrifuge bottles were weighed again, and the weights of the dry protein pellets were determined by subtracting the weights of the empty centrifuge bottles from

the weights of the bottles with the bacterial pellets. The bacterial pellets were stored at -80°C.

#### **2.2.4 Protein Purification**

To purify the PGP synthase protein after it was induced (see section 2.2.3), two different protocols were conducted to ensure maximal protein yield.

##### **2.2.4.1 BugBuster Protein Purification Protocol**

The bacterial pellets (as attained in section 2.2.3) were lysed with 5 mL/g bacterial pellet of BugBuster (Novagen) containing 1 kU/mL rLysozyme (Novagen), 25 U/mL benzonase nuclease (Novagen), and 1 protease inhibitors caplet (Sigma-Aldrich) in 50-mL centrifuge tubes (Becton Dickinson). The pellets were resuspended by mixing, and incubated at room temperature for 20 minutes with shaking. The samples were spun at 16,000xg for 15 minutes at 4°C in a Beckman J2-MC centrifuge. The remaining pellets were later used for inclusion body purification. The soluble fraction of protein was then isolated using Talon cobalt columns (Clontech). The columns were labelled for the induced and non-induced protein samples. The batches of 20 mL of culture that were set aside at 4°C (see section 2.2.3) were then added to the Talon cobalt columns. The BugBuster extracts were added to the columns as well. The columns were incubated at room temperature with slow shaking for 45 minutes to lyse the culture. The stoppers were removed from the columns, and the lysates were allowed to flow through.

The flow-throughs were collected, stored at  $-80^{\circ}\text{C}$ , and labelled as induced protein flow-through and non-induced protein flow-through. The columns were washed twice with 5 mL of BugBuster Wash 1 buffer (6.615 g/L  $\text{Na}_2\text{HPO}_4$ , 0.469 g/L sodium phosphate monobasic [ $\text{NaH}_2\text{PO}_4$  from Fisher Scientific], 17.5 g/L NaCl, pH 8.0), and the first washes were collected, stored at  $-80^{\circ}\text{C}$ , and labelled as induced protein wash 1 and non-induced protein wash 1. The columns were washed with 10 mL of BugBuster Wash 2 buffer (6.615 g/L  $\text{Na}_2\text{HPO}_4$ , 0.469 g/L  $\text{NaH}_2\text{PO}_4$ , 17.5 g/L NaCl, 0.511 g/L imidazole [Sigma-Aldrich], pH 7.5). The columns were inverted twice before the wash was allowed to flow through the columns. The second washes were collected, stored at  $-80^{\circ}\text{C}$ , and labelled as induced protein wash 2 and non-induced protein wash 2. The PGP synthase protein was then eluted with 1 mL of BugBuster elution buffer (6.615 g/L  $\text{Na}_2\text{HPO}_4$ , 0.469 g/L  $\text{NaH}_2\text{PO}_4$ , 17.5 g/L NaCl, 10.212 g/L imidazole, pH 7.0). The columns were inverted back and forth for 10 seconds prior to the flow through of the elution through the column. This was repeated five additional times, leading to an initial 6 mL of protein eluted per column. An additional two elutions were completed with 1 mL elution buffer and 20 minute incubations with shaking at room temperature before allowing the elution to flow through the column. Forty  $\mu\text{L}$  of the elution was retained, stored at  $-80^{\circ}\text{C}$ , and labelled as induced protein elution and non-induced protein elution. The remaining elution was then concentrated using Amicon Ultra-4 Centrifugal Filter Devices (Millipore). The elutions were added to the Amicon filters in 15-mL centrifuge tubes, and the tubes were spun at  $2,500\times g$  in an IEC DPR-6000 centrifuge for 15 minutes (Millipore 2004). The flow-throughs were retained, stored at  $-80^{\circ}\text{C}$ , and labelled as induced protein concentrated flow-through and non-induced protein concentrated flow-

through. The concentrated protein fraction was removed from the top of the concentrated column, stored at  $-80^{\circ}\text{C}$ , and labelled as induced protein concentrated elution and non-induced protein concentrated elution. The PGP synthase protein concentration was determined using the bicinchoninic acid (BCA) assay (see sections 2.2.5). The correct PGP synthase protein size was verified using SDS-polyacrylamide gel electrophoresis (PAGE), and staining with Coomassie blue (see sections 2.2.6 and 2.2.7) (EMD Biosciences 2004; Clontech Laboratories 2007).

The inclusion body cell pellets were re-suspended in the same volume of BugBuster as in the soluble protein fraction isolation as previously described in 50-mL centrifuge tubes. One KU/mL rLysozyme was added. The pellets were mixed by mixing until an even suspension was attained, and incubated at room temperature for 5 minutes with slow shaking. Six volumes of BugBuster, diluted 1-in-10 in ddH<sub>2</sub>O, were then added to the tubes. The tubes were mixed by mixing for 1 minute. The tubes were centrifuged at 5,000xg for 15 minutes at  $4^{\circ}\text{C}$  in a Beckman J2-MC centrifuge. The supernatants were discarded. The remaining inclusion body pellets were resuspended in one-half of the original volume of 1-in-10 diluted BugBuster in new 50-mL tubes. The suspension was mixed by mixing, and then centrifuged at 5,000xg for 15 minutes at  $4^{\circ}\text{C}$ . The supernatants were discarded. The remaining inclusion body pellets were again resuspended in one-half of the original volume of 1-in-10 diluted BugBuster in new 50-mL tubes. The suspension was mixed by mixing, and then centrifuged a third time at 5,000xg for 15 minutes at  $4^{\circ}\text{C}$ . The supernatants were discarded. The remaining inclusion body pellets were resuspended a third time in one-half of the original volume of

1-in-10 diluted BugBuster in new 50-mL tubes. The suspension was mixed by mixing, and then centrifuged for a fourth time at 5,000xg for 15 minutes at 4°C. The supernatants were discarded. The remaining inclusion body pellets were resuspended a final time in one-half of the original volume of 1-in-10 diluted BugBuster in new 50-mL tubes. The suspension was mixed by mixing, and then centrifuged at 16,000xg for 15 minutes at 4°C. The supernatant was discarded. The final pellets of inclusion bodies were resuspended in 4 mL PBS, stored at -80°C until they were used for SDS-PAGE, and labelled as induced protein inclusion bodies and non-induced protein inclusion bodies (EMD Biosciences 2004; Clontech Laboratories 2007).

#### **2.2.4.2 Urea Protein Purification Protocol**

As an alternative to the BugBuster Protein Purification Protocol (see section 2.2.4.1), a Urea Protein Purification Protocol was also conducted. The bacterial pellets, as attained in section 2.2.3, were suspended in 4 mL urea lysis buffer (17.533 g/L NaCl, 7.098 g/L Na<sub>2</sub>HPO<sub>4</sub>, 0.174 g/L phenylmethanesulfonyl fluoride [PMSF from Sigma-Aldrich], 480.08 g/L urea [Fisher Scientific], 0.050 g/L DNase, 0.952 g/L MgCl<sub>2</sub>, 1.563 g/L β-mercaptoethanol [Sigma-Aldrich], pH 8.0) in 15-mL centrifuge tubes. The bacteria were sonicated on ice for 20 seconds three times using a Sonifier Cell Disruptor 350. The tubes were spun at top speed for 15 minutes at 4°C in a Beckman J2-MC centrifuge. The supernatant was retained and labelled as the crude extract. Forty μL of crude extract was set aside for each of the samples to be used in SDS-PAGE gels, and were labelled as induced protein crude extract and non-induced protein crude extract.

Talon columns were equilibrated by adding 1.5 mL ddH<sub>2</sub>O to each column, mixing the columns, and spinning the columns at 3,000xg for 3 minutes in an IEC DPR-6000 centrifuge at room temperature. The previous step was repeated with another 1.5 mL ddH<sub>2</sub>O, and twice with 1.5 mL urea equilibrating buffer (29.220 g/L NaCl, 7.098 g/L Na<sub>2</sub>HPO<sub>4</sub>, 480.080 g/L urea, pH 8.0). The supernatants were then discarded. The crude extracts were added to the columns and allowed to incubate at 4°C for 1 hour with slight shaking. The columns were then spun at 3,000xg for 3 minutes. The flow-throughs were retained, stored at -80°C, and labelled as induced protein flow-through and non-induced protein flow-through. The columns were then washed with 5 mL urea wash 1 buffer (29.220 g/L NaCl, 7.098 g/L Na<sub>2</sub>HPO<sub>4</sub>, 480.080 g/L urea, pH 8.0) by mixing and then spinning for 3 minutes at 3,000xg. This wash was repeated two additional times, and the flow-throughs were retained, stored at -80°C, and labelled as induced protein wash 1 and non-induced protein wash 1. The columns were then washed with 5 mL urea wash 2 (29.220 g/L NaCl, 7.098 g/L Na<sub>2</sub>HPO<sub>4</sub>, 480.080 g/L urea, 0.681 g/L imidazole, pH 8.0) by mixing and then spinning for 3 minutes at 3,000xg. This wash was repeated once more, and the flow-throughs were retained, stored at -80°C, and labelled as induced protein wash 2 and non-induced protein wash 2. The protein was then eluted by adding 5 mL urea elution buffer (5.844 g/L NaCl, 480.080 g/L urea, 17.020 g/L imidazole, 2.423 g/L tris base, pH 7.5), mixing, shaking on ice for 3 minutes, and spinning at 3,000xg for 3 minutes. This was repeated twice more to produce 15 mL of eluted protein. Forty µL of the elution was retained, stored at -80°C, and labelled as induced protein elution and non-induced protein elution. The remaining elution was then concentrated using Amicon Ultra-4 Centrifugal Filter Devices (see section 2.2.4.1). The

protein concentration was then measured by the BCA assay, and the samples were run using SDS-PAGE gels that were stained with Coomassie blue (Lebediker 2006; Clontech Laboratories 2007).

### **2.2.5 Bicinchoninic Acid Protein Assay**

The BCA protein assay kit was purchased from Sigma-Aldrich. The Standard 2.1 mL Assay Protocol was used to determine protein concentrations. The reaction was carried out in glass test tubes (VWR). The BCA working reagent consisted of 2 mL Reagent A (bicinchoninic acid solution) and 0.04 mL Reagent B (copper[II] sulfate pentahydrate 4% solution) per tube. To create the standard curve, 100  $\mu$ L of diluted BSA protein standard was added to seven tubes to reach 0, 2.5, 5, 10, 20, 35, and 70  $\mu$ g/mL concentrations. For each unknown protein sample, 10  $\mu$ L of sample and 90  $\mu$ L of ddH<sub>2</sub>O were added, with the working reagent, to each glass test tube. All test tubes (standards and unknown samples) were then incubated at 37°C for 30 minutes standing in a water bath. The tubes were then allowed to cool to room temperature, and the liquid was transferred to spectrophotometer cuvetts (Fisher Scientific). The GeneQuant pro spectrophotometer BCA562 program was then used to determine the unknown protein sample concentrations (Sigma-Aldrich 2005).

## 2.2.6 SDS-PAGE

Acrylamide gels were cast using the Bio-Rad Mini-PROTEAN Tetra Handcast System that was cleaned with 70% ethanol before use. Ten mL of 12% acrylamide mix (117.980 g/L acrylamide [Bio-Rad], 3.232 g/L bis-acrylamide [Bio-Rad], 1.010 g/L SDS, 45.833 g/L tris base, pH 8.8) was mixed with 10 mg ammonium persulfate (APS from Sigma-Aldrich) and 4  $\mu$ L tetramethylethylenediamine (TEMED from Sigma-Aldrich) to make two gels. Alternatively, 10 mL of 8% acrylamide mix (78.457 g/L acrylamide, 2.149 g/L bis-acrylamide, 1.010 g/L SDS, 45.833 g/L tris base, pH 8.8) was mixed with 10 mg APS and 4  $\mu$ L TEMED to make two gels. As well, 10 mL of 5% stacking gel mix (49.360 g/L acrylamide, 1.352 g/L bis-acrylamide, 1.018 g/L SDS, 15.525 g/L tris base, pH to 6.8) was mixed with 10 mg APS and 10  $\mu$ L TEMED. The 12% and 8% gels were poured into the Bio-Rad Handcast System, covered with ddH<sub>2</sub>O, and allowed to set for 15 minutes. The ddH<sub>2</sub>O was removed, and the 5% stacking gel was poured on top of the set gels and allowed to set with ten-well or fifteen-well Bio-Rad combs, that were previously soaked in methanol [Fisher Scientific], for 15 minutes. The set gels were placed in the Bio-Rad Mini-PROTEAN Tetra Cell, and the apparatus was filled with running buffer (18.8 g/L glycine [Fisher Scientific], 3.02 g/L tris base, 5 g/L SDS). Equal amounts of protein samples, as determined by the BCA assay (see section 2.2.5), were mixed with 2  $\mu$ L 5X protein gel loading buffer (100 g/L SDS, 5 g/L bromophenol blue sodium salt, 500 g/L glycerol, 250  $\mu$ L  $\beta$ -mercaptoethanol, 30.285 g/L tris base, pH 6.8) and ddH<sub>2</sub>O to a total of 10  $\mu$ L in 1.5-mL microcentrifuge tubes. Five  $\mu$ L of Page Ruler Plus Pre-stained Protein Ladder (Fermentas) was mixed with 5  $\mu$ L ddH<sub>2</sub>O and

placed in a microcentrifuge tube. The tops of the tubes were punctured with a needle, and the samples and ladder were placed in boiling water for 5 minutes. The tubes were spun at maximum speed in a microcentrifuge to collect the samples, and then the samples and ladder were loaded into the set gels in the Bio-Rad Tetra Cell apparatus. The gels were run at 130-150 V for 60 minutes until the dye front reached the bottom of the gels (Harlow and Lane 1999).

### **2.2.7 Coomassie Blue Staining**

After gel electrophoresis, the gels were covered with Coomassie blue stain (2.5 g/L Coomassie blue sodium salt, 500 g/L methanol, 100 g/L glacial acetic acid) in clean plastic containers. The gels were then incubated overnight at room temperature with shaking. The Coomassie stain was then removed, and the gel was destained by successive incubations with destaining solution (250 g/L methanol, 75 g/L glacial acetic acid) at room temperature with shaking (Harlow and Lane 1999).

### **2.2.8 Drying the gels**

After Coomassie blue staining, the SDS-PAGE gels were dried. First the gels were washed briefly in water. The gels were then sandwiched between plastic wrap (Saran) and filter paper (Fisher Scientific), with the top of the gel facing the plastic wrap and the back of the gel against the filter paper. The sandwiched gel was then placed into a Bio-Rad Model 583 gel dryer filter paper side down. The gel dryer's vacuum was turned on, and gentle heat was applied for 2 hours. The vacuum was then released slowly, and the gel was removed and stored at room temperature (Harlow and Lane 1999).

### **2.2.9 PGP Synthase Peptide Design**

Peptides were designed using the National Center for Biotechnology Information (NCBI) Basic Local Alignment Search Tool (BLAST) against the N- and C-terminals of the PGP synthase protein to find conserved sequences between species. These peptides were then used to create an antibody against PGP synthase (see section 2.2.11). The peptides were ordered from The University of Calgary's Peptide Services, and had the following sequences: N-terminal, 25-mer GPVFWRLLGLLPGRPGLAALLGC; C-terminal 16-mer CPGRQVKLWVKMVTPL.

## 2.2.10 Protein Cross-Linking

In order for the PGP synthase peptides to be made into phage antibodies, they were first cross-linked to BSA using sulfo-*m*-maleimidobenzoyl-*N*-hydroxysuccinimide ester (sulfo-MBS) to allow them to be more naturally immunogenic (Jacob, Arnon et al. 1985).

### 2.2.10.1 Amino Group Preparation

For the 25-mer peptide, 2.624 mg of BSA (Sigma-Aldrich) was dissolved in 400  $\mu$ L of conjugation buffer (0.877 g/L EDTA in PBS, pH 7.2) in a 1.5-mL microcentrifuge tube. For the 16-mer peptide, 2.389 mg of BSA was dissolved in 360  $\mu$ L conjugation buffer. As well, for BSA-BSA conjugation, 2.624 mg of BSA was dissolved in 400  $\mu$ L of conjugation buffer. A ten-fold molar excess of sulfo-MBS crosslinker (Pierce) was then added to each sample. For the 25-mer peptide, 50  $\mu$ L of sulfo-MBS (4.16 g/L in conjugation buffer) was added to the 400  $\mu$ L. For the 16-mer peptide, 45  $\mu$ L of sulfo-MBS was added to the 360  $\mu$ L. For the BSA, 50  $\mu$ L of sulfo-MBS was added to the 400  $\mu$ L. The three tubes (corresponding to the 25-mer peptide, the 16-mer peptide, and the BSA-BSA conjugation) with the sulfo-MBS then sat at room temperature for 30 minutes with slow shaking. Three Zeba desalting columns (Pierce) were placed in 15-mL centrifuge tubes, and centrifuged at 1,000 $\times$ g for 2 minutes in an IEC DPR-6000 centrifuge to remove the storage resin. The columns were placed into new centrifuge tubes, and 2.5 mL of conjugation buffer was placed in each column to equilibrate the

columns. The columns were centrifuged at 1,000xg for 2 minutes to remove the conjugation buffer. The columns were placed into new tubes, and the 25-mer peptide, the 16-mer peptide, and the BSA-BSA sulfo-MBS samples were added to the tubes. The columns were spun at 1,000xg for 2 minutes to collect the desalted samples. The samples were placed back into the columns, and the columns were placed back into the same tubes. The columns were spun at 1,000xg for 2 minutes to collect the amino group samples (Pierce Biotechnology 2005; Pierce Biotechnology 2007).

#### **2.2.10.2      Sulphydryl Group Preparation**

$\beta$ -mercaptoethanol was added to remove disulphide bonds between the peptides and BSA. Three mg of 25-mer peptide was mixed into 1 mL conjugation buffer with 7  $\mu$ L  $\beta$ -mercaptoethanol in a 1.5-mL centrifuge tube. Two mg of 16-mer peptide was mixed into 1 mL conjugation buffer with 7  $\mu$ L  $\beta$ -mercaptoethanol. 52.48 mg of BSA was mixed into 2 mL conjugation buffer with 14  $\mu$ L  $\beta$ -mercaptoethanol. These three tubes were incubated for 30 minutes at room temperature with slow shaking. Three Zeba desalting columns were placed in 15 mL-centrifuge tubes, and centrifuged at 1,000xg for 2 minutes in an IEC DPR-6000 centrifuge to remove the storage resin. The columns were placed into new tubes, and 2.5 mL of conjugation buffer was placed in each column to equilibrate the columns. The columns were centrifuged at 1,000xg for 2 minutes to remove the conjugation buffer. The columns were placed into new tubes, and the 25-mer peptide, the 16-mer peptide, and the BSA was added to the tubes. The columns were spun at 1,000xg for 2 minutes to collect the desalted samples. The samples were placed back into the columns, and the columns were placed back into the same tubes.

The columns were spun at 1,000xg for 2 minutes to collect the sulfhydryl group samples (Pierce Biotechnology 2005; Pierce Biotechnology 2007).

### **2.2.10.3 Crosslinking**

The amino and sulfhydryl peptides were mixed together, and incubated at room temperature for 30 minutes with slow shaking. The absorbance was measured at absorbance at 280 nm (OD280) on a GeneQuant pro spectrophotometer. The samples were diluted to the required volume of 75 mL, and placed into three 50-mL centrifuge tubes per sample (Pierce Biotechnology 2005).

### **2.2.11 Peptide Phage Display**

Peptide phage display was used to produce phage scFv antibodies against PGP synthase. Due to the lack of sufficient protein substrate produced by the PGP synthase protein purification techniques (see section 2.2.4), the antibodies were produced against peptides corresponding to the N- and C-terminals of PGP synthase.

#### **2.2.11.1 Production of Helper Phage**

T-phage resistant *E. coli* (TG1) was streaked onto a 100-mm minimal media agar plate (15 g/L agar [Fisher Scientific], 105 g/L potassium phosphate dibasic [K<sub>2</sub>HPO<sub>4</sub> from Mallinckrodt], 45 g/L KH<sub>2</sub>PO<sub>4</sub>, 10 g/L ammonium sulfate [(NH<sub>4</sub>)<sub>2</sub>SO<sub>4</sub> from Sigma-Aldrich], 5 g/L sodium citrate [Sigma-Aldrich], 0.246 g/L magnesium sulphate [MgSO<sub>4</sub>

from Sigma-Aldrich], 5 g/L thiamine hydrochloride [B1 from Sigma-Aldrich], 0.040 g/L L-amino acid stock [Sigma-Aldrich], 2 g/L glucose [Sigma-Aldrich]), and grown overnight in an incubator at 37°C. A TG1 bacterial colony was selected, and grown in 5 mL 2X TY broth (5 g/L NaCl, 16 g/L tryptone, 10 g/L yeast extract) overnight at 37°C with shaking at 250 rpm. The next day, three 10-mL culture tubes (Becton Dickinson) with 200 µL 2X TY broth were inoculated with 2 µL of the overnight TG1 culture, and the three tubes were grown to an OD<sub>600</sub> of 0.4. Ten µL of one hundred-fold serial dilutions of KM13 helper phage (10<sup>7</sup> pfu/mL) were then added to the three tubes. The tubes were placed standing in a 37°C water bath for 30 minutes. Each 210 µL of culture were then added to 3 mL of 42°C molten H-top agar (8 g/L agar, 8 g/L NaCl, 10 g/L tryptone). The 3.21 mL were then poured onto three warm 100-mm TYE plates (15 g/L agar, 8 g/L NaCl, 10 g/L tryptone, 5 g/L yeast extract), and allowed to set. The plates were incubated overnight at 37°C in an incubator. The next day, a small plaque from one of the TYE plates was picked, and added to a 10-mL culture tube with 5 mL 2X TY with TG1 at an OD<sub>600</sub> of 0.4. The 5-mL culture was grown for 2 hours with shaking at 37°C. The 5 mL was then added to 500 mL of 2X TY, and grown with shaking at 37°C for 1 hour. Fifty mg/L kanamycin was then added to the culture, and it was grown overnight at 30°C with shaking at 250 rpm. The next day, the culture was spun at 10,800xg in a Beckman J2-MC centrifuge at 4°C for 15 minutes. Four hundred mL of the supernatant was mixed with 100 mL PEG/NaCl (200 g/L carbowax polyethylene glycol 8000 [Fisher Scientific], 146.108 g/L NaCl), and left on ice for 1 hour with slow shaking. The supernatant-PEG/NaCl mixture was then spun at 10,800xg at 4°C for 30 minutes. The PEG/NaCl supernatant was discarded, and the pellet was suspended in 8 mL PBS and

2 mL PEG/NaCl by mixing. The mixture was left on ice for 20 minutes with slow shaking, and then spun at 3,300xg at 4°C for 30 minutes. The PEG/NaCl supernatant was aspirated, and the pellet was resuspended in 5 mL PBS. This was spun at 11,600xg at 4°C for 10 minutes to remove bacterial debris. The supernatant (helper phage) was stored with 150 g/L glycerol in 2-mL cryovials (Wheaton) at -80°C. To titre the helper phage, 45 µL of the frozen helper phage was mixed with 5 µL trypsin stock solution (10 g/L trypsin Type XIII [Sigma-Aldrich], 0.111 g/L calcium chloride [CaCl<sub>2</sub> from Mallinckrodt], 6.057 g/L tris base, pH 7.4) in a 1.5-mL microcentrifuge tube, and incubated for 30 minutes at 37°C in a water bath. One hundred-fold serial dilutions of the trypsin-treated helper phage and untreated helper phage were then made. Ten µL of trypsin-treated phage or untreated phage was diluted in 1 mL of PBS. This was repeated five times to make six serial dilutions for the trypsin-treated or untreated phage. Twelve culture tubes with 1 mL 2X TY broth were inoculated with TG1 bacteria, and grown until OD<sub>600</sub> was 0.4. Fifty µL of each helper phage dilution was added to the twelve culture tubes. The culture tubes were then mixed with 3 mL molten H-top agar, and poured onto 100-mm TYE plates. The twelve plates were grown overnight at 37°C in an incubator. The titre of the trypsin-treated phage was confirmed to be 10<sup>5</sup> to 10<sup>8</sup> pfu/mL lower than the untreated phage. If the titre was not sufficiently lower in the trypsin-treated phage, another helper phage plaque would have been selected to prepare more helper phage. The titre used in this project for the KM13 helper phage was 3.6 x 10<sup>15</sup> pfu/mL (Winter 2002).

### **2.2.11.2 Production of I and J Phage Libraries**

TG1 cells were streaked onto a 100-mm minimal media agar plate, and grown overnight in an incubator at 37°C. A TG1 bacterial colony was selected, and grown in 5 mL of 2X TY broth overnight at 37°C with shaking at 250 rpm. The next day, the I and J libraries were grown in two flasks with 200 mL 2X TY broth with 100 mg/L ampicillin and 10 g/L glucose, inoculated with 2 mL overnight TG1 culture, at 37°C with shaking at 250 rpm until the OD600 was 0.4. One hundred fifty mL of the broth was used to make glycerol stocks with 150 g/L glycerol. The stocks were stored in 2-mL cryule vials at -80°C.  $2 \times 10^{11}$  pfu KM13 helper phage (2.8 µL of helper phage stock) were then added to the remaining 50 mL of library I and J bacterial culture. The two cultures were incubated standing at 37°C in a water bath for 30 minutes. The cultures were then spun at 3,000xg in a Beckman J2-MC centrifuge at 4°C for 10 minutes. The supernatants were discarded, and the bacterial pellets were resuspended in two flasks with 100 mL of 2X TY with 100 mg/L ampicillin, 50 mg/L kanamycin, and 1 g/L glucose. The library cultures were incubated overnight at 30°C with shaking at 250 rpm. The next day, the cultures were spun at 3,300xg at 4°C for 30 minutes. Eighty mL of the supernatants was mixed with 20 mL PEG/NaCl, and left on ice for 1 hour with slow shaking. The two library-PEG/NaCl mixtures were then spun at 3,300xg at 4°C for 30 minutes. The PEG/NaCl supernatants were aspirated, and the library pellets were resuspended in 4 mL PBS. The resuspensions were spun at 11,600xg at 4°C for 10 minutes to remove bacterial debris. The supernatants (library I and J phage) were stored with 150 g/L glycerol in 2-mL cryule vials at -80°C. To titre the library phage, one hundred-fold serial

dilutions of the library phage were made. One  $\mu\text{L}$  of library I or J phage was diluted in 100  $\mu\text{L}$  of PBS. This was repeated five times to make six serial dilutions for the I and J phage libraries. Twelve culture tubes with 900  $\mu\text{L}$  2X TY broth were inoculated with TG1 bacteria that had been grown until OD600 was 0.4. The twelve tubes were incubated standing at 37°C in a water bath for 30 minutes. Ten  $\mu\text{L}$  of each library phage dilution was spotted onto 100-mm TYE plates with 100 mg/L ampicillin and 10 g/L glucose. The twelve plates were grown overnight at 37°C in an incubator. The titre of the phage was confirmed to be at least  $10^{12}$  cfu/mL. If the titre was not sufficient, another library phage colony would have been selected to prepare more library phage. The titres used in this project for the library I phage was  $6.0 \times 10^{12}$  cfu/mL, and for library J phage was  $2.2 \times 10^{17}$  cfu/mL (Winter 2002).

### **2.2.11.3 Phage Display**

Phage display consisted of three main sections. There was the production of TG1 bacteria, antigen binding, and the selection process. These processes were repeated three times for three rounds of selection, and are described in the following sections. The schematic and day-to-day schedule of phage display can be seen in Figure 9 and Table 1.

# Selection Round 1

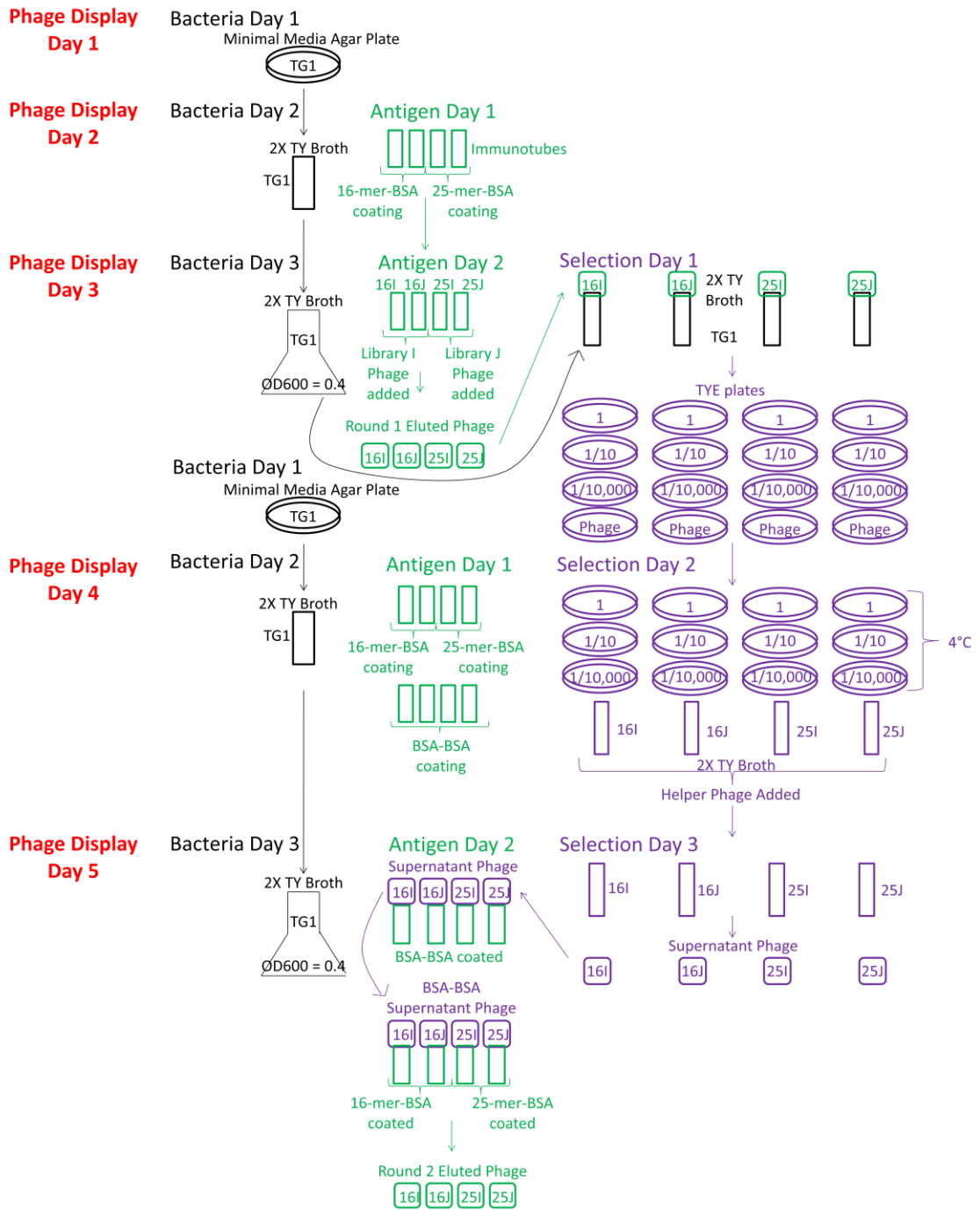


(Figure 9 continued on next page)

(Figure 9 continued from previous page)

## Selection Round 2

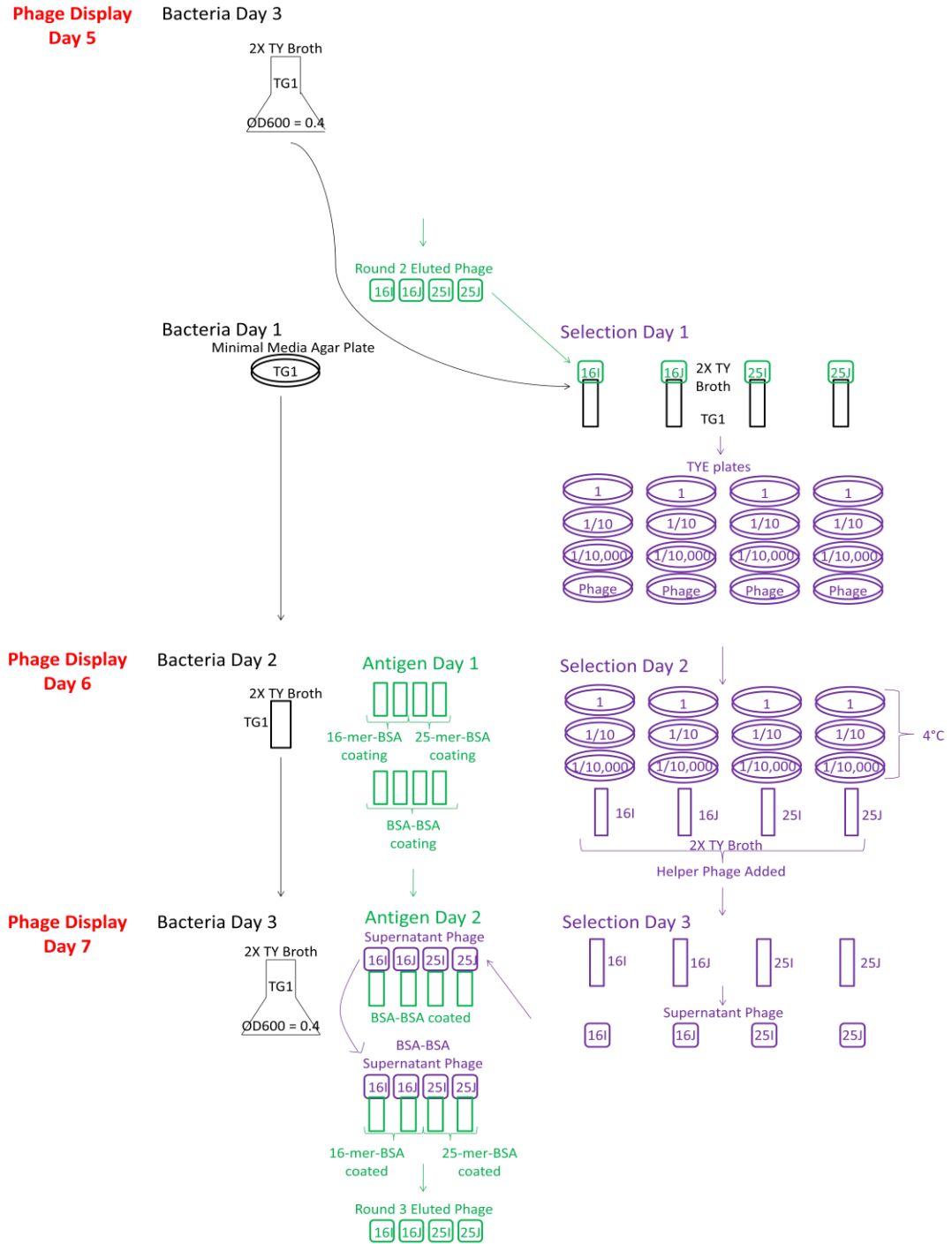


(Figure 9 continued on next page)

(Figure 9 continued from previous page)

### Selection Round 3

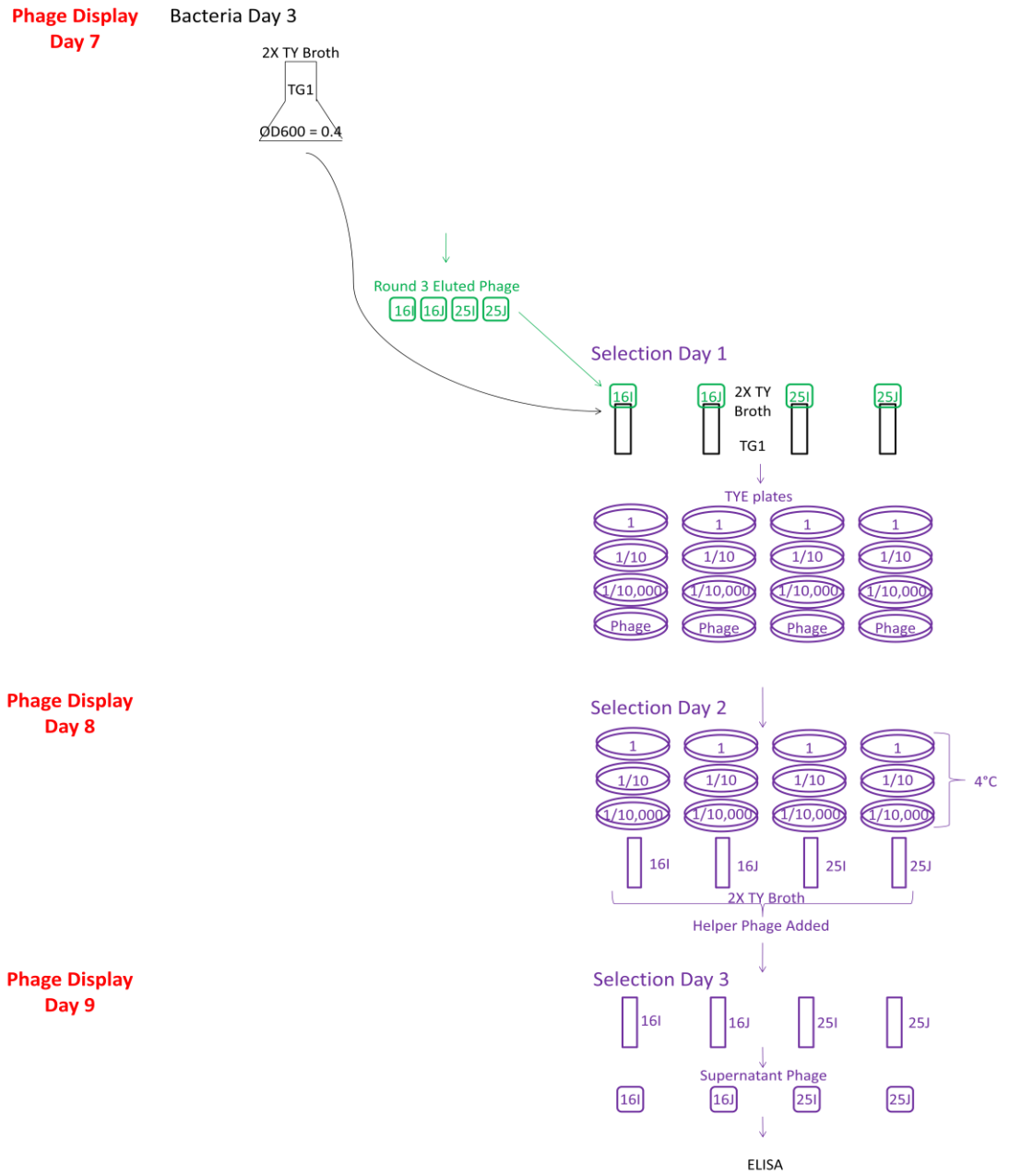


Figure 9: Phage Display Schematic

Adapted from: Winter 2002

Table 1: Phage Display Day-to-Day Schedule

Adapted from: Winter 2002

<b>Phage Display</b>	<b>Bacteria</b>	<b>Antigen</b>	<b>Selection</b>
<b>Day 1</b>	Day 1		
<b>Day 2</b>	Day 2	Day 1	
<b>Day 3</b>	Day 3, Day 1	Day 2	Day 1
<b>Day 4</b>	Day 2	Day 1	Day 2
<b>Day 5</b>	Day 3, Day 1	Day 2	Day 3, Day 1
<b>Day 6</b>	Day 2	Day 1	Day 2
<b>Day 7</b>	Day 3	Day 2	Day 3, Day 1
<b>Day 8</b>			Day 2
<b>Day 9</b>			Day 3

#### **2.2.11.3.1 Phage Display – TG1 Bacteria**

Initially (Bacteria Day 1), TG1 was streaked onto a 100-mm minimal media agar plate, and was grown overnight in an incubator at 37°C. The next day (Bacteria Day 2), 5 mL of 2X TY was inoculated with one colony from the previous day's TG1 minimal media agar plate in a 10-mL culture tube. The culture was grown overnight at 37°C with shaking at 250 rpm. The next day (Bacteria Day 3), 100 mL of fresh TG1 bacteria was grown from the previous day's 5 mL culture by diluting it 1-in-100 in fresh 2X TY broth. It was grown until the OD600 was 0.4 (Winter 2002).

#### **2.2.11.3.2 Phage Display – Antigen Binding**

Initially (Antigen Day 1), Maxisorp immuno test tubes (immunosorbent tubes from Nunc) were coated with 4 mL of 10 – 100 mg/L of antigen diluted in PBS. For the first immunotube coating, the antigens were the 16-mer and 25-mer peptides conjugated to BSA. For the second and third immunotube coatings, the antigens were the 16-mer peptide conjugated to BSA, the 25-mer peptides conjugated to BSA, and BSA conjugated to itself. For each antigen, two immunotubes were coated, corresponding to one tube each for the I and J phage libraries (Winter 2002).

The next day (Antigen Day 2), the immunotubes were washed three times with PBS. The tubes were then filled to the brim with M-PBS (20 g/L skim milk powder [Wal-Mart] in PBS) to block for 2 hours at room temperature. For the first coating, all four immunotubes were blocked. For the second and third coatings, the BSA-BSA conjugated immunotubes were blocked first, and the peptide immunotubes were blocked after the BSA-BSA immunotubes were finished blocking. The blocked immunotubes were then washed three times with PBS. For the first coating, the immunotubes were filled with  $10^{12}$  to  $10^{13}$  phage from library I or J in 4 mL PBS. For the second and third coatings, selection phage in 4 mL PBS was used (see section 2.2.11.3.3 – Selection Day 3). The immunotubes were labelled corresponding to the peptide and phage library as follows: 16I, 16J, 25I, and 25J. The immunotubes were incubated for 1 hour at room temperature with over-and-under rotation. They were then incubated for 1 hour at room temperature standing. For the first coating, the supernatant was then discarded. For the second and third coatings, the BSA-BSA supernatant was then poured into the blocked peptide immunotubes. This allowed the phage antibodies that had bound to BSA or the sulfo-MBS crosslinker to be removed prior to amplification. The peptide immunotubes with the supernatant from the BSA-BSA immunotubes were incubated for 1 hour at room temperature with over-and-under rotation. They were then incubated for 1 hour at room temperature standing. After the phage incubation, the immunotubes were washed with PBS-T (1 mL Tween-20 [Sigma-Aldrich] per L PBS). For the first coating, the immunotubes were washed ten times. For the second and third coatings, the immunotubes were washed twenty times. The PBS-T was then shaken out of the tubes. This phage was eluted from the immunotubes by adding 500  $\mu$ L of diluted trypsin-PBS (50  $\mu$ L

trypsin stock with 450  $\mu$ L PBS). The tubes were incubated for 10 minutes at room temperature with over-and-under rotation. Half the eluted phage was stored at 4°C, and the remaining 250  $\mu$ L was used in the following phage selection process (Winter 2002).

### **2.2.11.3.3 Phage Display – Phage Selection**

Initially, (Selection Day 1) 250  $\mu$ L of eluted phage from each immunotube (see section 2.2.11.3.2 – Antigen Day 2) was added to 10-mL culture tubes containing 1.75 mL of TG1 at an OD600 of 0.4 (see section 2.2.11.3.1 – Bacteria Day 3). The tubes were incubated for 30 minutes at 37°C in a water bath without shaking. For each culture corresponding to each immunotube, dilution plates were made by spotting 10  $\mu$ L, 10  $\mu$ L of a 1-in-100 dilution, and 10  $\mu$ L of a 1-in-10,000 dilution onto 100-mm TYE plates with 100 mg/L ampicillin and 10 g/L glucose. The 10  $\mu$ L were spread using sterile glass spreaders. The remaining TG1 cultures were spun at maximum speed in an Eppendorf 5415C microcentrifuge for 5 minutes. The bacterial pellets were then resuspended in 50  $\mu$ L 2X TY broth. The 50  $\mu$ L were then spread onto phage TYE plates containing 100 mg/L ampicillin and 10 g/L glucose. All plates were grown overnight in an incubator at 37°C (Winter 2002).

The next day (Selection Day 2), 2 mL of 2X TY broth with 150 g/L glycerol was added to the phage TYE plates (not the dilution plates). The cells were loosened with sterile glass spreaders, and mixed thoroughly. One mL of the phage-infected bacteria was stored at -80°C with 150 g/L glycerol in cryovials. Fifty  $\mu$ L of the phage-bacteria

mixture was used to inoculate 50 mL of 2X TY containing 100 mg/L ampicillin and 10 g/L glucose. Once the cultures reached an OD<sub>600</sub> of 0.4,  $5 \times 10^{10}$  pfu of helper phage was added to 10 mL of the cultures. The cultures were incubated without shaking at 37°C in a water bath for 30 minutes. The cultures were then spun at 3,000xg for 10 minutes at 4°C in a Beckman J2-MC centrifuge. The bacterial pellets were resuspended in 50 mL of 2X TY with 100 mg/L ampicillin, 50 mg/L kanamycin, and 1 g/L glucose. The cultures were incubated at 30°C overnight with shaking at 250 rpm.

The next day (Selection Day 3), the 30°C overnight cultures were spun at 3,300xg for 15 minutes at 4°C in a Beckman J2-MC centrifuge. Ten mL PEG/NaCl was mixed with 40 mL of the supernatants, and the mixtures were left on ice for 1 hour with slow shaking. The mixtures were then spun at 3,300xg for 30 minutes at 4°C. The PEG/NaCl was poured off, and the mixtures were spun at 3,300xg for 5 minutes at 4°C. The PEG/NaCl was aspirated, and the cell pellets were resuspended in 2 mL PBS in 2.0-mL microcentrifuge tubes (Axygen). The tubes were spun at maximum speed in an Eppendorf 5415C microcentrifuge for 10 minutes to remove any bacterial debris. One mL of this phage was used for the next round of antigen binding (see section 2.2.11.3.2 – Antigen Day 1). The remaining 1 mL, or 2 mL for the final round of selection, of phage was stored at 4°C (Winter 2002).

## **2.2.12 Enzyme-Linked Immunosorbent Assay (ELISA)**

ELISA was used to confirm that the phage antibodies made by phage display were specific for PGP synthase (see section 2.2.11).

### **2.2.12.1 Monoclonal Phage ELISA**

Individual colonies from the titration plates from each round of phage selection were inoculated into 100  $\mu$ L of 2X TY with 100 mg/L ampicillin and 10 g/L glucose in ninety-six-well cell culture plates (Nunc). There were four ninety-six-well plates used, corresponding to the 16-mer-peptide, I library; the 16-mer-peptide, J library; the 25-mer-peptide, I library; and the 25-mer-peptide, J library. These plates were grown overnight at 37°C with shaking at 250 rpm. After the overnight growth, a ninety-six-well transfer device (Boekel Scientific) was used to transfer small inoculums (2  $\mu$ L) from the four grown plates to four new ninety-six-well cell culture plate containing 200  $\mu$ L 2X TY with 100 mg/L ampicillin and 10 g/L glucose. Glycerol stocks of the original four ninety-six-well cell culture plates were made by adding glycerol to a final concentration of 150 g/L, and these plates were stored at -80°C. The second ninety-six-well cell culture plates were grown at 37°C for 2 hours with shaking at 250 rpm. Twenty-five  $\mu$ L of 2X TY with 100 mg/L ampicillin, 10 g/L glucose, and  $10^9$  pfu of helper phage was added to each well. The plates were grown at 37°C for 1 hour with shaking at 250 rpm. The plates were then spun at 1,800xg for 10 minutes at 4°C in a Beckman Coulter Allegra 25R centrifuge. The supernatant was aspirated, and the cell pellets were resuspended in 200  $\mu$ L of 2X TY

with 100 mg/L ampicillin and 50 mg/L kanamycin per well. The plates were then grown overnight at 30°C with shaking at 250 rpm. The plates were spun at 1,800xg for 10 minutes at 4°C. Fifty  $\mu$ L of the supernatant was then used in polyclonal phage ELISA (see section 2.2.12.2). The remaining 50  $\mu$ L of phage supernatant was moved to four new ninety-six-well plates and stored at 4°C (Winter 2002).

### **2.2.12.2 Polyclonal Phage ELISA**

Ninety-six-well flexible assay plates (Becton Dickinson) were coated with 100  $\mu$ L per well of antigen in the same buffer and at the same concentration as used for phage display selection (see section 2.2.11). Two plates were coated with the 16-mer peptide BSA conjugation (one for the library I phage and one for the library J phage), two plates were coated with the 25-mer peptide BSA conjugation (one for the library I phage and one for the library J phage), and four plates were coated with BSA-BSA conjugation (one for the 16-mer-peptide, library I phage; one for the 16-mer-peptide, library J phage; one for the 25-mer-peptide, library I phage; and one for the 25-mer-peptide, library J phage). The eight plates were left overnight at room temperature to allow time for the antigens to bind to the plates. The next day, the plates were washed three times with PBS. Two hundred  $\mu$ L of M-PBS was added to each well, and the plates were allowed to block for 2 hours at room temperature. The eight plates were then washed three times with PBS. Twenty-five  $\mu$ L of phage from monoclonal ELISA (see section 2.2.12.1) was then added with 75  $\mu$ L of M-PBS to the corresponding plates (four sets of BSA-BSA and peptide-BSA plates). These plates were incubated standing for 1 hour at room temperature. The

phage solution was then discarded, and the plates were washed three times with PBS-T. Two hundred  $\mu\text{L}$  of a 1-in-5,000 dilution of Protein L-HRP-anti-M13 secondary antibody (Pierce) in M-PBS was then added to the plates. The plates were incubated for 1 hour at room temperature, and then washed three times with PBS-T. One hundred  $\mu\text{L}$  of substrate solution (100 mg/L 3,3',5,5'-tetramethylbenzidine [TMB from Sigma-Aldrich], 8.203 g/mol sodium acetate [Sigma-Aldrich], pH 6.0, 60 mg/L hydrogen peroxide [Sigma-Aldrich] added before use) was added to each well. The plates were then left at room temperature for 15 minutes until a blue color developed. The reaction was stopped by adding 50  $\mu\text{L}$  of 1 M sulphuric acid (Sigma-Aldrich) to each well, and the blue color turned yellow to confirm the reaction was stopped (Winter 2002).

### **2.2.12.3 ELISA Analysis**

The polyclonal ELISA plates were read using a Molecular Devices Spectra Max 190 plate reader. The absorbance at 650 nm (OD650) was subtracted from the absorbance at 450 nm (OD450). A positive phage reaction was found if the OD450 – OD650 was above background values in a well on the peptide ELISA plate, but not in the corresponding BSA-BSA well.

### 2.2.13 Production of Soluble Antibody Fragments

HB2151 *E. coli* was streaked onto a 100-mm minimal agar plates and grown overnight at 37°C in an incubator. Five mL of 2X TY was inoculated with one colony of HB2151 from the overnight plate. The broth was grown at 37°C with shaking at 250 rpm until the OD600 was 0.4. Two hundred µL of the exponentially-growing bacteria was infected with 10 µL of phage from the monoclonal ELISA 4°C plates (see section 2.2.12) in 1.5-mL microcentrifuge tubes. These tubes were grown standing at 37°C in a water bath for 30 minutes. The cultures were then moved to 10-mL culture tubes with 5 mL 2X TY with 100 mg/L ampicillin and 10 g/L glucose. These tubes were grown overnight with shaking at 37°C with shaking at 250 rpm. One mL of each overnight culture was added to 50 mL 2X TY containing 100 mg/L ampicillin and 1 g/L glucose. The cultures were grown with shaking at 250 rpm at 37°C until the OD600 was 0.9. One hundred fifty g/L glycerol was added to the remaining 4 mL of overnight cultures, and aliquots of 1 mL were frozen at -80°C in 2-mL cryule vials to be used in the future to grow more phage antibody. 2.145 g/L IPTG was then added to the 0.9 OD600 50 mL cultures, and they were grown with shaking at 250 rpm at 30°C overnight. The next day, the cultures were then spun three times at 1,800xg for 10 minutes in an IEC DPR-6000 centrifuge to remove bacterial debris. The supernatant is used as the phage antibody (Winter 2002).

## **2.2.14 Western Blotting**

To determine if the PGP synthase protein was affected by ceramide treatment, western blotting was conducted with the help of Lauren Luo.

### **2.2.14.1 Cell Treatments**

Cells were grown as in section 2.1.1. They were then grown to 70 – 80% confluency, and starved for 12 hours in  $\alpha$ -MEM with no FBS. Cells were then treated with 10 mg/L C<sub>2</sub>-ceramide diluted in 100% ethanol or the same volume of ethanol alone in  $\alpha$ -MEM supplemented with 10% FBS for 1 or 4 hours. Cells were harvested after treatments by scraping with sterile cell scrapers, and then pelleted by centrifugation in an IEC DPR-6000 centrifuge at 1,000xg in 15-mL centrifuge tubes. Cells were then lysed to obtain the proteins (see section 2.2.14.2).

### **2.2.14.2 Cell Lysis**

The cell pellets were washed by resuspending them in 1 mL cold PBS followed by centrifugation at 1,000xg for 5 minutes. The supernatants were aspirated, and the pellets were washed again. The supernatants were aspirated, and the pellets were put on ice. Two hundred  $\mu$ L of lysis buffer (1.461 g/L EDTA, 10 g/L nonidet P 40 substitute [NP-40 from Fluka], 5 g/L sodium deoxycholate [Sigma-Aldrich], 10.636 g/L sodium pyrophosphate [Sigma-Aldrich], 0.184 g/L sodium orthovanadate [Sigma-Aldrich], 2.099 g/L sodium fluoride [NaF from Sigma-Aldrich], 0.058 g/L NaCl, 1.211 g/L tris

base, pH 7.5, with 0.174 g/L PMSF, 1.6 mg/L aprotinin [Sigma-Aldrich], and 5 mg/L leupeptin [Sigma-Aldrich] added right before use) was added to each tube, and the pellets were suspended by mixing for 30 seconds. The suspension was then moved to a 1.5-mL microcentrifuge tube, and the tubes were left on ice for 20 minutes with slow shaking. The tubes were then spun at maximum speed in a Hettich-Zentrifugen Mikro 20 microcentrifuge at 4°C for 15 minutes. The supernatant was quantified using the BCA protein assay kit (see section 2.2.5), and stored at -80°C prior to use.

### **2.2.14.3 SDS-PAGE**

SDS-PAGE was conducted as in section 2.2.6. The controls used were: BSA as a negative control to the phage antibodies, and the PGP synthase protein purified by the urea protein purification protocol (section 2.2.4.2) as a positive control to the phage antibodies. As well, peptide competition was used to determine which protein bands were due to non-specific antibody binding.

### **2.2.14.4 Protein Transfer to Polyvinylidene Fluoride (PVDF) Membranes**

To prepare for transfer, one rectangle of PVDF membrane (Millipore) was cut to match the size of one SDS-PAGE gel. The membrane was labelled in pencil, soaked in methanol for 15 seconds, and washed in ddH<sub>2</sub>O for 2 minutes. For each membrane, two pieces of filter paper (VWR) were cut be just a bit larger in size than the membrane. The membrane, two filter papers, and four sponges were soaked in 4°C transfer buffer (3.025 g/L tris base, 14.4 g/L glycine, 200 mL methanol per L) for 15 minutes. The gels

were then removed from the Bio-Rad Mini-PROTEAN Tetra Cell apparatus, and the transfer sandwich (Bio-Rad) was assembled in transfer buffer in the following order: black side, two sponges, one filter paper, gel, PVDF membrane, one filter paper, two sponges, and clear side. The labelled membrane side was oriented so that it faced the gel. Air bubbles were removed by rolling with a glass pipette, and the transfer sandwich was closed. The sandwich was placed in the Bio-Rad Mini Trans-Blot Cell apparatus with the black side of the sandwich facing the black side of the cell, and the clear side of the sandwich facing the red side of the cell. A magnet and an ice pack were then placed in the transfer apparatus. The apparatus was filled with transfer buffer and placed in a glass dish to prevent spillage. The apparatus was moved to a 4°C cold room, placed on a magnetic spinner, and connected to a power supply. Transfer occurred for 1 hour at 100 V, followed by 40 V overnight.

#### **2.2.14.5 Primary and Secondary Antibody Incubations**

The transferred PVDF membranes were washed in tris-buffered saline (TBS: 3 g/L tris base, 8 g/L NaCl, 0.2 g/L KCl, pH 7.4) for 5 minutes. The membranes were checked for protein transfer by shaking them with Ponceau S stain (2 g/L Ponceau S [Sigma-Aldrich], 30 g/L trichloroacetic acid [Sigma-Aldrich], 30 g/L sulfosalicylic acid [Sigma-Aldrich]) for 30 seconds, and then rinsing them with ddH<sub>2</sub>O until the red stain dissipated. The membranes were washed in methanol for 20 minutes with shaking. An equal volume of ddH<sub>2</sub>O was then added to the methanol, and the membranes were shaken for an additional 20 minutes. The membranes were blocked for 1 – 2 hours at room temperature with shaking in blocking buffer (50 g/L skim milk in T-TBS [1 mL Tween-

20 (Sigma-Aldrich) per L TBS]). The membranes were then incubated with the primary antibody overnight at 4°C in heat-sealed pouches (Fisher) with rotation. After the overnight incubation, the membranes were rinsed twice in T-TBS, washed for 15 minutes in T-TBS with shaking, and washed twice for 5 minutes in T-TBS with shaking. The membranes were then incubated with the secondary antibody for 1 – 2 hours at room temperature with rotation in heat-sealed bags. After the incubation, the membranes were rinsed twice in T-TBS, washed for 15 minutes in T-TBS with shaking, and washed twice for 5 minutes in T-TBS with shaking.

When the 16J-G6 or 16J-H12 phage antibody clones were used as the primary antibody, they were diluted 1-in-3 in T-TBS. The phage antibodies were detected using horse radish peroxidase (HRP)-conjugated protein A (Pierce) or protein L (Pierce), diluted 1-in-3,000 in antibody buffer (10 g/L skim milk in T-TBS). When the GAPDH rabbit polyclonal immunoglobulin G (IgG) primary antibody (Santa Cruz Biotechnology, Inc.) was used, it was diluted 1-in-4,000 in antibody buffer. The secondary antibody used for the GAPDH primary antibody was the HRP-conjugated goat anti-rabbit IgG (Santa Cruz Biotechnology, Inc.), diluted 1-in-5,000 in antibody buffer.

#### **2.2.14.6 Enhanced Chemiluminescence (ECL) Plus Detection**

After the membranes were washed following incubation with the secondary antibody, the ECL Plus Detection kit (GE Healthcare) was used. The membranes were incubated in the ECL plus mixture (solution A [ECL Plus substrate from GE Healthcare] and solution B [Acridan solution from GE Healthcare] in a 40:1 ratio) for 5 minutes (GEHealthcare 2006). The membranes were then covered with plastic to prevent them from drying out. They were then imaged using the Molecular Dynamics STORM 860 scanner. The image was then processed using the ImageQuant 5.2 program. Following STORM image capture, the membranes were exposed to Amersham Hyperfilm ECL (GE Healthcare) in a dark room. The films were then developed in the AGFA CP 1000 automatic film processor. The films were scanned using an Epson Expression 1680 scanner, and processed in Adobe Photoshop 4.0.

#### **2.2.14.7 Stripping of Membranes**

Following ECL Plus detection, the membranes were stripped in 4.0 g/L NaOH for 3 minutes with shaking. The membranes were then washed in ddH<sub>2</sub>O for 15 minutes with shaking. The membranes were reprobed with different primary and secondary antibodies (see section 2.2.14.5).

## **CHAPTER 3 - RESULTS**

### **3.1 Overview**

The following section describes the results of the analyses used to determine how Dlc-2 and Rho signaling modulate the ceramide induction of PGP synthase. The CHO cell lines used in this project were Cl22, E91, RSC6, and RhoMT2. As stated previously, the E91 cell line contains the promoter trap retrovirus within the Dlc-2 gene. The Cl22 cell line, which expresses the ecotropic retrovirus receptor gene, served as the control cell line for E91. The RSC6 cell line was created using shRNAi that targets the Dlc-2 mRNA. The RhoMT2 cell line serves as the RSC6 control cell line, as the shRNAi sequence is mutated so that it does not target the Dlc-2 mRNA. These cell lines were used to determine if there is transcriptional control of the PGP synthase gene, post-transcriptional control of mRNA stability, and post-translational control of the PGP synthase protein by Dlc-2 and ceramide.

### 3.2 Transcriptional Control

To determine if PGP synthase is being regulated at the transcriptional level by ceramide and Rho, Real-Time RT-PCR was conducted. Three batches of the CI22, E91, RSC6, and RhoMT2 cell lines were treated with 10 mg/L ceramide (30  $\mu$ M) or the same volume of ethanol. The cells' RNA was then extracted and converted to cDNA. The cDNA was then used in Real-Time RT-PCR reactions. The  $2^{-\Delta\Delta C_t}$  method (Livak and Schmittgen 2001), with GAPDH as the reference gene, was used to calculate relative expression levels, as shown in Figure 10.

The CI22 cell line showed rather stable expression of the PGP synthase gene, with peaks in induction at 6 and 12 hours after ceramide treatment. The E91 and RSC6 cell lines also showed stable PGP synthase expression. The RhoMT2 cell line showed stable PGP synthase expression as well, but with a significantly different peak in induction at 6 hours after ceramide treatment. For the most part, however, PGP synthase expression is not being induced by ceramide treatment. The significantly different peak in induction after 6 hours of treatment in the RhoMT2 cell line may be due to off-target effects of the shRNA. Due to the large standard deviations present, I cannot state that there are differences between cell lines. Therefore, this Real-Time RT-PCR data suggests that PGP synthase is not regulated at the transcriptional level by ceramide and Rho.

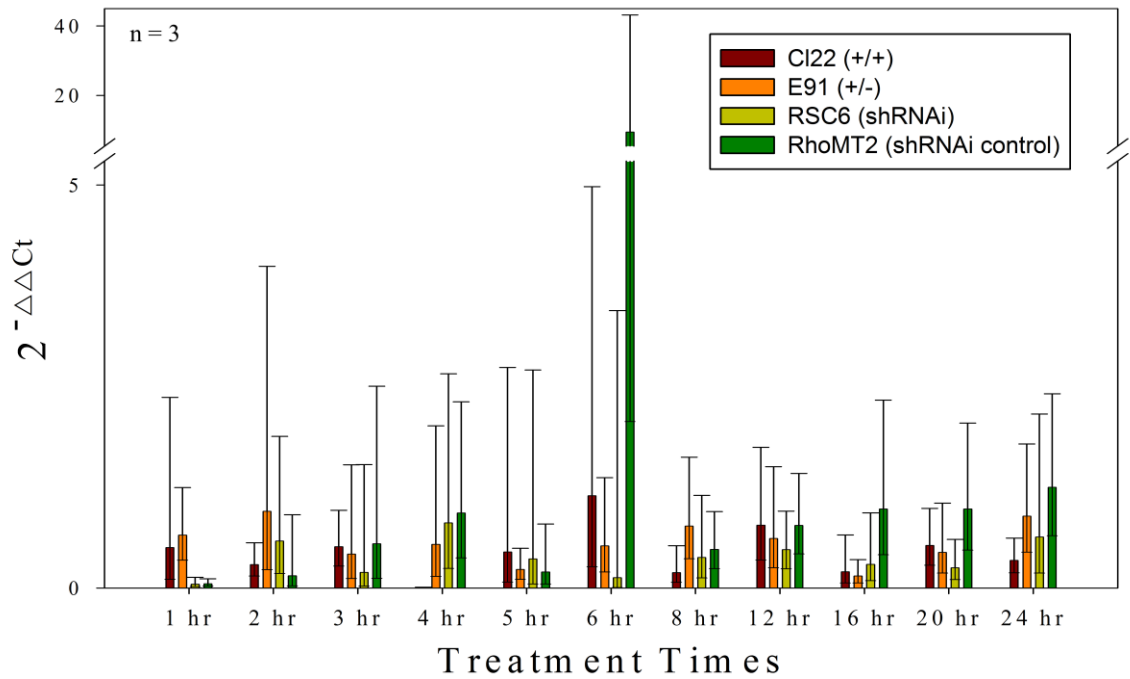


Figure 10: Real-Time RT-PCR

Cells were treated with 10 mg/L  $C_2$ -ceramide or the same volume of ethanol for 1, 2, 3, 4, 5, 6, 8, 12, 16, 20, and 24 hours. Relative gene expression was determined using the  $2^{-\Delta\Delta Ct}$  method (Livak and Schmittgen 2001) with GAPDH as the reference gene. The results are the mean of three independent cell treatments. The bars represent the standard deviation. ANOVA significance at the 0.05 level is denoted by the star (\*).

To ensure the Real-Time RT-PCR reactions took place properly, agarose gels were used to confirm the presence of only one PCR product per reaction well. Representative gel images can be seen in Figures 11 – 14. The CI22 representative image from the third batch of 20-hour C<sub>2</sub>-ceramide and ethanol-treated cells is shown in Figure 11. There is one PCR product at 100 bp present in all wells. The E91 representative image from the same cell treatment is shown in Figure 12, and shows only one PCR product at 100 bp. The RSC6 representative image from the same cell treatment is shown in Figure 13, and also shows only one PCR product at 100 bp. Finally, the RhoMT2 representative image from the same cell treatment is shown in Figure 14, and shows only one PCR product at 100 bp.

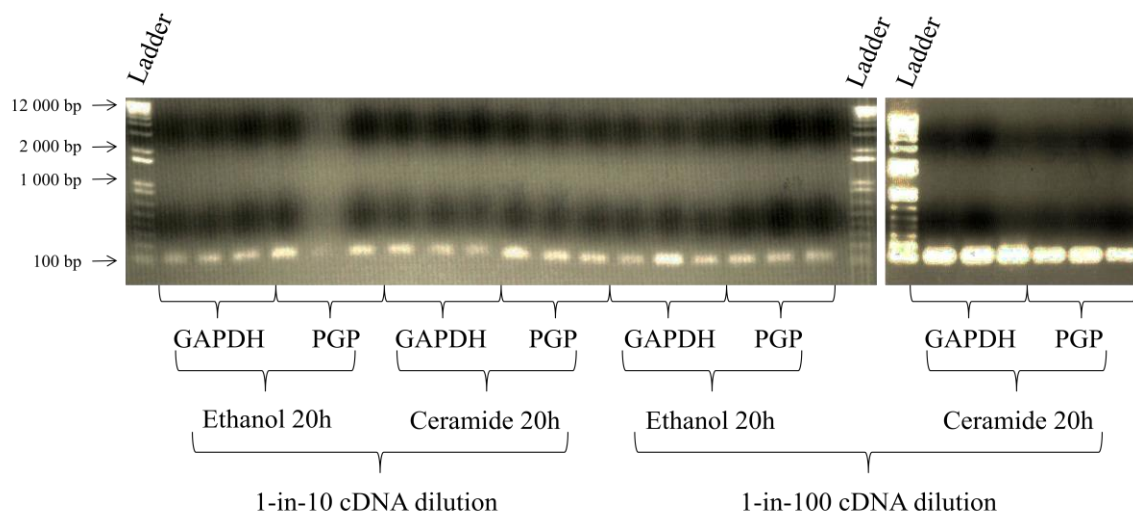


Figure 11: CI22 Agarose Gel

The Real-Time RT-PCR products from the third round of 20-hour C<sub>2</sub>-ceramide and ethanol cell treatments were run on 1% agarose gels, as described in section 2.2.7.

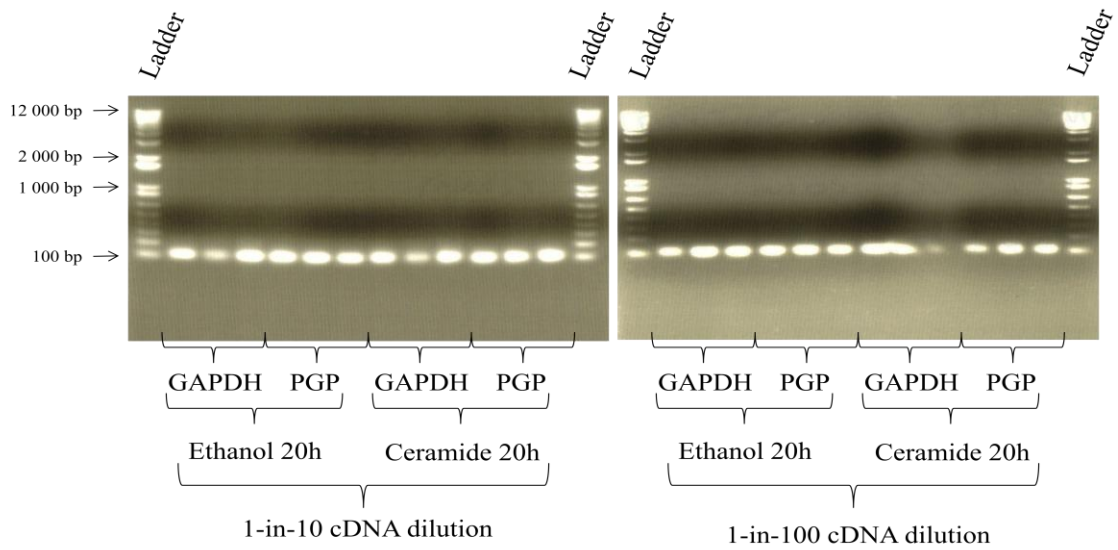


Figure 12: E91 Agarose Gel

The Real-Time RT-PCR products from the third round of 20-hour  $C_2$ -ceramide and ethanol cell treatments were run on 1% agarose gels, as described in section 2.2.7.

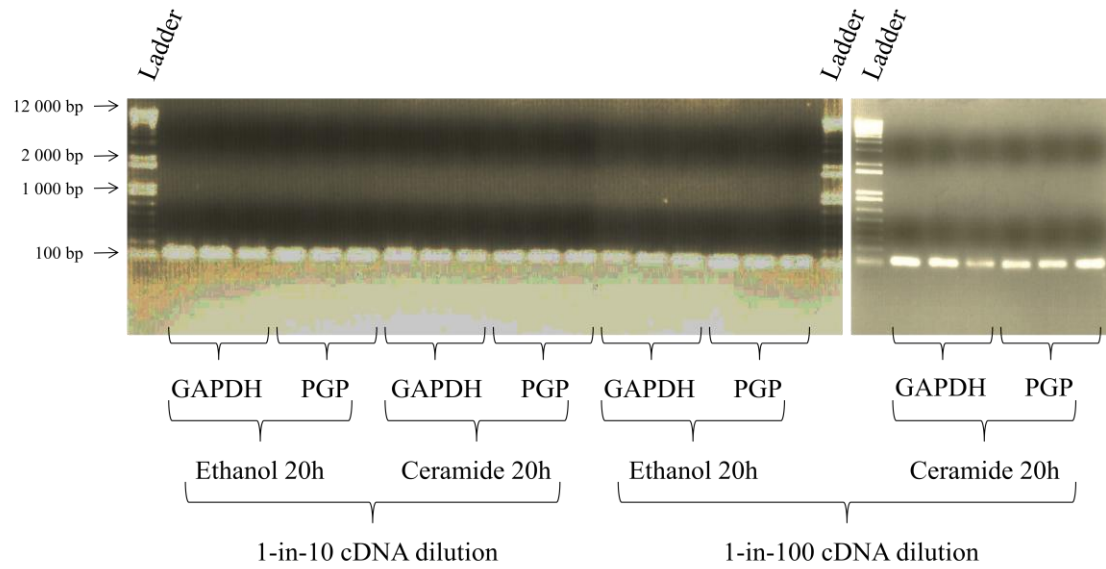


Figure 13: RSC6 Agarose Gel

The Real-Time RT-PCR products from the third round of 20-hour C<sub>2</sub>-ceramide and ethanol cell treatments were run on 1% agarose gels, as described in section 2.2.7.

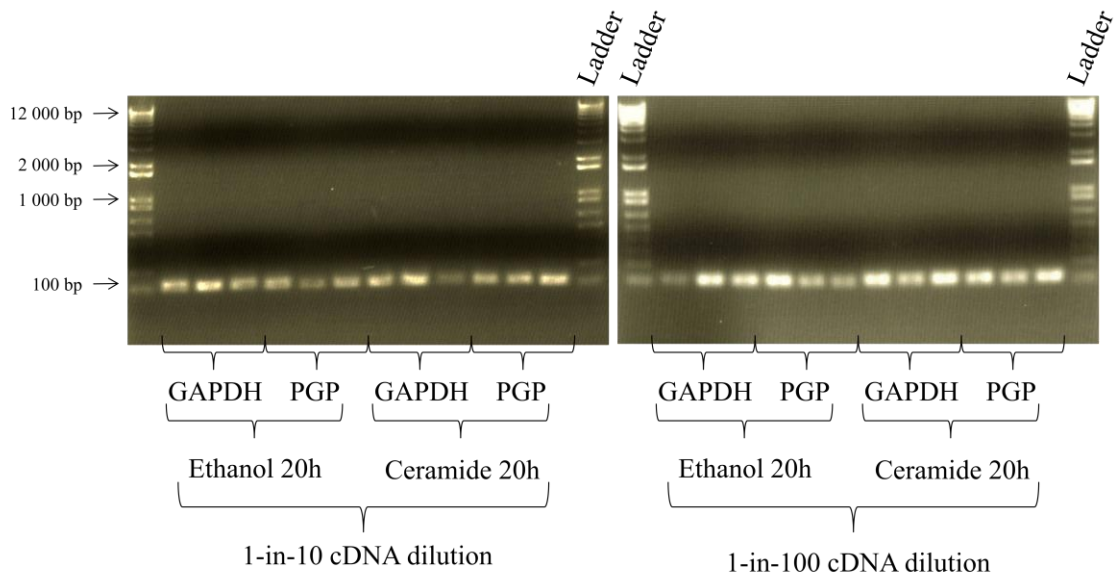


Figure 14: RhoMT2 Agarose Gel

The Real-Time RT-PCR products from the third round of 20-hour C<sub>2</sub>-ceramide and ethanol cell treatments were run on 1% TAE agarose gels, as described in section 2.2.7.

### 3.3 Post-Transcriptional Control

To determine if PGP synthase is being regulated post-transcriptionally by ceramide and Rho, Real-Time RT-PCR was conducted. Three batches of the CI22, E91, RSC6, and RhoMT2 cell lines were treated with 10 mg/L ceramide, the same volume of ethanol, or not treated for 4 hours. The cells were then treated with 10 mg/L AD for 0, 1, 2, 3, 4, 5, and 6 hours. The cells' RNA was then extracted and converted to cDNA. The cDNA was then used in Real-Time RT-PCR reactions. The Ct values are shown in Figures 15 –18.

The CI22 cell line shows rather straight lines for the GAPDH and PGP synthase Ct curves, as displayed in Figure 15. There is slight variation in the Ct values, but they start and end at roughly the same values of 23 and 31 for GAPDH and PGP synthase, respectively. Therefore, PGP synthase mRNA stability is not being affected by ceramide in CI22 cells. The E91 cell line also shows straight lines (as displayed in Figure 16), starting and ending at Ct values of about 25 and 32 for GAPDH and PGP synthase, respectively. Therefore, PGP synthase mRNA stability is not being affected in E91 cells. However, for the GAPDH ceramide-treated curve, the 0-hour time point is significantly different than the remaining 1 – 6 hour time points. This may have been due to the fact that there was less mRNA present. This difference is probably not due to the ceramide treatment itself, as the other three cell lines do not behave in a similar manner. The RSC6 cell line, as displayed in Figure 17, begins to show an increase in Ct values for GAPDH after 4 hours of AD treatment. This suggests there is less mRNA present in the

Real-Time RT-PCR reactions. The 5 and 6 hour Ct values are significantly different than the 2 – 4 hour Ct values for the ceramide, ethanol, and no treatment curves. This suggests that GAPDH mRNA stability is decreasing in the RSC6 cells. However, the PGP synthase mRNA stability is unchanged, with a Ct value varying slightly around 33. Therefore, PGP synthase mRNA stability is not being affected in RSC6 cells. The RhoMT2 cell line, as displayed in Figure 18, begins to show an increase in Ct values for GAPDH and PGP synthase after 4 hours of AD treatment. The 5 and 6 hour Ct values are significantly different than the 2 – 4 hour Ct values for GAPDH for the ceramide, ethanol, and no treatment curves. For PGP synthase, the 5 and 6 hour Ct values are significantly different than the 2 – 4 hour Ct values for the ethanol or no treatment curves, and the 3 – 4 hour Ct values for the ceramide curve. This suggests that mRNA stability is decreasing in the RhoMT2 cells. Due to the fact that no other cell line shows significant mRNA stability differences in the PGP synthase curves, this change in the RhoMT2 curve is probably due to off-target effects of shRNA.

In all four cell lines, the set of ceramide, ethanol, and no treatment Ct curves for GAPDH or PGP synthase were not significantly different from each other. Therefore, ceramide and ethanol are not affecting mRNA stability. The RSC6 and RhoMT2 GAPDH curves show a decrease in mRNA stability. Therefore, it seems that the use of shRNAi is affecting mRNA stability. This may be due to off-target effects, as the shRNA was not meant to target GAPDH mRNA, but the GAPDH mRNA stability is being affected. Finally, due to the lack of mRNA stability change in the C122, E91, and RSC6 cell lines for PGP synthase, it seems that PGP synthase is not being regulated post-transcriptionally by ceramide and Rho.

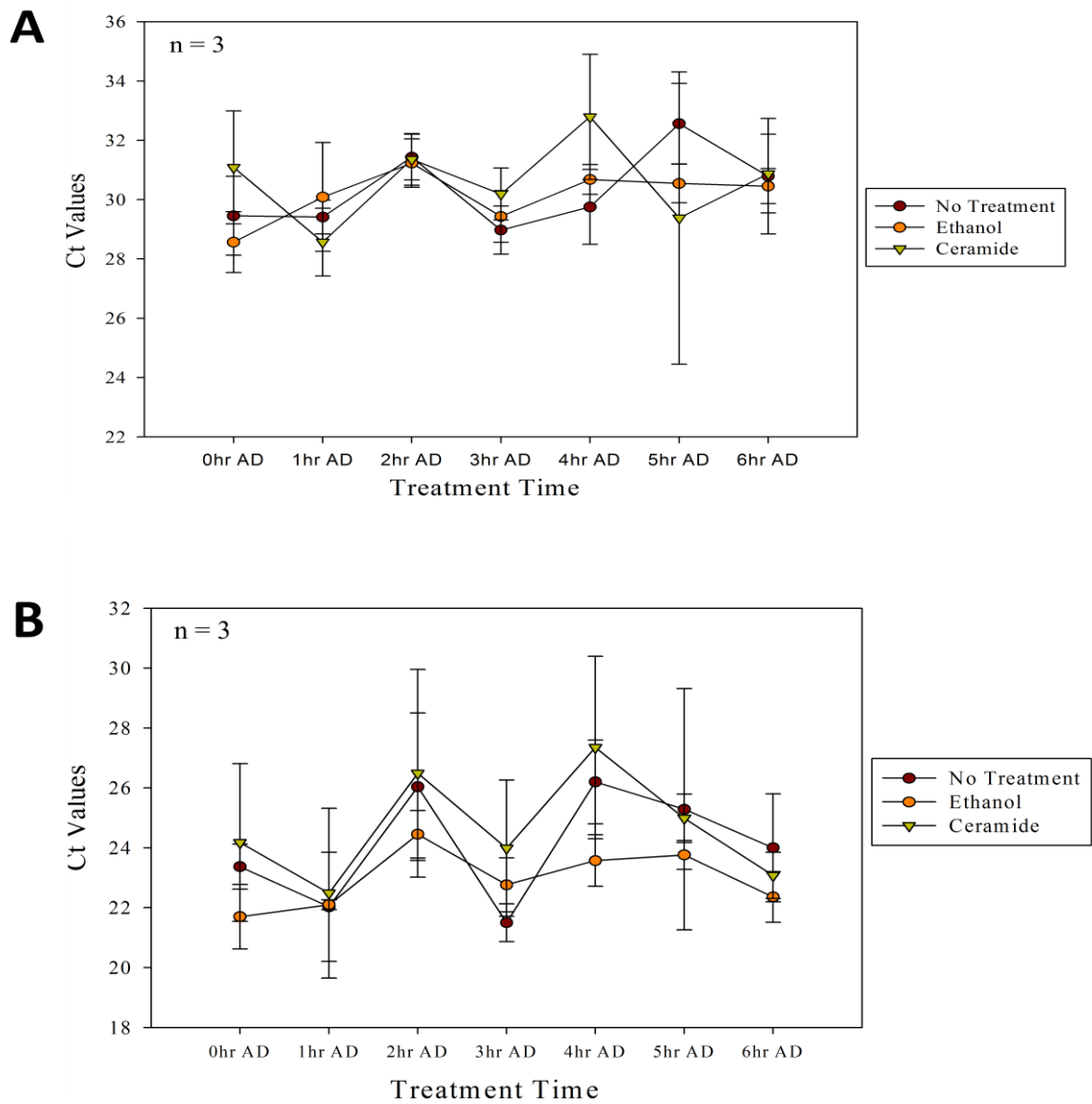


Figure 15: CI22 Real-Time RT-PCR

Cells were treated with 10 mg/L C<sub>2</sub>-ceramide, the same volume of ethanol, or nothing for 4 hours. They were then treated with 10 mg/L AD for 0, 1, 2, 3, 4, 5, and 6 hours. The mean Ct values of PGP synthase (part **A**) and GAPDH (part **B**) are presented with bars representing standard deviation of three independent cell treatments.

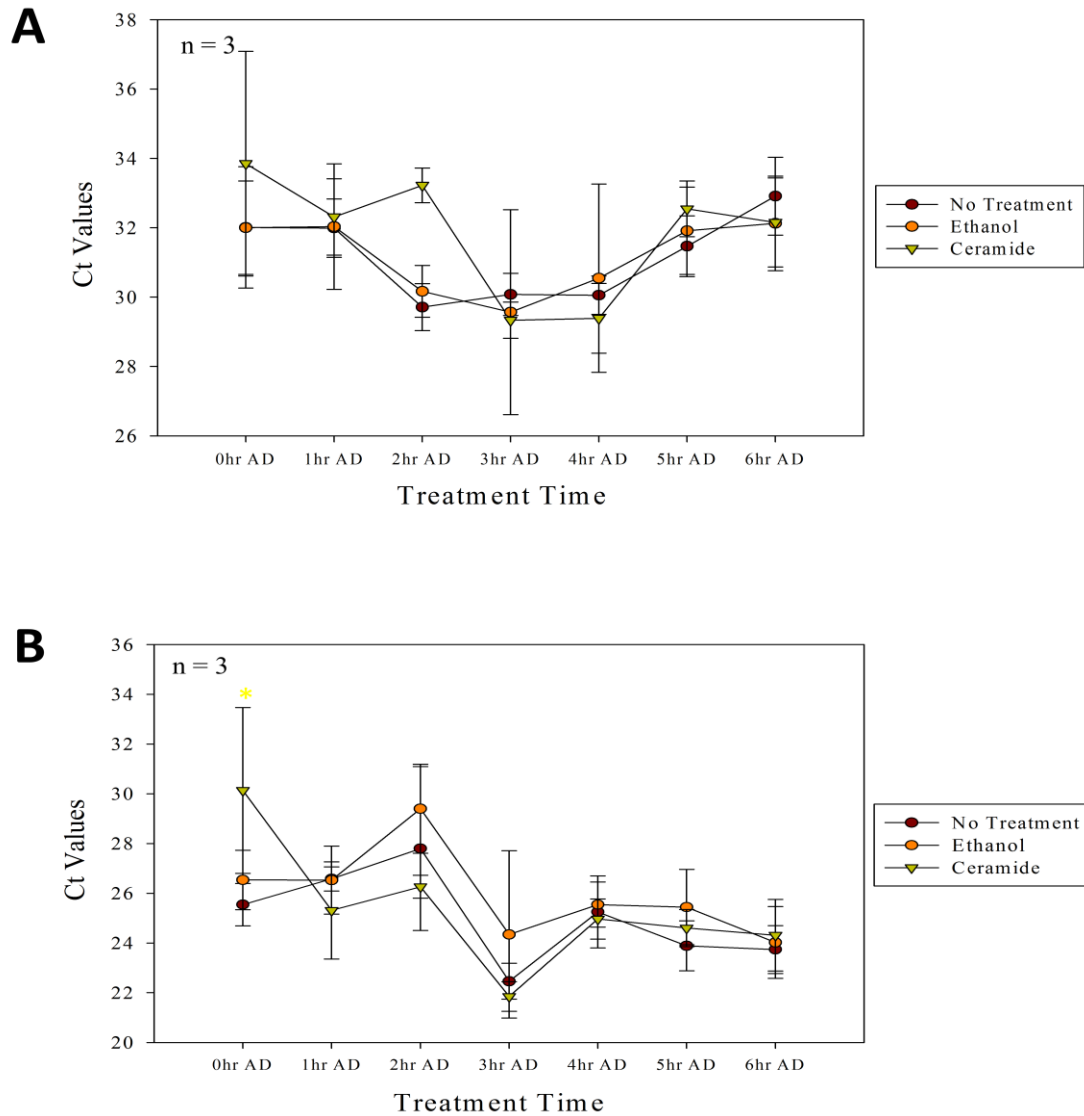


Figure 16: E91 Real-Time RT-PCR

Cells were treated with 10 mg/L C<sub>2</sub>-ceramide, the same volume of ethanol, or nothing for 4 hours. They were then treated with 10 mg/L AD for 0, 1, 2, 3, 4, 5, and 6 hours. The mean Ct values of PGP synthase (part **A**) and GAPDH (part **B**) are presented with bars representing standard deviation of three independent cell treatments. ANOVA significance at the 0.001 level is denoted by the star (\*) corresponding to the treatment color, as shown in the figure legend.

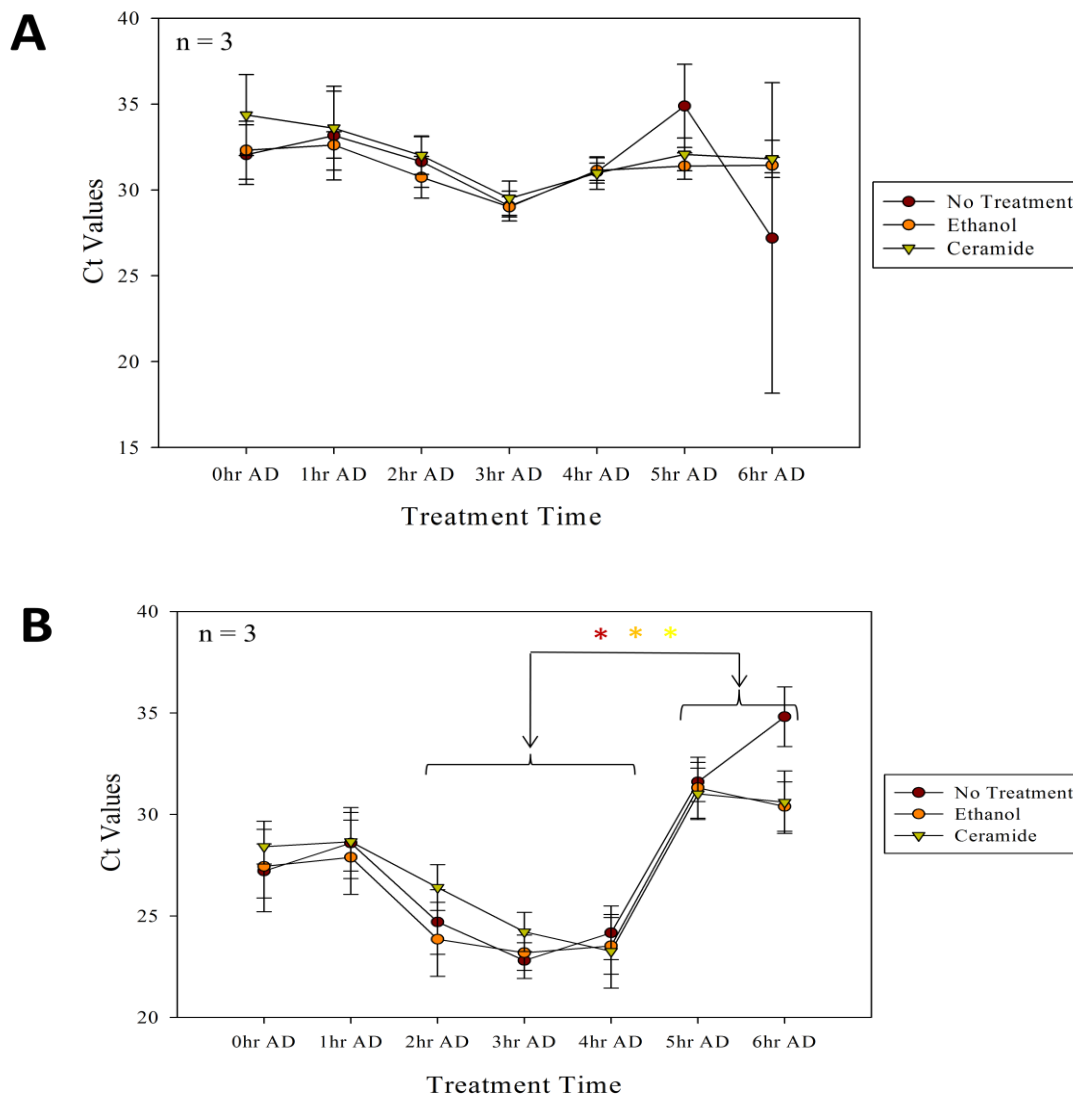


Figure 17: RSC6 Real-Time RT-PCR

Cells were treated with 10 mg/L C<sub>2</sub>-ceramide, the same volume of ethanol, or nothing for 4 hours. They were then treated with 10 mg/L AD for 0, 1, 2, 3, 4, 5, and 6 hours. The mean Ct values of PGP synthase (part **A**) and GAPDH (part **B**) are presented with bars representing standard deviation of three independent cell treatments. ANOVA significance at the 0.001 level is denoted by the star (\*) corresponding to the treatment color, as shown in the figure legend.

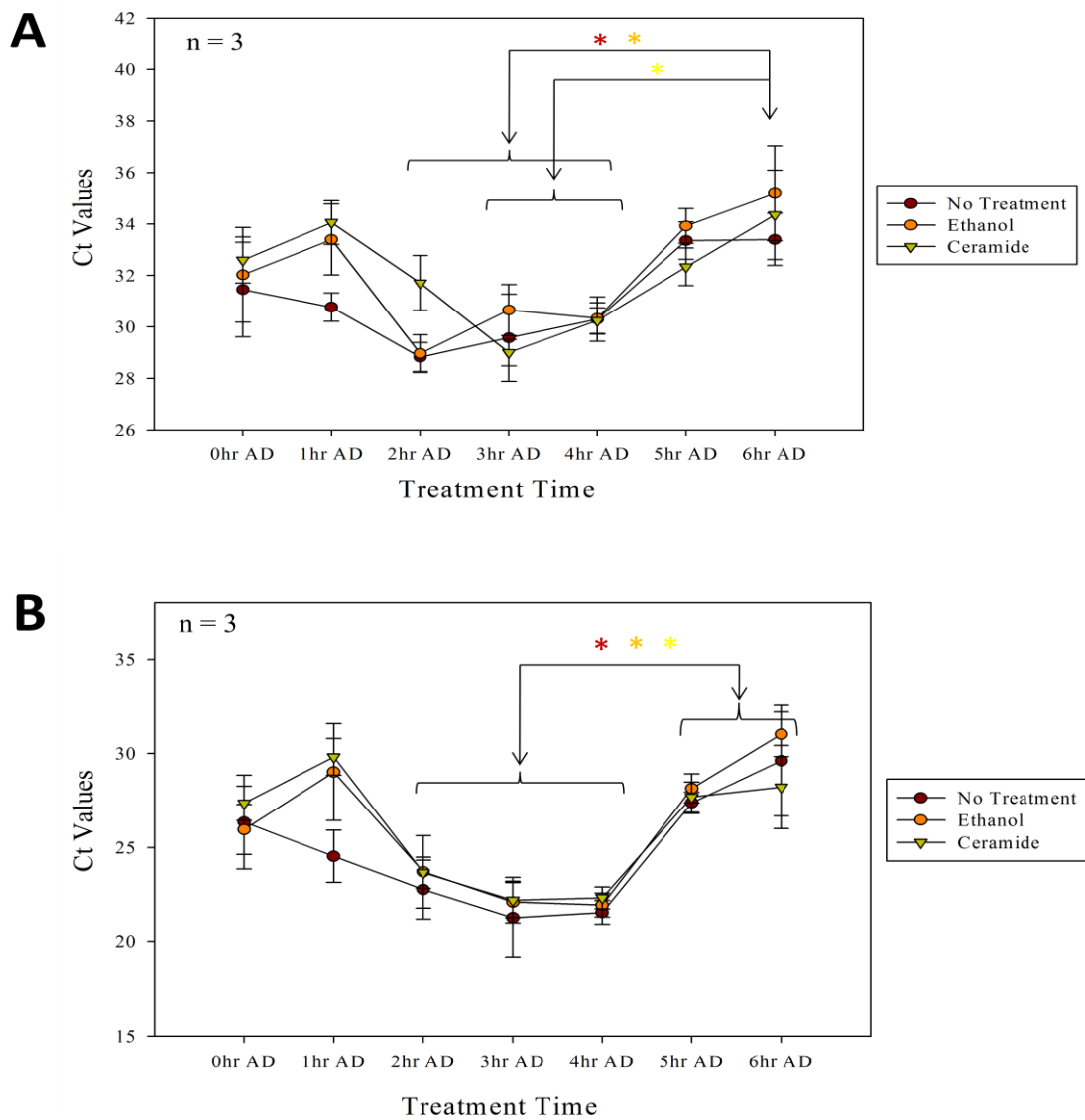


Figure 18: RhoMT2 Real-Time RT-PCR

Cells were treated with 10 mg/L  $C_2$ -ceramide, the same volume of ethanol, or nothing for 4 hours. They were then treated with 10 mg/L AD for 0, 1, 2, 3, 4, 5, and 6 hours. The mean Ct values of PGP synthase (part **A**) and GAPDH (part **B**) are presented with bars representing standard deviation of three independent cell treatments. ANOVA significance at the 0.001 level is denoted by the star (\*) corresponding to the treatment color, as shown in the figure legend.

### 3.4 Post-Translational Control

The following section shows the results of the experiments used to determine if PGP synthase protein levels were being affected by ceramide and Rho. The PGP synthase protein was purified for use as an antigen in phage display to develop an antibody against it, as there are currently no high-quality antibodies available against hamster PGP synthase. Initially, PGP synthase protein was induced in pTF16 *E. coli* with the pET-1not1 plasmid. A mini-preparation was used to confirm the correct plasmid was present in the *E. coli*. The DNA isolated from bacterial colonies was digested with *Sall* and *NotI* restriction enzymes, and the reaction products were run on an agarose gel, as shown in Figure 19. There are two restriction products at 5,500 and 2,300 bp. Colony 3 was arbitrarily chosen for use in subsequent experiments.

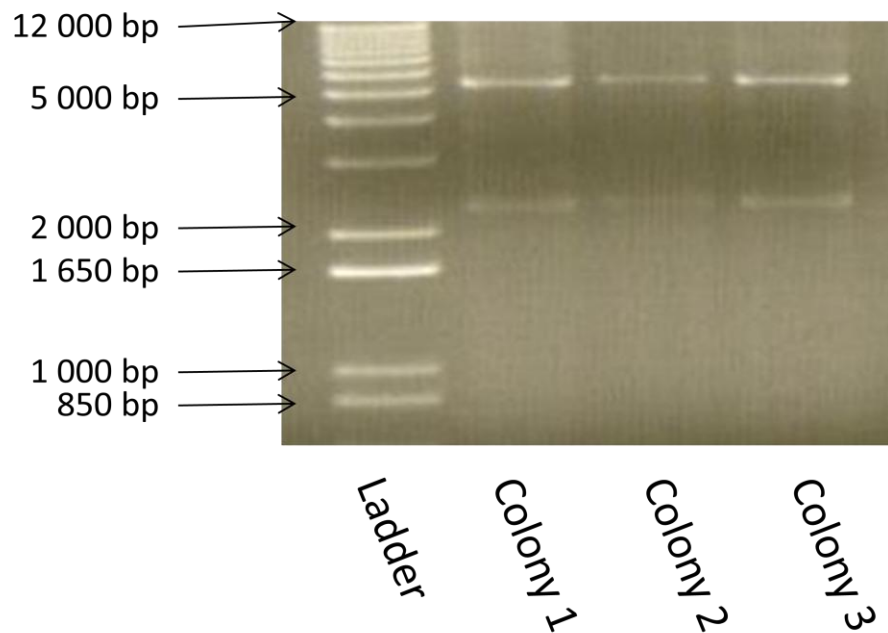


Figure 19: Mini-Preparation Agarose Gel

Agarose gel electrophoresis of DNA isolated from three colonies of pTF16 *E. coli* with the pET-1not1 (PGP synthase gene) plasmid using the mini-preparation protocol (section 2.2.2). The DNA was digested with *SalI* and *NotI* restriction enzymes. The products were then run on a 1% TAE agarose gel.

After confirmation by mini-preparation that the proper PGP synthase plasmid was in pTF16 *E. coli*, the protein was induced by L-(+)-arabinose and IPTG addition. A non-induced control was also grown in parallel to all batches of induced PGP synthase protein. The protein was purified using BugBuster or urea methods, and purified through Talon cobalt columns. The protein was concentrated in Amicon Ultra columns. The purification and column products were run on SDS-PAGE gels that were then stained with Coomassie blue and dried, as shown in Figures 20 – 26.

Figures 20 – 22 show the results of the BugBuster protein purification method with a 2-hour protein induction. Three samples of pTF16 *E. coli* were grown in parallel, with two samples being induced (samples A and B), and the third sample acting as the non-induced control. As shown in Figure 20, the induced sample A crude extract and flow-through lanes are full of many proteins that are not of interest. Washes 1 and 2 remove more proteins that do not specifically bind to the cobalt columns through histidine tags. The protein elution shows a protein at a mass of 45 kDa, as determined using a standard curve, being released from the column. The predicted molecular weight of CHO PGP synthase is 62.329 (Kawasaki, Kuge et al. 1999). Therefore, PGP synthase is not detected in the induced sample A. Figure 21, the induced sample B Figure, is very similar to Figure 20. The induced sample B crude extract and flow-through lanes are full of many proteins, and the washes remove more proteins. In this sample, there is a fainter band at 45 kDa when compared to the sample A gel. The non-induced sample is shown in Figure 22. The crude extract and flow-through in this case have fewer proteins when compared to the two induced protein samples. This may be due to the fact that

L-(+)-arabinose and IPTG were not added. As well, there are no visible proteins in the washes or elution. In summary, Figures 20 – 22 show that PGP synthase cannot be detected when using the BugBuster protein purification method. This does not mean that the protein is not present, but it may be at an amount too small to detect using Coomassie blue.

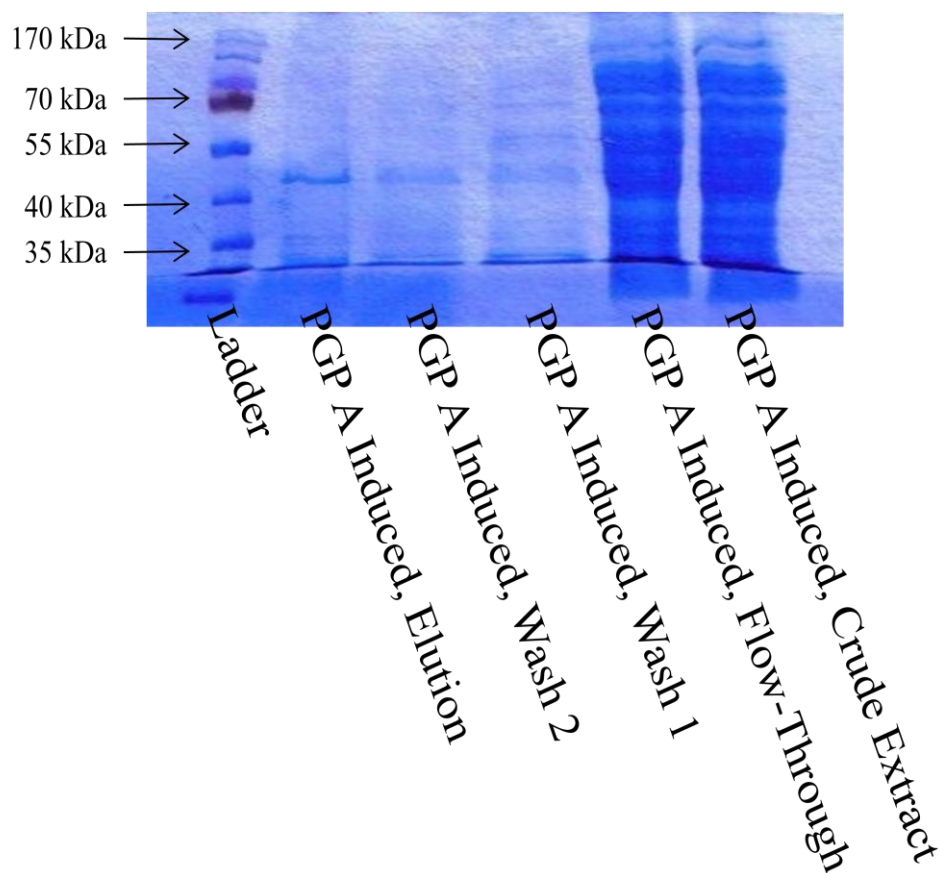


Figure 20: Induced Sample A Using the BugBuster Protein Purification Method  
PGP synthase protein was induced for 2 hours (section 2.2.3), and then purified using the BugBuster purification protocol and Talon columns (section 2.2.4.1). The column products were then run on a 12% SDS-PAGE gel (section 2.2.6). The gel was stained with Coomassie blue for 4 hours, and then destained overnight (section 2.2.7).

The gel was then dried (section 2.2.8).

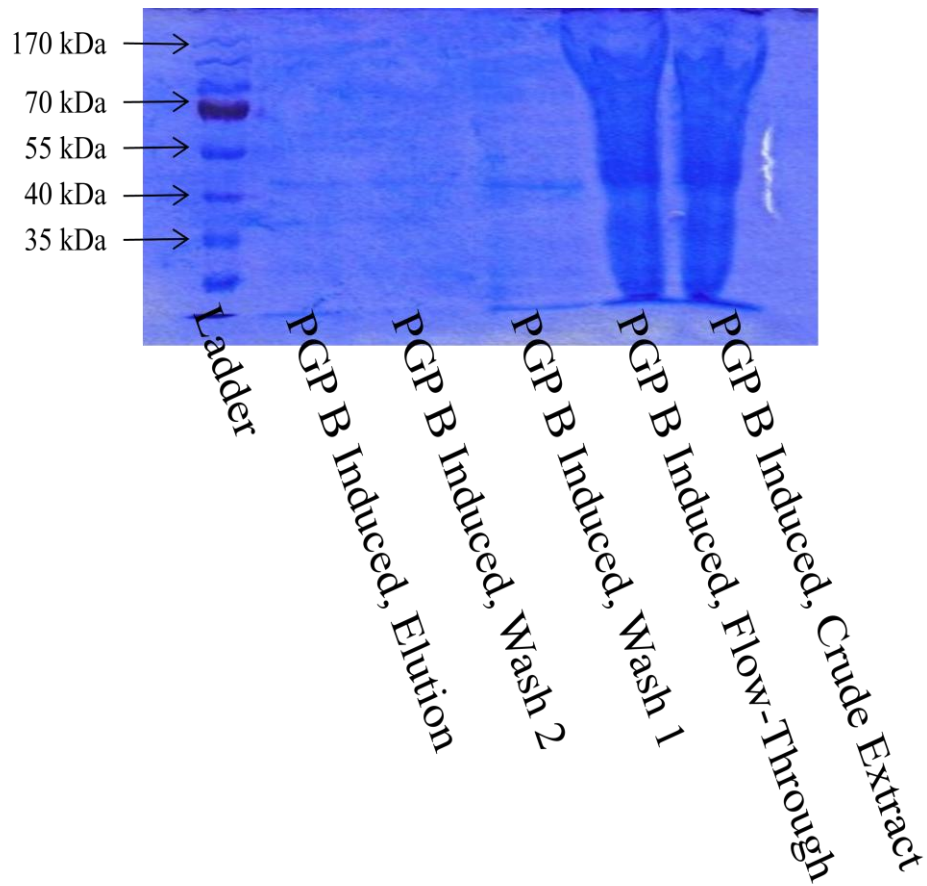


Figure 21: Induced Sample B Using the BugBuster Protein Purification Method  
PGP synthase protein was induced for 2 hours (section 2.2.3), and then purified using the BugBuster purification protocol and Talon columns (section 2.2.4.1). The column products were then run on a 12% SDS-PAGE gel (section 2.2.6). The gel was stained with Coomassie blue for 4 hours, and then destained overnight (section 2.2.7).  
The gel was then dried (section 2.2.8).

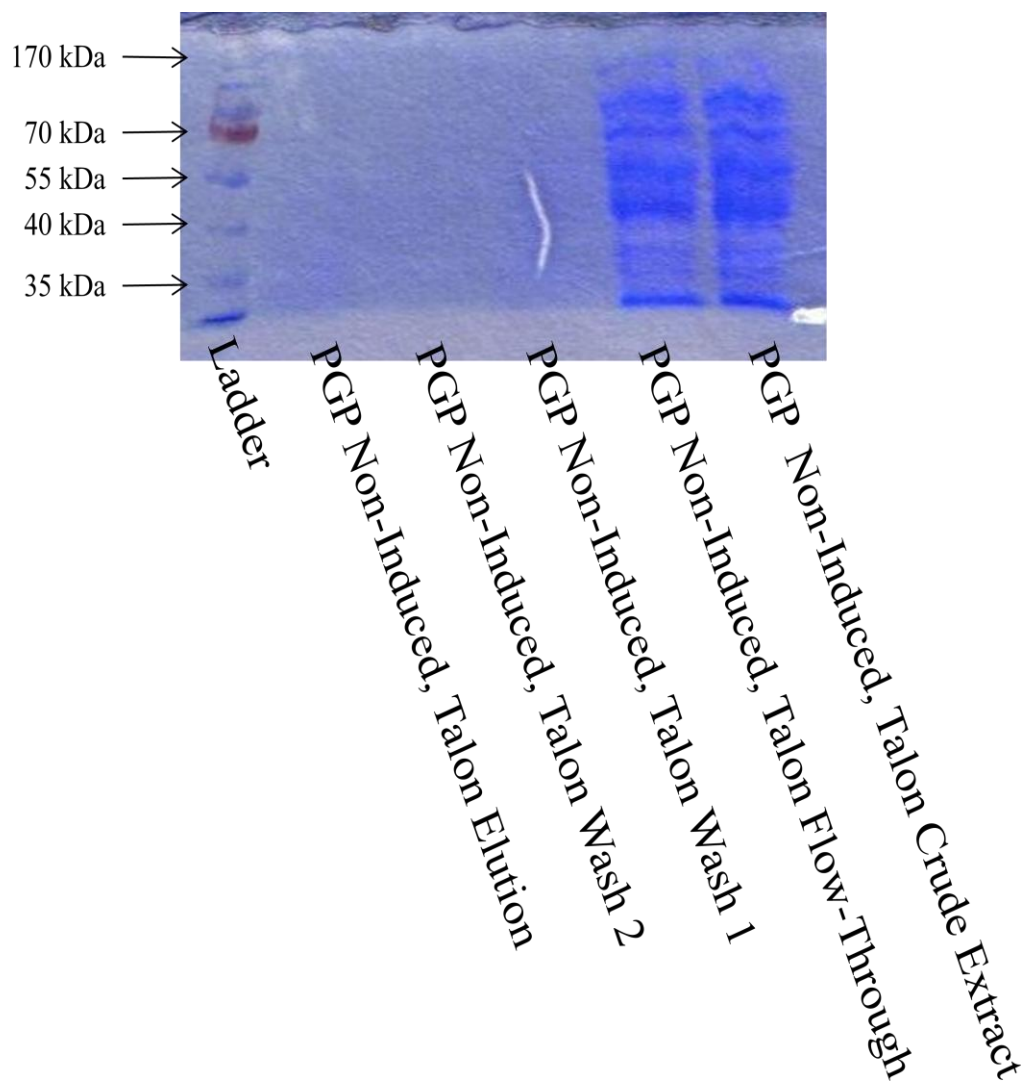


Figure 22: Non-Induced Sample Using the BugBuster Protein Purification Method  
 PGP synthase protein was grown non-induced, in parallel to the induced protein samples A and B (section 2.2.3). It was then purified using the BugBuster purification protocol and Talon columns (section 2.2.4.1). The column products were then run on a 12% SDS-PAGE gel (section 2.2.6). The gel was stained with Coomassie blue for 4 hours, and then destained overnight (section 2.2.7). The gel was then dried (section 2.2.8).

Figures 23 and 24 show the results of the BugBuster protein purification with inclusion body purification method, and a 2-hour protein induction. Two samples of pTF16 *E. coli* were grown in parallel, with one sample being induced and one sample acting as the non-induced control. As shown in Figure 23, the induced sample soluble fraction (protein crude extract) is full of many proteins that are not of interest. Washes 1, 3, and 5 show the removal of proteins, and there are more proteins present in the Talon column flow-through. However, there are no visible proteins in the column washes or elution. Figure 24, shows the non-induced protein sample. The soluble fraction once again shows many proteins that are not of interest, although there are fewer proteins present in the non-induced protein sample compared to the induced protein sample. There are proteins visible in washes 1 and 3. However, there is no protein visible in wash 5, the column flow-through, the column washes, or the column elution. Therefore, Figures 23 and 24 show that PGP synthase cannot be detected when using the BugBuster protein purification with inclusion body purification method. As in Figures 20 – 22 showing the BugBuster protein purification method, this does not mean that the protein is not present, but that it may be at an amount too small to detect using Coomassie blue.

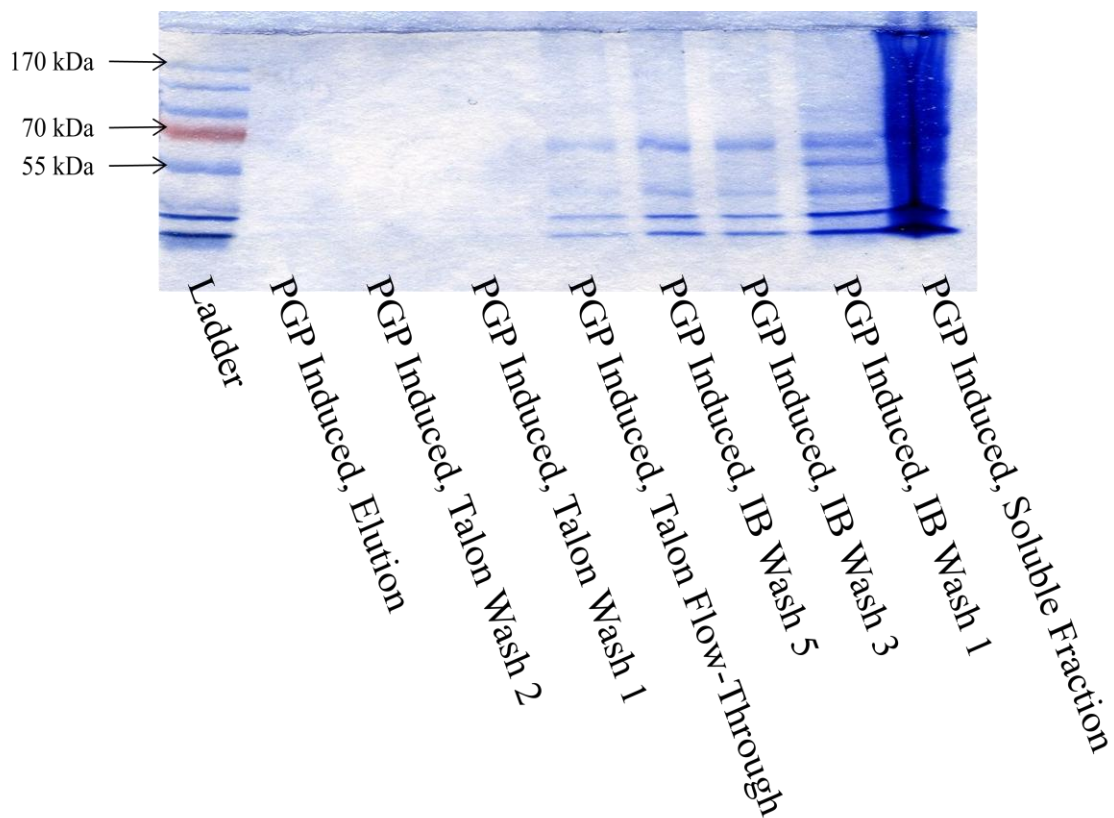


Figure 23: Induced Sample Using the BugBuster Protein Purification  
with Inclusion Body Purification Method

PGP synthase protein was induced for 2 hours (section 2.2.3), and then purified using the BugBuster purification protocol with inclusion body purification and Talon columns (section 2.2.4.1). The column products were then run on a 12% SDS-PAGE gel (section 2.2.6). The gel was stained with Coomassie blue for 4 hours, and then destained overnight (section 2.2.7). The gel was then dried (section 2.2.8).

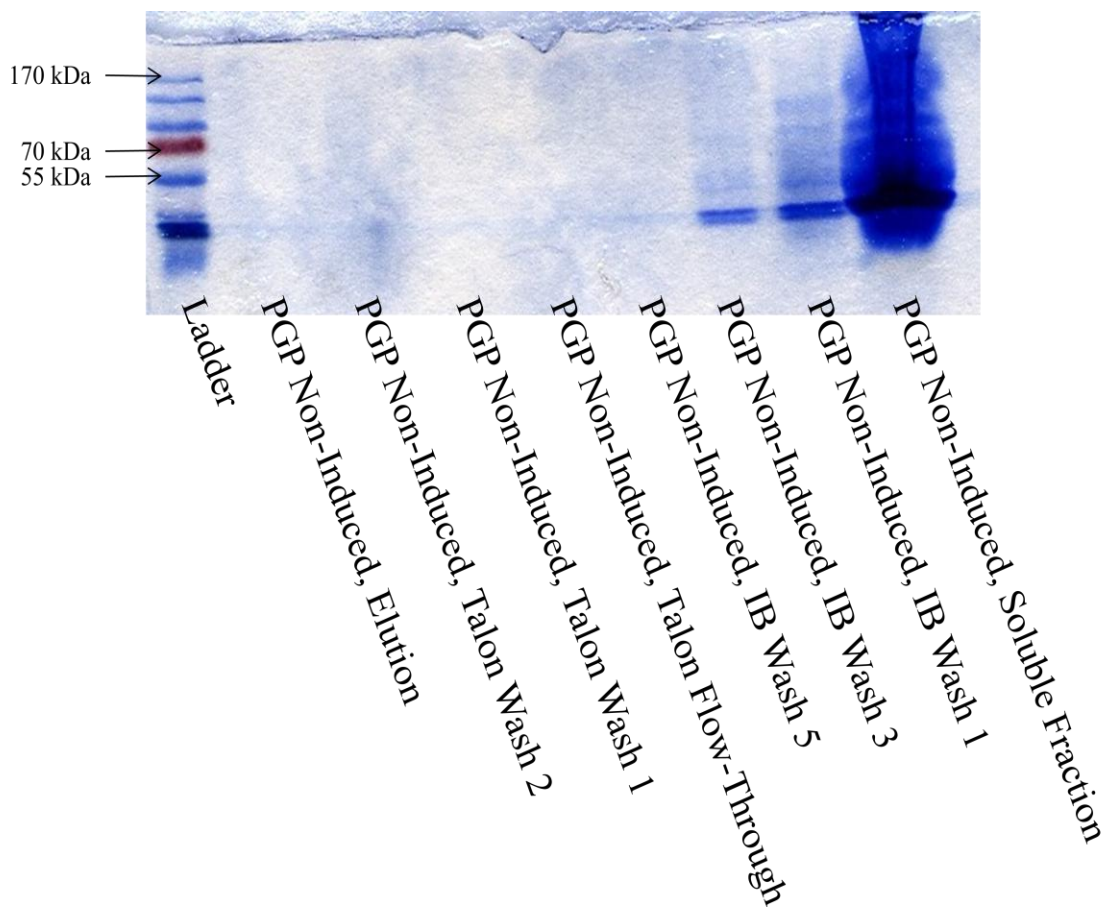


Figure 24: Non-Induced Sample Using the BugBuster Protein Purification with Inclusion Body Purification Method

PGP synthase protein was grown non-induced, in parallel to the induced protein sample (section 2.2.3). It was then purified using the BugBuster purification protocol with inclusion body purification and Talon columns (section 2.2.4.1). The column products were then run on a 12% SDS-PAGE gel (section 2.2.6). The gel was stained with Coomassie blue for 4 hours, and then destained overnight (section 2.2.7).

The gel was then dried (section 2.2.8).

Figures 25 and 26 show the results of the urea protein purification method, with a 2-hour protein induction. Two samples of pTF16 *E. coli* were grown in parallel, with one sample being induced and one sample acting as the non-induced control. As shown in Figure 25, the induced sample crude extract and column flow-through are full of many proteins that are not of interest. Wash 1, wash 2, and the column elution also show faint protein bands. The concentrated protein flow-through also shows a very faint protein band. The concentrated protein elution shows clear protein bands at 125, 96, 69, 65, 57, and 40 kDa, as determined using a standard curve. Figure 26, shows the non-induced protein sample. The crude extract and column flow-through again show many proteins that are not of interest. Once again, there are fewer proteins present in the non-induced protein sample compared to the induced protein sample. There are no proteins visible in wash 1, wash 2, the column elution, or the concentrated protein flow-through. There is a 40 kDa band in the concentrated elution. It is most likely that the circled 57 kDa band in the induced sample elution is the PGP synthase protein (Figure 25), as this band is not present in the non-induced sample (Figure 26). As well, this band is quite close to the predicted CHO PGP synthase weight of 62.329 (Kawasaki, Kuge et al. 1999). The 5 kDa discrepancy in molecular mass may be due to the manner in which the protein is translated in the *E. coli*, or by the way the protein runs in the SDS-PAGE gel. Therefore, Figures 25 and 26 show that PGP synthase can be detected when using the urea protein purification method and Amicon columns.

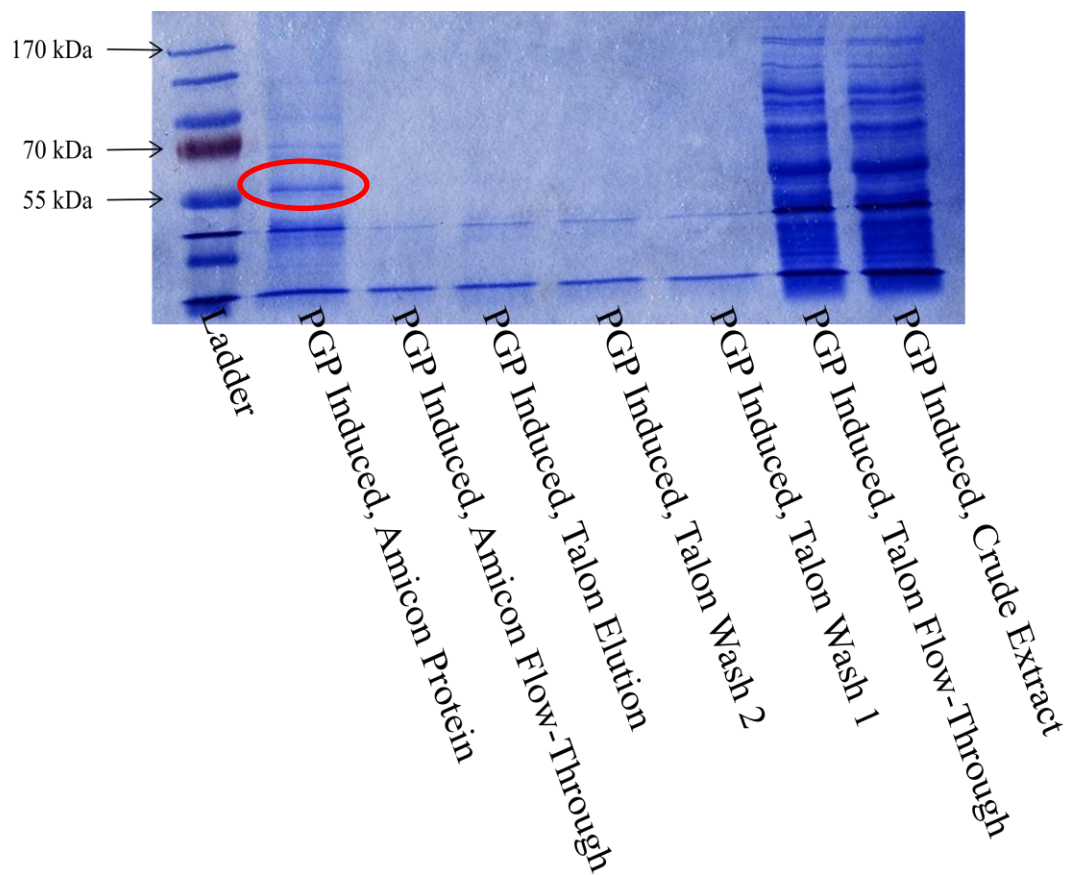


Figure 25: Induced Sample Using the Urea Protein Purification Method

PGP synthase protein was induced for 2 hours (section 2.2.3), and then purified using the urea purification protocol and Talon columns (section 2.2.4.2). The protein elution was then concentrated using Amicon columns. The products were then run on a 12% SDS-PAGE gel (section 2.2.6). The gel was stained with Coomassie blue for 4 hours, and then destained overnight (section 2.2.7). The gel was then dried (section 2.2.8).

The 57 kDa PGP synthase band is circled.

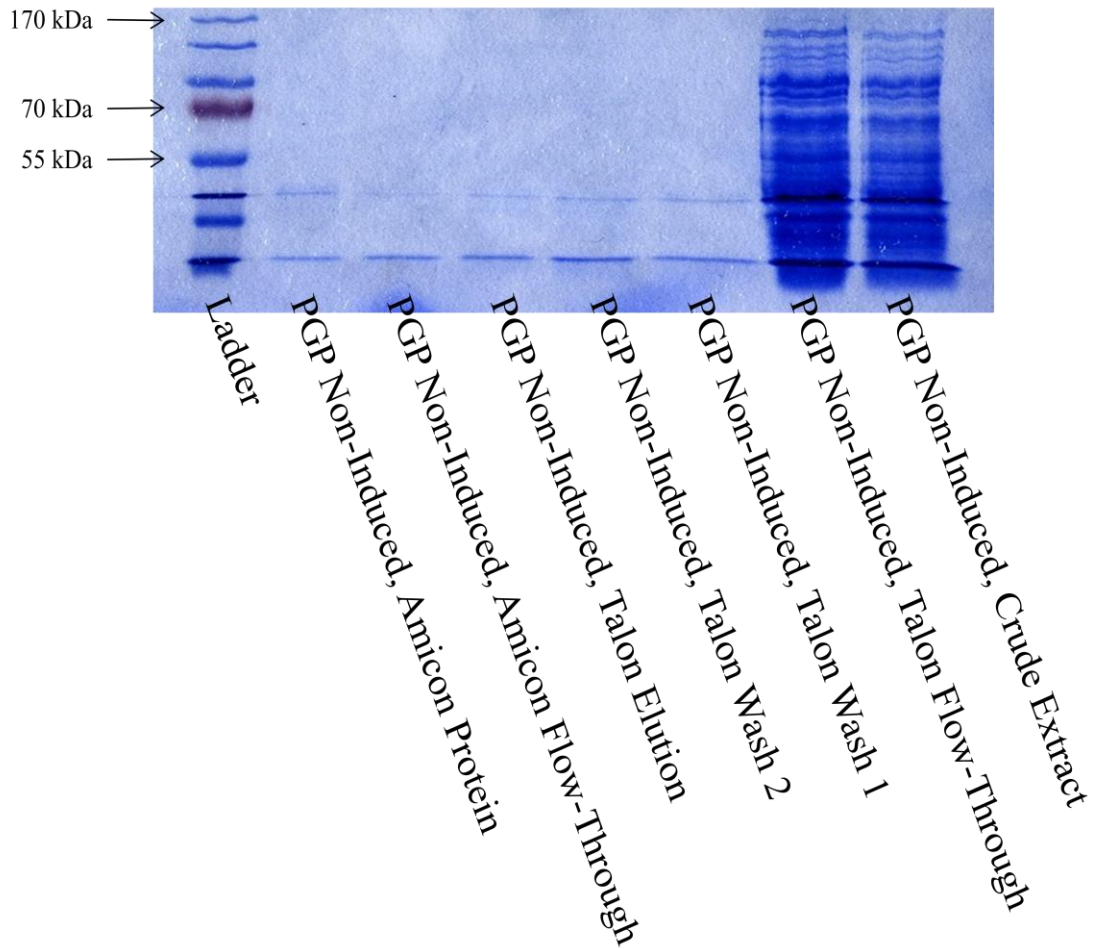


Figure 26: Non-Induced Sample Using the Urea Protein Purification Method

PGP synthase protein was grown non-induced, in parallel to the induced protein sample (section 2.2.3). It was then purified using the urea purification protocol and Talon columns (section 2.2.4.2). The protein elution was then concentrated using Amicon columns. The products were then run on a 12% SDS-PAGE gel (section 2.2.6). The gel was stained with Coomassie blue for 4 hours, and then destained overnight (section 2.2.7). The gel was then dried (section 2.2.8).

Following protein induction and purification using BugBuster and urea, it was determined that there was not sufficient PGP synthase protein to conduct phage display screening using the purified PGP synthase protein as the antigen. Therefore, peptides corresponding to the N- and C-terminals of the PGP synthase protein conjugated to BSA were used. Three rounds of phage display selection were conducted, with additional panning against BSA conjugated to itself to remove BSA cross-reacting phage antibodies. Phage ELISA was used to screen for positive phage antibody clones. The ELISA graphs can be seen in Figures 27 – 30. These graphs show the difference between absorbance at 450 nm and 650 nm for each well of a ninety-six-well plate. The graphs show the ELISA reactions for each pair of peptide-phage library reactions (16I, 16J, 25I, and 25J) with the corresponding BSA reactions underneath.

Figure 27 shows the 16-mer peptide, phage library I ELISA reactions. The following wells had positive ELISA reactions in the peptide plate: C1, D5, and H5. In the corresponding BSA plate, well E3 had a positive reaction. Therefore, the following clones had the potential to be phage antibody clones: 16I-C1, 16I-D5, and 16I-H5. These clones were potential phage antibodies because they had a positive ELISA reaction in the peptide well, but not in the corresponding BSA well. Figure 28 shows the 16-mer peptide, phage library J ELISA reactions. The following clones were considered for phage antibody production: 16J-E6, 16J-F3, 16J-F8, 16J-F12, 16J-G3, 16J-G4, 16J-G6, 16J-G12, and 16J-H7. Figure 29 shows the 25-mer peptide, phage library I ELISA reactions. There were no potential phage antibody clones, as the only well with a positive ELISA in the peptide plate, well F4, also had a positive ELISA reaction in the

corresponding BSA plate. Figure 30 shows the 25-mer peptide, phage library J ELISA reactions. Clones 25J-A4, 25J-D8, and 25J-H6 were considered for phage antibody production. The clones that proved to be the best phage antibodies were clones 16J-G6 and 16J-H12, and these clones were used in western blotting.

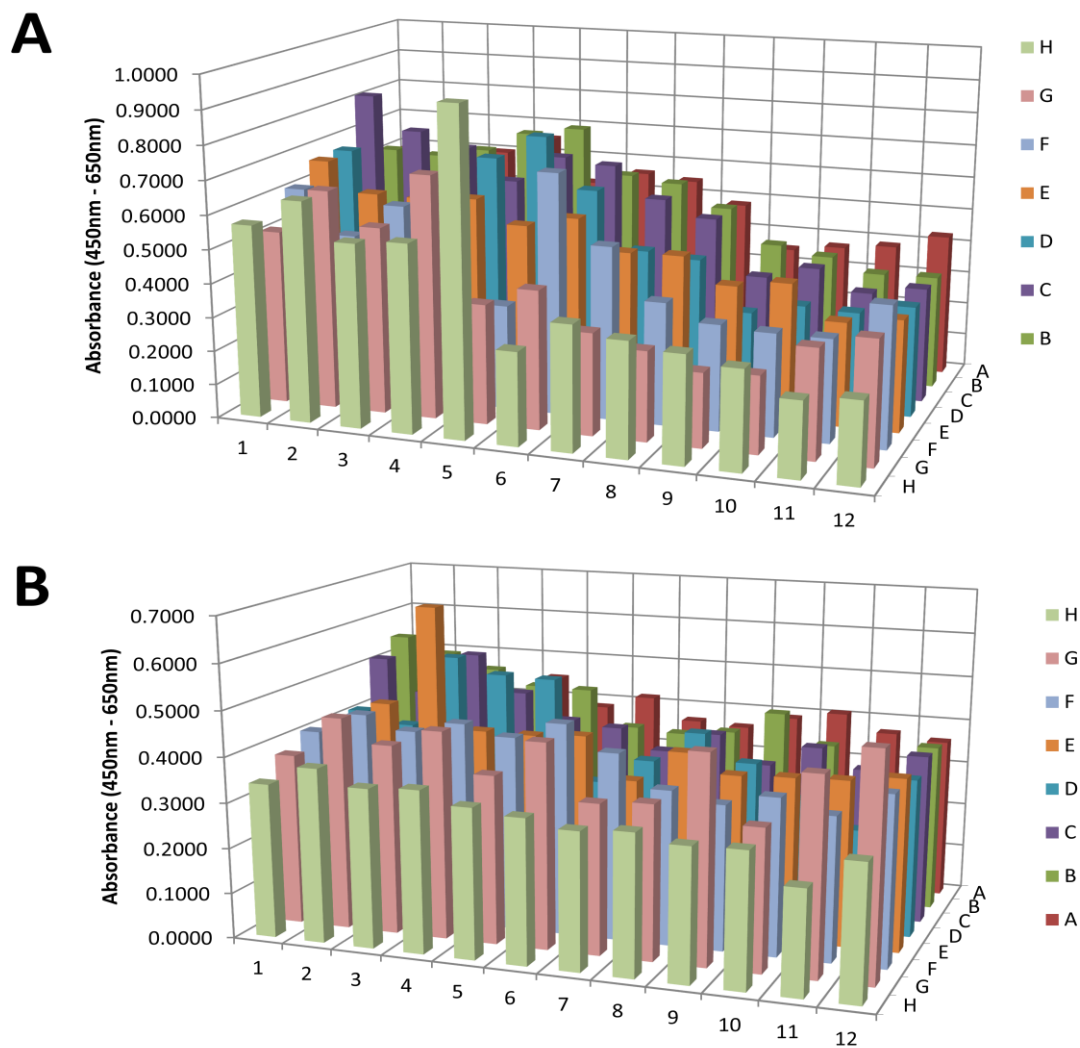


Figure 27: 16-mer Peptide, Tomlinson Phage Library I ELISA

The above graphs depict the positive ELISA reactions (section 2.2.12), when the difference between the absorbance at 450 nm and the absorbance at 650 nm (y-axis of graphs) was above the background value. The x-z axes represent the positions in the ninety-six-well plates in which the ELISA was conducted. Part **A** of the Figure represents the 16-mer peptide, library I ELISA, and part **B** is the corresponding BSA-BSA conjugated reactions.

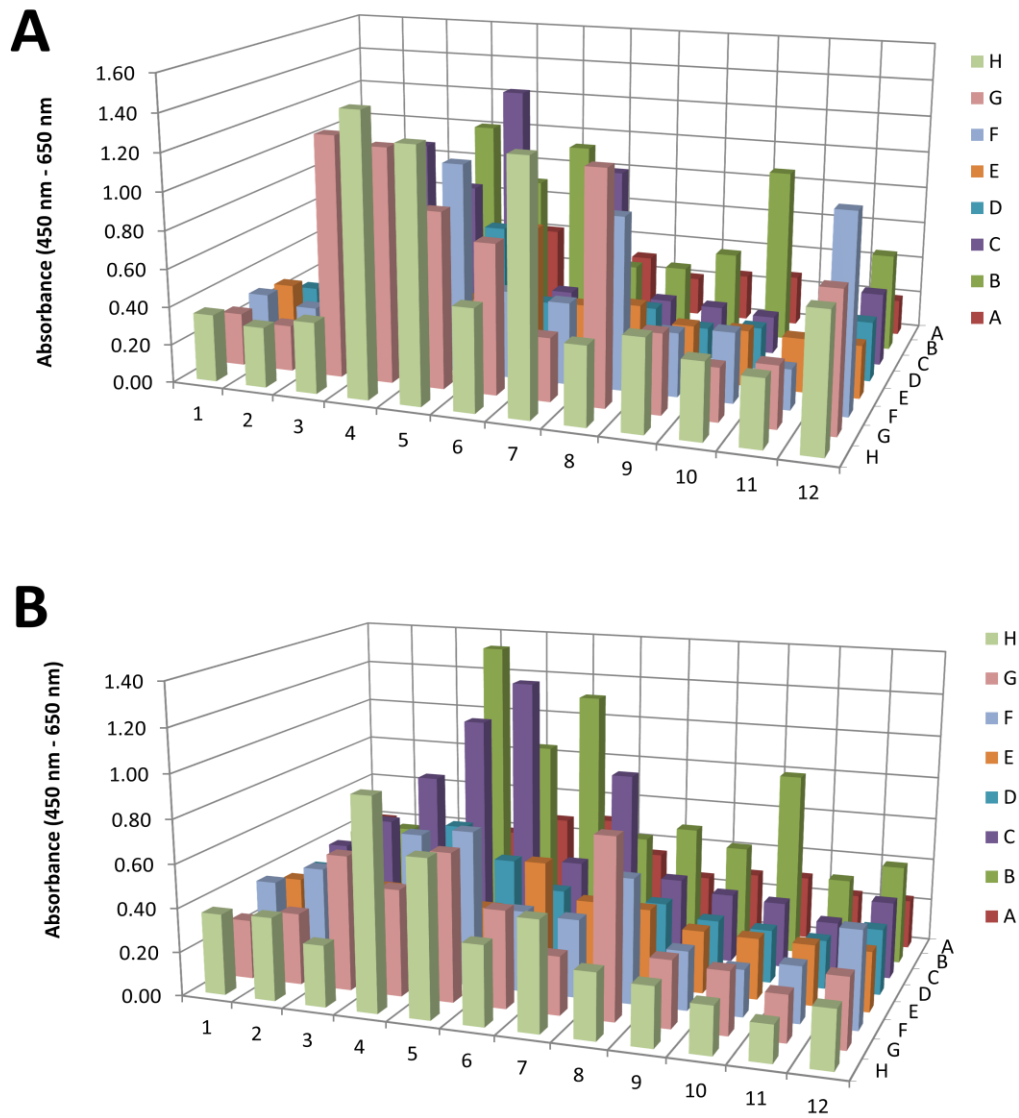


Figure 28: 16-mer Peptide, Tomlinson Phage Library J ELISA

The above graphs depict the positive ELISA reactions (section 2.2.12), when the difference between the absorbance at 450 nm and the absorbance at 650 nm (y-axis of graphs) was above the background value. The x-z axes represent the positions in the ninety-six-well plates in which the ELISA was conducted. Part **A** of the Figure represents the 16-mer peptide, library J ELISA, and part **B** is the corresponding BSA-BSA conjugated reactions.

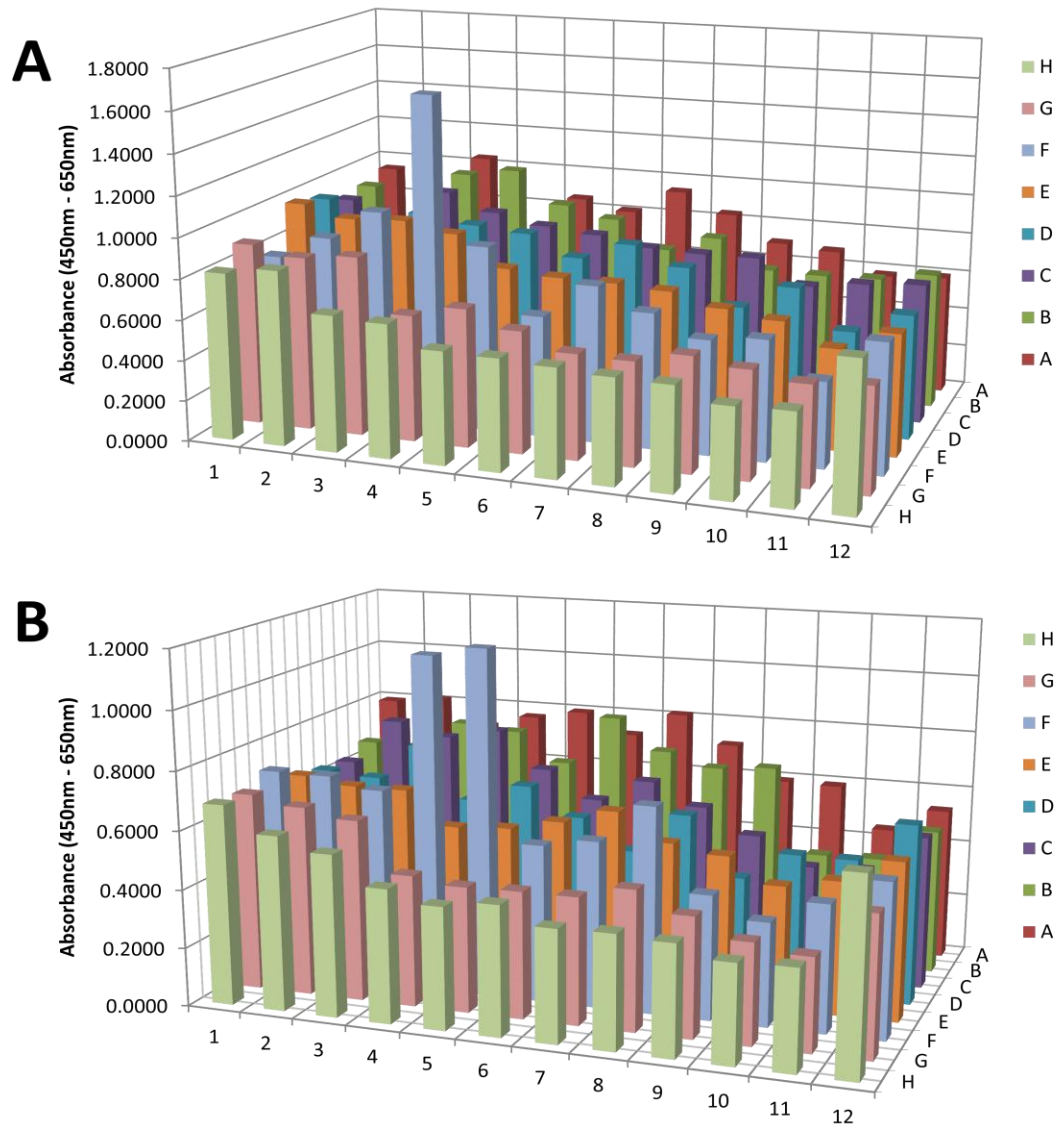


Figure 29: 25-mer Peptide, Tomlinson Phage Library I ELISA

The above graphs depict the positive ELISA reactions (section 2.2.12), when the difference between the absorbance at 450 nm and the absorbance at 650 nm (y-axis of graphs) was above the background value. The x-z axes represent the position in the ninety-six-well plates in which the ELISA was conducted. Part **A** of the Figure represents the 25-mer peptide, library I ELISA, and part **B** is the corresponding BSA-BSA conjugated reactions.

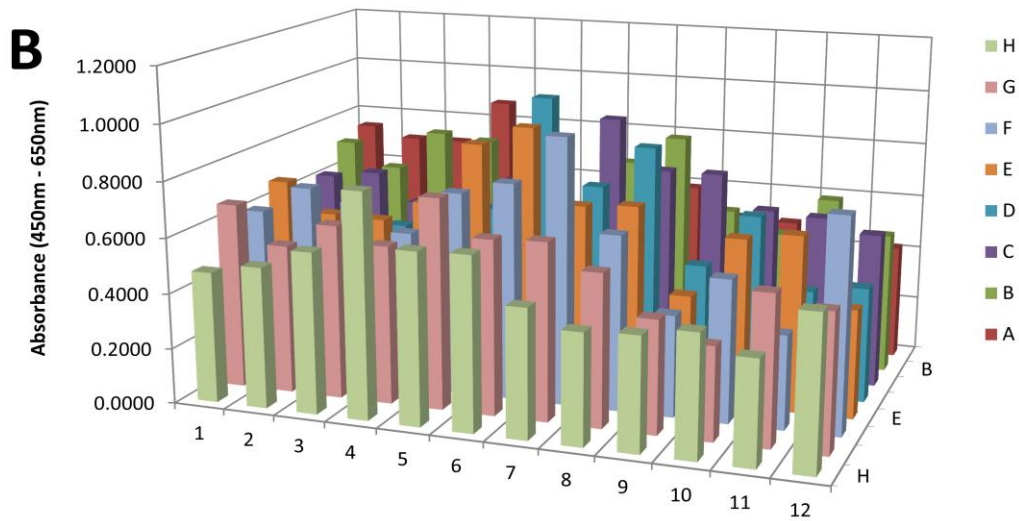
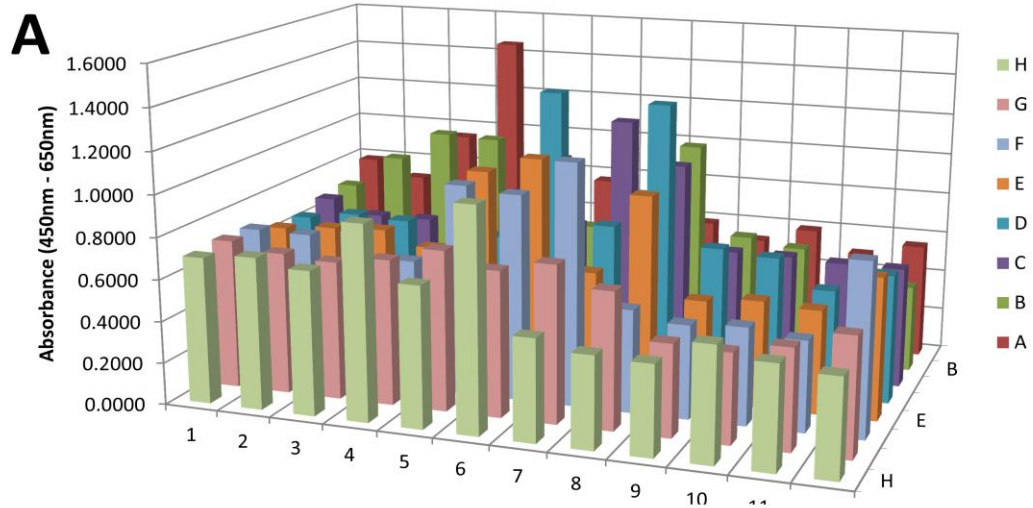


Figure 30: 25-mer Peptide, Tomlinson Phage Library J ELISA

The above graphs depict the positive ELISA reactions (section 2.2.12), when the difference between the absorbance at 450 nm and the absorbance at 650 nm (y-axis of graphs) was above the background value. The x-z axes represent the position in the ninety-six-well plates in which the ELISA was conducted. Part **A** of the Figure represents the 25-mer peptide, library J ELISA, and part **B** is the corresponding BSA-BSA conjugated reactions

Western blotting was used to determine if PGP synthase protein levels were regulated by ceramide and Rho, as shown in Figures 31 – 34. The western blots consisted of CHO cells treated for 1 or 4 hours with 10 mg/L C<sub>2</sub>-ceramide or the same volume of ethanol. BSA was present to serve as a negative control. As well, induced PGP synthase protein purified from pTF16 *E. coli* using the urea protein purification method was used as a positive control.

Figure 31 represents the western blots from the first batch of cells treated for 1 hour. Part A of the Figure shows the result from the incubations with phage antibody clone 16J-G6, and Protein L was used for detection. The PGP synthase band is denoted by an arrow, and is present in the CHO cell lanes at 55 kDa, as determined by a standard curve. There are non-specific protein bands at 155, 72, 50, and 37 kDa. There are no bands in the BSA lane, which confirms that the 16J-G6 phage antibody clone is not reactive towards BSA. However, the purified PGP synthase protein lane only shows a band at 71 kDa, and this is not the correct mass for PGP synthase. Part B of the Figure shows a membrane run in parallel with Part A. The primary antibody was clone 16J-G6, and the 16-mer peptide from which the phage antibody was produced was present to compete out the phage antibody. Protein L was used for detection. The 55 kDa PGP synthase band that was present in part A is not present in part B. Therefore, the peptide competition prevented the 16J-G6 antibody from binding to the 55 kDa band on the membrane, confirming that this band is indeed PGP synthase. The presence of bands at 155, 72, 50, and 37 kDa in the CHO lanes confirms that those bands are due to non-specific interactions. As well, there is a band present at 71 kDa in the purified PGP

synthase protein lane, which confirms that this band is non-specific. Part C of the Figure shows the membrane from part A. The membrane was initially probed with rabbit polyclonal GAPDH primary antibody, and goat anti-rabbit secondary antibody. The membrane was then stripped, and re-probed with 16J-G6, as shown in part A of the Figure. In part C, the GAPDH bands are present in the CHO cell lanes at 37 kDa. This band may be appearing in part A as a non-specific band. This may be due to the milder stripping conditions used after GAPDH probing. In the CHO cell lanes there are non-specific bands at 50 and 72 kDa. These bands may also be present in part A of the Figure. There are no bands present in the BSA lane, but the non-specific 71 kDa band is present in the purified PGP synthase protein lane. Part D of the Figure shows the membrane from part B. This membrane was probed in parallel with the membrane from part C with rabbit polyclonal GAPDH primary antibody, and goat anti-rabbit secondary antibody. The membrane was then stripped, and re-probed with 16J-G6 with the 16-mer peptide present, as shown in part B of the Figure. The banding in this membrane is very similar to the banding in part C. The GAPDH bands are present in the CHO cell lanes at 37 kDa, and there are non-specific bands at 50 and 72 kDa. There is also the non-specific 71 kDa band in the purified PGP synthase protein lane. Part E of the Figure presents the 55 kDa band densities relative to GAPDH. This represents PGP synthase protein levels. All cell lines show slight decreases in protein levels after ceramide treatment, with the largest change occurring in the E91 cell line. This suggests that PGP synthase protein levels are negatively regulated by ceramide and Rho.

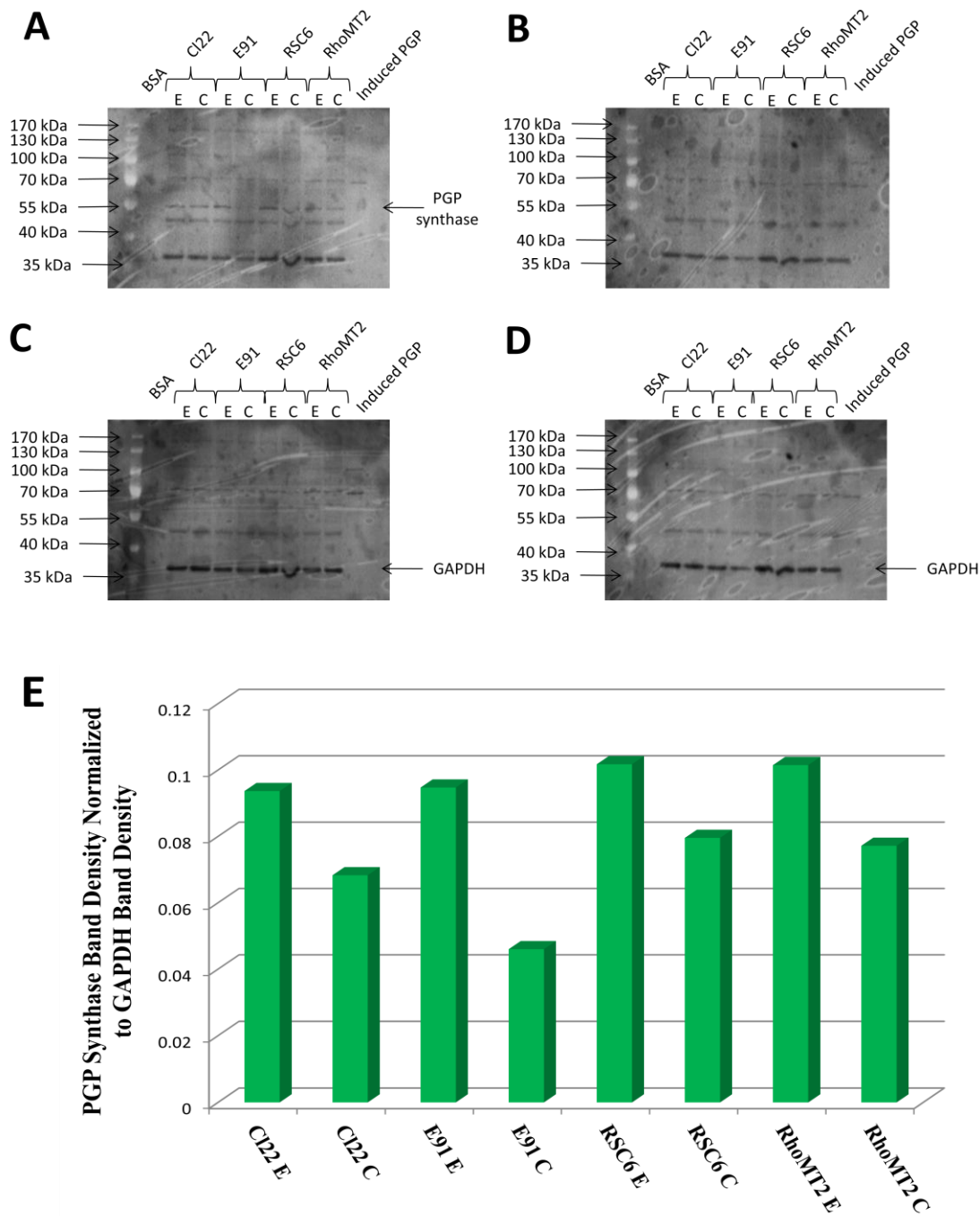


Figure 31: Western Blots from First Batch of 1-hour Cell Treatments

With the assistance of Lauren Luo, two 12% SDS-PAGE gels were run in parallel, as in section 2.2.14, with samples from CI22, E91, RSC6, and RhoMT2 cells treated with 10 mg/L ceramide (C) or the same volume of ethanol (E) for 1 hour. BSA served as a

negative control, and induced PGP synthase protein from pTF16 *E. coli* with the pET-1not1 plasmid served as a positive control. Images **A and C** are from membrane A, and images **B and D** are from membrane B. Image **A** shows membrane A incubated with phage primary antibody 16J-G6 without 16-mer peptide, and detected with Protein L antibody-binding proteins. Image **B** shows membrane B, run in parallel with membrane A, incubated with phage primary antibody 16J-G6 with 16-mer peptide competition, and with Protein L detection. Image **C** shows membrane A incubated with GAPDH primary antibody and anti-rabbit secondary antibody. Image **D** shows membrane B, run in parallel with membrane A, incubated with GAPDH primary antibody and anti-rabbit secondary antibody. Image **E** shows the band density of the 55 kDa band (PGP synthase) present in image **A** relative to the 37 kDa band (GAPDH) present in image **C**.

Figure 32 represents the western blots from the second batch of cells treated for 1 hour. Part A of the Figure shows the result from the incubations with phage antibody clone 16J-H12, and Protein L was used for detection. The PGP synthase band is denoted by an arrow, and is present in the CHO cell lanes at 55 kDa, as determined by a standard curve. There are non-specific protein bands at 50, 37, and 34 kDa. There are no bands in the BSA lane, which confirms that the 16J-H12 phage antibody clone is not reactive towards BSA. The purified PGP synthase protein lane shows the non-specific 71 kDa band that was also present when using the 16J-G6 antibody. Part B of the Figure shows a membrane run in parallel with Part A. The primary antibody was clone 16J-H12, and the 16-mer peptide from which the phage antibody was produced was present to compete out the phage antibody. Protein L was used for detection. The 55 kDa PGP synthase band that was present in part A is not present in part B. Therefore, the peptide competition prevented the 16J-H12 antibody from binding to the 55 kDa band on the membrane, confirming that this band is indeed PGP synthase. The presence of bands at 50, 37, and 34 kDa in the CHO lanes confirms that those bands are due to non-specific interactions. The non-specific 71 kDa band is present in the purified PGP synthase protein lane. Part C of the Figure shows the membrane from part A. The membrane was initially probed with rabbit polyclonal GAPDH primary antibody, and goat anti-rabbit secondary antibody. The membrane was then stripped, and re-probed with 16J-H12, as shown in part A of the Figure. In part C, the GAPDH bands are present in the CHO cell lanes at 37 kDa. Part D of the Figure shows the membrane from part B. This membrane was probed in parallel with the membrane from part C with rabbit polyclonal GAPDH primary antibody, and goat anti-rabbit secondary antibody. The membrane was then

stripped, and re-probed with 16J-H12 with the 16-mer peptide present, as shown in part B of the Figure. The banding in this membrane is very similar to the banding in part C. The GAPDH bands are present in the CHO cell lanes at 37 kDa. Part E of the Figure presents the 55 kDa band densities relative to GAPDH, representing the PGP synthase protein levels. The CI22 cell line shows a slight decrease in PGP synthase protein level after ceramide treatment, which is consistent with the results from Figure 31. The E91 cell line shows a large decrease in PGP synthase protein levels, which is also consistent with Figure 31. However, the RSC6 and RhoMT2 cell lines show very slight increases in protein level, which is not consistent with Figure 31. Therefore, part E suggests that PGP synthase protein levels are negatively regulated by ceramide and Rho due to the large decrease in protein levels after ceramide treatment in the E91 cell line. As well, the off-target effects of the shRNAi in the RSC6 and RhoMT2 cell lines may be affecting protein levels in a manner that makes them inconsistent.

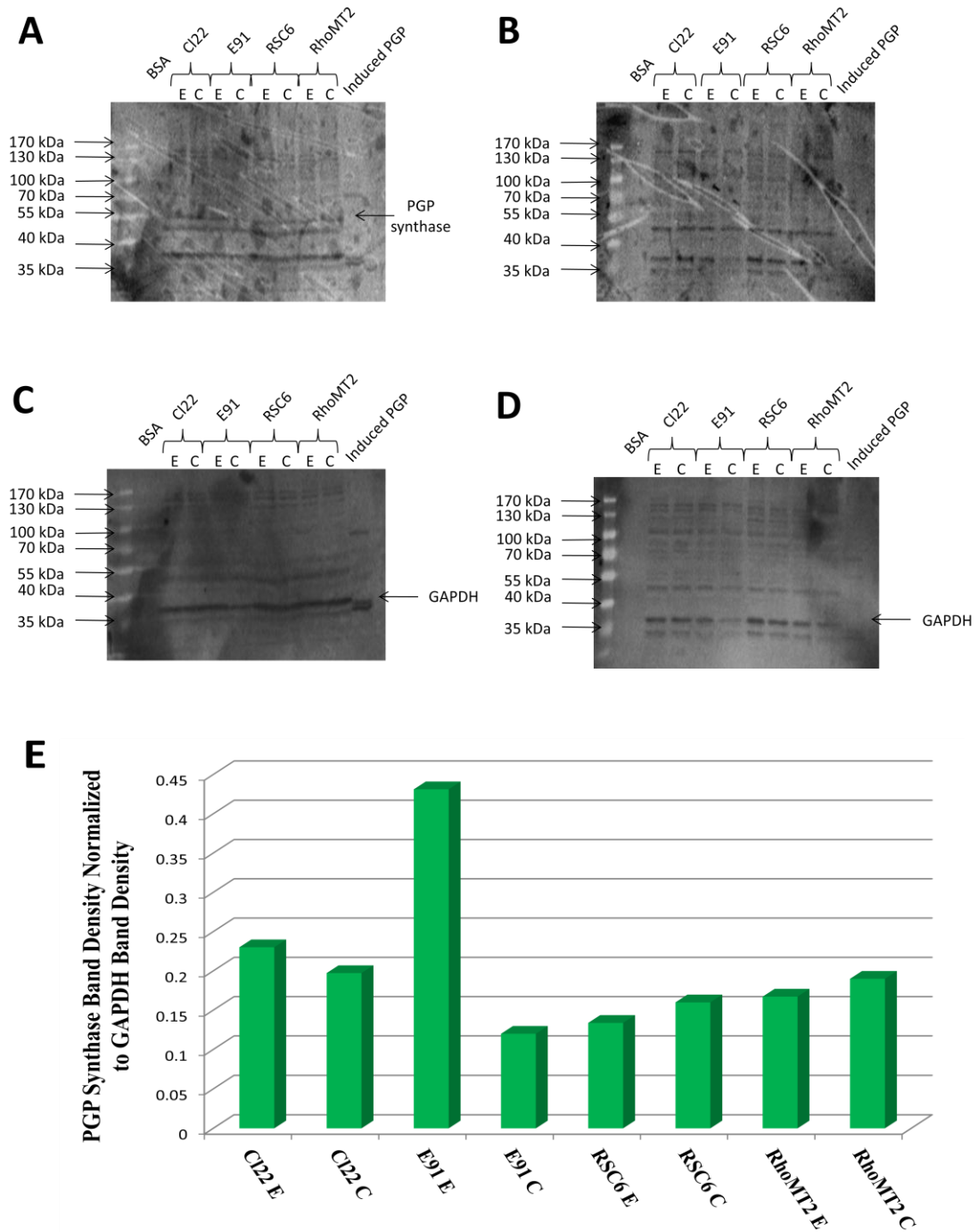


Figure 32: Western Blots from Second Batch of 1-hour Cell Treatments

With the assistance of Lauren Luo, two 12% SDS-PAGE gels were run in parallel, as in section 2.2.14, with samples from CI22, E91, RSC6, and RhoMT2 cells treated with 10 mg/L ceramide (C) or the same volume of ethanol (E) for 1 hour. BSA served as a

negative control, and induced PGP synthase protein from pTF16 *E. coli* with the pET-1not1 plasmid served as a positive control. Images **A and C** are from membrane A, and images **B and D** are from membrane B. Image **A** shows membrane A incubated with phage primary antibody 16J-H12 without 16-mer peptide, and detected with Protein L antibody-binding proteins. Image **B** shows membrane B, run in parallel with membrane A, incubated with phage primary antibody 16J-H12 with 16-mer peptide competition, and with Protein L detection. Image **C** shows membrane A incubated with GAPDH primary antibody and anti-rabbit secondary antibody. Image **D** shows membrane B, run in parallel with membrane A, incubated with GAPDH primary antibody and anti-rabbit secondary antibody. Image **E** shows the band density of the 55 kDa band (PGP synthase) present in image **A** relative to the 37 kDa band (GAPDH) present in image **C**.

Figure 33 represents the western blots from the first batch of cells treated for 4 hours. Part A of the Figure shows the result from the incubations with phage antibody clone 16J-G6, and Protein L was used for detection. The PGP synthase band is denoted by an arrow, and is present in the CHO cell lanes at 55 kDa, as determined by a standard curve. As well, there is a PGP synthase band at 57 kDa in the purified PGP synthase protein lane. Part B of the Figure shows a membrane run in parallel with Part A. The primary antibody was clone 16J-G6, and the 16-mer peptide from which the phage antibody was produced was present to compete out the phage antibody. Protein L was used for detection. The 55 kDa PGP synthase band that was present in part A is not present in part B. Part C of the Figure shows the membrane from part A. The membrane was initially probed with rabbit polyclonal GAPDH primary antibody, and goat anti-rabbit secondary antibody. The membrane was then stripped, and re-probed with 16J-G6, as shown in part A of the Figure. In part C, the GAPDH bands are present in the CHO cell lanes at 37 kDa. Part D of the Figure shows the membrane from part B. This membrane was probed in parallel with the membrane from part C with rabbit polyclonal GAPDH primary antibody, and goat anti-rabbit secondary antibody. The membrane was then stripped, and re-probed with 16J-G6 with the 16-mer peptide present, as shown in part B of the Figure. The banding in this membrane is very similar to the banding in part C. The GAPDH bands are present in the CHO cell lanes at 37 kDa. Part E of the Figure presents the 55 kDa band densities relative to GAPDH, representing the PGP synthase protein levels. All four cell lines show decreases in PGP synthase protein level after ceramide treatment. The E91 cell line shows the slightest decrease, and the

RSC6 and RhoMT2 cell lines show the largest decreases. Therefore, part E suggests that PGP synthase protein levels are negatively regulated by ceramide and Rho.

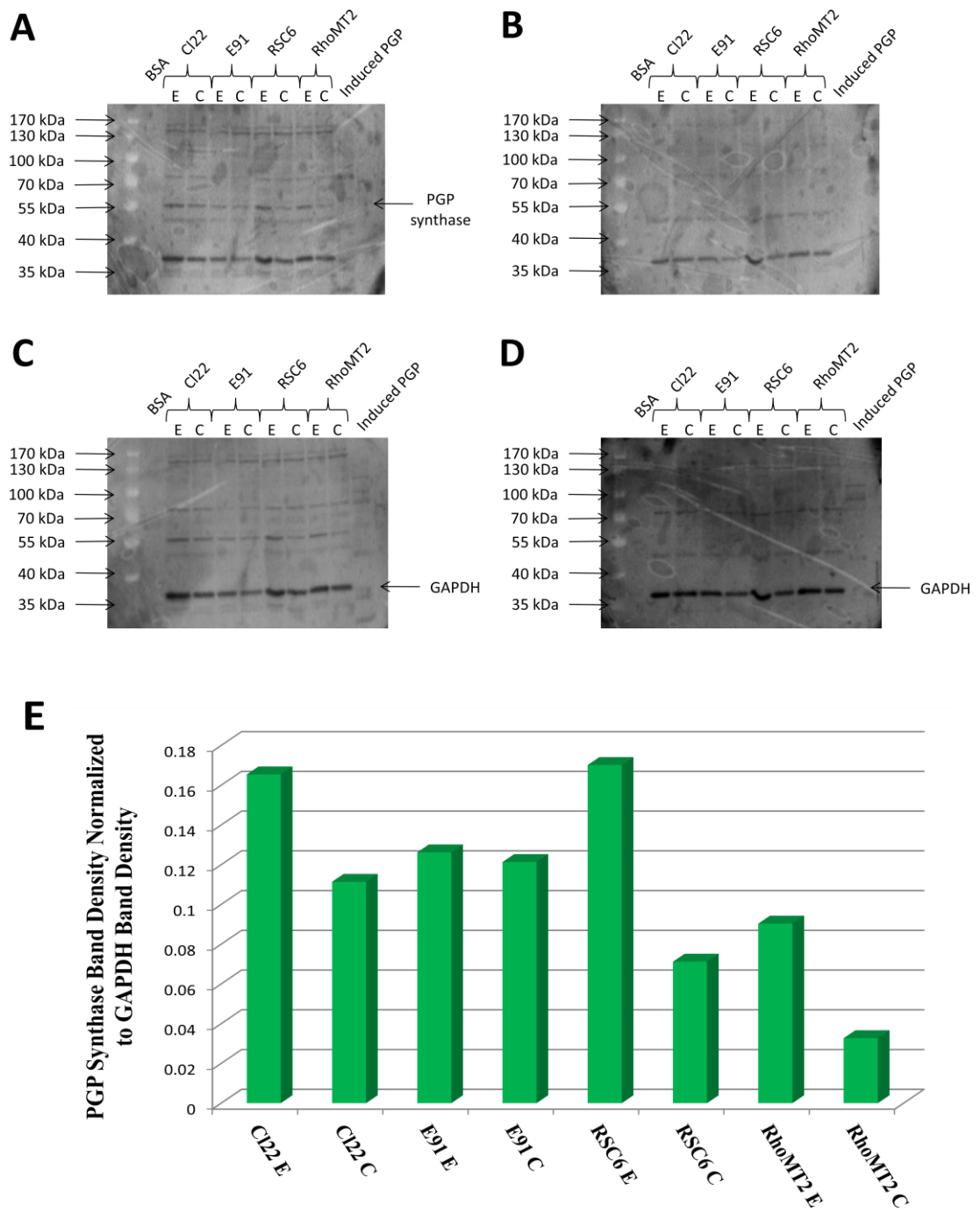


Figure 33: Western Blots from First Batch of 4-hour Cell Treatments

With the assistance of Lauren Luo, two 12% SDS-PAGE gels were run in parallel, as in section 2.2.14, with samples from C122, E91, RSC6, and RhoMT2 cells treated with 10 mg/L ceramide (C) or the same volume of ethanol (E) for 4 hours. BSA served as a

negative control, and induced PGP synthase protein from pTF16 *E. coli* with the pET-1not1 plasmid served as a positive control. Images **A and C** are from membrane A, and images **B and D** are from membrane B. Image **A** shows membrane A incubated with phage primary antibody 16J-G6 without 16-mer peptide, and detected with Protein L antibody-binding proteins. Image **B** shows membrane B, run in parallel with membrane A, incubated with phage primary antibody 16J-G6 with 16-mer peptide competition, and with Protein L detection. Image **C** shows membrane A incubated with GAPDH primary antibody and anti-rabbit secondary antibody. Image **D** shows membrane B, run in parallel with membrane A, incubated with GAPDH primary antibody and anti-rabbit secondary antibody. Image **E** shows the band density of the 55 kDa band (PGP synthase) present in image **A** relative to the 37 kDa band (GAPDH) present in image **C**.

Figure 34 represents the western blots from the second batch of cells treated for 4 hours. Part A of the Figure shows the result from the incubations with phage antibody clone 16J-H12, and Protein L was used for detection. The PGP synthase band is denoted by an arrow, and is present in the CHO cell lanes at 55 kDa, as determined by a standard curve. As well, there is a PGP synthase band at 57 kDa in the purified PGP synthase protein lane. Part B of the Figure shows a membrane run in parallel with Part A. The primary antibody was clone 16J-H12, and the 16-mer peptide from which the phage antibody was produced was present to compete out the phage antibody. Protein L was used for detection. The 55 kDa PGP synthase band that was present in part A is not present in part B. The 60 kDa band in the purified PGP synthase protein lane is also not present in part B, suggesting that this is indeed PGP synthase. This also supports the fact that clone 16J-H12 is binding to PGP synthase proteins. The 5 kDa discrepancy in molecular mass between the 55 kDa CHO PGP synthase and the 60 kDa *E. coli* PGP synthase may be due to the manner in which the protein is translated in the *E. coli*, or if the proteins run differently in SDS-PAGE gels. Part C of the Figure shows the membrane from part A. The membrane was initially probed with rabbit polyclonal GAPDH primary antibody, and goat anti-rabbit secondary antibody. The membrane was then stripped, and re-probed with 16J-H12, as shown in part A of the Figure. In part C, the GAPDH bands are present in the CHO cell lanes at 37 kDa. Part D of the Figure shows the membrane from part B. This membrane was probed in parallel with the membrane from part C with rabbit polyclonal GAPDH primary antibody, and goat anti-rabbit secondary antibody. The membrane was then stripped, and re-probed with 16J-H12 with the 16-mer peptide present, as shown in part B of the Figure. The banding

in this membrane is very similar to the banding in part C. The GAPDH bands are present in the CHO cell lanes at 37 kDa. Part E of the Figure presents the 55 kDa band densities relative to GAPDH, representing the PGP synthase protein levels. The CI22 cell line shows an increase in PGP synthase protein level after ceramide treatment, which is inconsistent with Figure 33. The E91, RSC6, and RhoMT2 cell lines show decreases in PGP synthase protein level after ceramide treatment. The decreases are larger in the RSC6 and RhoMT2 cell lines, suggesting that the off-target effects of shRNA are affecting protein PGP synthase levels. This is consistent with Figure 33. Therefore, part E suggests that PGP synthase protein levels are negatively regulated by ceramide and Rho in E91, RSC6 and RhoMT2 cell lines.

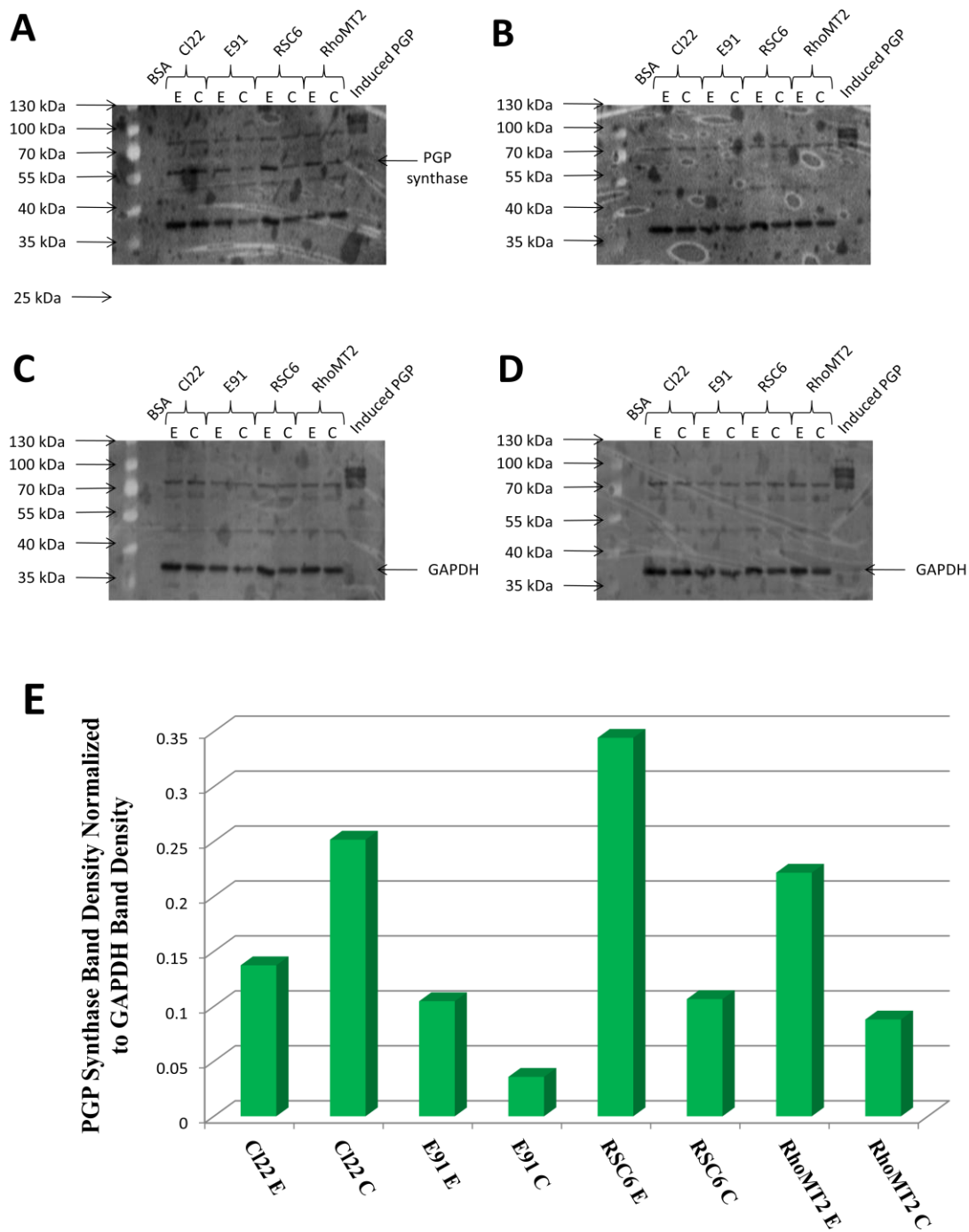


Figure 34: Western Blots from Second Batch of 4-hour Cell Treatments

With the assistance of Lauren Luo, two 12% SDS-PAGE gels were run in parallel, as in section 2.2.14, with samples from C122, E91, RSC6, and RhoMT2 cells treated with 10 mg/L ceramide (C) or the same volume of ethanol (E) for 4 hours. BSA served as a

negative control, and induced PGP synthase protein from pTF16 *E. coli* with the pET-1not1 plasmid served as a positive control. Images **A and C** are from membrane A, and images **B and D** are from membrane B. Image **A** shows membrane A incubated with phage primary antibody 16J-H12 without 16-mer peptide, and detected with Protein L antibody-binding proteins. Image **B** shows membrane B, run in parallel with membrane A, incubated with phage primary antibody 16J-H12 with 16-mer peptide competition, and with Protein L detection. Image **C** shows membrane A incubated with GAPDH primary antibody and anti-rabbit secondary antibody. Image **D** shows membrane B, run in parallel with membrane A, incubated with GAPDH primary antibody and anti-rabbit secondary antibody. Image **E** shows the band density of the 55 kDa band (PGP synthase) present in image **A** relative to the 37 kDa band (GAPDH) present in image **C**.

## **CHAPTER 4 – DISCUSSION**

### **4.1 Introduction**

It has already been determined that ceramide causes induction of PGP synthase enzyme activity in CHO cell lines with intact Dlc-2, but not when Dlc-2 function is lost (Hatch, Gu et al. 2008). The hypotheses of this project were that: the induction of PGP synthase is due in part to the transcriptional control of the PGP synthase gene by Rho proteins upon ceramide stimulation, and that these proteins are mediated by Dlc-2; Rho proteins are affecting PGP synthase mRNA stability; and the PGP synthase protein stability is being altered by Rho proteins upon ceramide stimulation, and this is mediated by the RhoGAP domain of Dlc-2. The following sections discuss the experimental results of this project with respect to the previous three hypotheses.

### **4.2 Transcriptional Control**

Real-Time RT-PCR was used to determine if PGP synthase is being regulated at the transcriptional level by ceramide and Rho. It is known that PGP synthase enzyme activity is induced in CHO cell lines with intact Dlc-2, but not when Dlc-2 function is lost (Hatch, Gu et al. 2008). It is also known that ceramide and Rho may be involved in similar transcription pathway. For example, both Rho and ceramide have been found to activate the JNK and p38 MAPK pathways (Jaffe and Hall 2005; Chen, Lin et al. 2008). Therefore, we hypothesized that the increase in enzyme activity of PGP synthase after ceramide treatment was due to an increase in transcription of the PGP synthase gene. It

was then expected that the CI22 and RhoMT2 cell lines would show induction in PGP synthase after ceramide treatment when compared to the E91 and RSC6 cell lines, respectively. This is due to the fact that the CI22 and RhoMT2 cell lines contain functioning Dlc-2, but the E91 and RSC6 cell lines do not. We hypothesized that cells with functioning Dlc-2 would have greater PGP synthase induction at the transcriptional level after ceramide treatment, as these cells show an increase in PGP synthase enzyme activity. However, as displayed in Figure 9, the only significant induction in PGP synthase expression was a peak after 6 hours of treatment in the RhoMT2 cell line. The CI22 cell line showed only a biphasic trend, with peaks at 6 and 12 hours after treatment. There was no significant pattern of CI22 expression being greater than E91, or of RhoMT2 expression being greater than RSC6. Therefore, the Real-Time RT-PCR data suggest that PGP synthase is not regulated at the transcriptional level by ceramide and Rho.

### **4.3 Post-Transcriptional Control**

Real-Time RT-PCR was used to determine if PGP synthase mRNA was being affected by ceramide and Rho. As displayed in Figures 15 – 18, the set of ceramide, ethanol, and no treatment PGP synthase mRNA stability curves in the CI22, E91, RSC6, and RhoMT2 cell lines are not different from each other. Therefore, ceramide treatment is not affecting PGP synthase mRNA stability. The CI22 and E91 PGP synthase mRNA curves do not show changes in mRNA stability. Therefore, PGP synthase mRNA stability is not being regulated by Rho proteins. There is no consequence of the lack of Dlc-2 RhoGAP in the E91 cell line compared to the functional Dlc-2 RhoGAP in the

Cl22 cell line. In conclusion, PGP synthase is not being regulated post-transcriptionally by ceramide and Rho.

However, as shown in Figure 18, RhoMT2 mRNA is less stable than the other three cell lines. As well, the RSC6 and RhoMT2 GAPDH mRNA is less stable than the Cl22 and E91 mRNA. These effects may be due to off-target effects of shRNAi. shRNA is cleaved in the cytoplasm by the protein Dicer to form short interfering RNA (siRNA) (Anthony and Cantlon 2007). The siRNA then bind to RNA-induced silencing complex (RISC), which cleaves mRNAs with compatible sequences to the siRNA (Anthony and Cantlon 2007). It has been found that siRNAs cause siRNA-specific, rather than mRNA target-specific off-target gene expression profiles (Jackson and Linsley 2004). These profiles were very reproducible, and the off-target effects could not be eliminated by decreasing siRNA concentrations (Jackson and Linsley 2004). Therefore, it is apparent that siRNAs, and thus shRNAi, commonly cause off-target effects, and these effects may have influenced the mRNA stability in the RSC6 and RhoMT2 cell lines.

#### **4.4 Post-Translational Control**

Western blotting with a phage antibody against PGP synthase was used to determine if the PGP synthase protein was being affected by Rho proteins upon ceramide stimulation, mediated by the RhoGAP domain of Dlc-2. Initially, the antibody was to be developed against the PGP synthase protein purified from *E. coli*. It was determined that the best method of purifying the PGP synthase protein was the urea protein purification method. In this project, the urea protein purification method yielded a 57 kDa PGP

synthase protein. However, when Kawasaki et al. purified a recombinant PGP synthase protein in *E. coli*, a PGP synthase band at 60 kDa was present on SDS-PAGE (Kawasaki, Kuge et al. 2001). This group did not use the full length PGP synthase cDNA, but cloned a portion of the cDNA into the pQE9 vector (Kawasaki, Kuge et al. 2001). In this project, the full-length cDNA was cloned into the pET-1not1 (pET28a) vector. Therefore, the use of the pET-1not-1 vector and the full-length cDNA, rather than the pQE9 vector and not the full-length cDNA, may account for the differences in PGP synthase molecular weight compared to Kawasaki et al. Kawasaki et al. then used the recombinant PGP synthase protein to produce a polyclonal antibody through immunizing a rabbit (Kawasaki, Kuge et al. 2001). However, in this project, the urea protein purification method did not yield a sufficient amount of protein for use in phage display antibody production. This may have been due to the formation of inactive protein inclusion bodies, as this has been known to occur when using the pET28a vector (Kim, Choeng et al. 2010). The presence of inclusion bodies is probably why the urea protein purification protocol was more successful than the BugBuster protein purification methods. Urea is a strong denaturant, and can be used to solubilize inclusion bodies (Lebendiker 2006). This project also used Talon cobalt columns, which bind to histidine-tagged proteins with greater specificity than the nickel-charged resins that were by Kawasaki et al (Clontech Laboratories 2007). However, despite the fact that this project used urea and cobalt columns, it was necessary to use peptides as the antigens for phage display antibody production.

ELISA was used to confirm potential phage antibodies. In total, there were twelve potential phage antibodies produced by the 16-mer, C-terminal peptide and three potential antibodies produced by the 25-mer, N-terminal peptide. Of those fifteen antibodies, three were produced from the Tomlinson I phage library, and the other twelve were produced from Tomlinson J phage library. Therefore, the 16-mer, C-terminal peptide was more immunogenic than the 25-mer, N-terminal peptide. Also, the J phage library was more successful than the I phage library. The two clones used in the subsequent western blots were 16J-G6 and 16J-H12.

Western blots were used to determine if PGP synthase protein levels were regulated by ceramide and Rho, and are displayed in Figures 31 – 34. The blots displayed a 55 kDa PGP synthase protein. The recombinant PGP synthase protein that was purified in *E. coli* was present in the 4 hour treatment blots. The presence of this band corroborates the fact that the 16J-G6 and 16J-H12 phage antibodies are binding to PGP synthase. However, when Kawasaki et al. used their PGP synthase antibody in western blots, there were two bands present in the CHO samples (Kawasaki, Kuge et al. 2001). There was a band at 60 kDa, and a fainter band at 62 kDa (Kawasaki, Kuge et al. 2001). This doublet was seen in the CHO cells used by Kawasaki et al. that were transformed to overproduce PGP synthase, and in mitochondrial fractions of wild-type CHO cells (Kawasaki, Kuge et al. 2001). The doublet was not present in the wild-type CHO cell lysates (Kawasaki, Kuge et al. 2001). Therefore, the fainter, higher PGP synthase doublet band may be present in the CHO cells used in this project, but not at a level that can be detected by the phage antibodies. However, the fact that the phage antibodies detect PGP synthase bands in CHO cell lysates suggests that the phage

antibodies have higher PGP synthase binding affinity than the rabbit polyclonal antibody used by Kawasaki et al.

We hypothesized that PGP synthase protein induction after ceramide treatment is prevented by Rho protein activity, mediated by the RhoGAP domain of Dlc-2.

Therefore, it was to be expected that the Cl22 and RhoMT2 cell lines would show an increase in PGP synthase protein levels after ceramide treatment, and the E91 and RSC6 cell lines would not. After 1 hour of ceramide treatment, the Cl22 cell line showed a slight decrease in protein levels, and the E91 cell line showed a large decrease. This suggests that PGP synthase protein levels are negatively regulated by ceramide and Rho, but the short treatment time of 1 hour may not be sufficient to see the effects of ceramide. Hatch et al. incubated CHO cell lines with ceramide for 24 hours, and then determined that there was an increase in PGP synthase enzyme activity (Hatch, Gu et al. 2008). The RSC6 and RhoMT2 cell lines showed both a small decrease and a small increase. Therefore, off-target effects of the shRNAi in the RSC6 and RhoMT2 cell lines may be affecting protein levels in a manner that makes them behave inconsistently. siRNAs have been found to block the translation of unintended protein targets, which may then cause unintended effects at the level of protein translation (Jackson and Linsley 2004). After 4 hours of ceramide treatment, the Cl22 cell line showed a slight decrease in PGP synthase protein levels and an increase in PGP synthase protein levels. The E91 cell line showed decreases in PGP synthase protein levels. Therefore, after 4 hours of ceramide treatment, PGP synthase protein levels may start to be induced. However, this trend is inconsistent between cell treatments, so more investigation would be required to confirm

this is the case. Rho proteins, however, are negatively regulating PGP synthase protein levels, as the E91 cell line continues to show a decrease in PGP synthase protein levels. Therefore, ceramide treatment of longer than 4 hours may be required to induce PGP synthase protein levels in cells with functional Dlc-2, but cells without functional Dlc-2 would not experience the increase in PGP synthase.

Rho proteins act as molecular switches (Jaffe and Hall 2005). RhoGAP proteins, such as Dlc-2, are the protein that can inactivate Rho (Jaffe and Hall 2005). When Dlc-2 is functioning properly, this leads to less active Rho proteins. In this case, it seems that ceramide may start to increase PGP synthase protein levels, as shown in one batch of the Cl22 cells. However, when Dlc-2 is not functioning properly, there are more active Rho proteins. In this case, there is a decrease in PGP synthase protein levels after ceramide treatment. The mechanism of control by more of the active Rho proteins, in cells with Dlc-2 interrupted, may be due to more active ROCKs (Schmandke and Strittmatter 2007). ROCKs have been found to phosphorylate the myosin phosphatase (Totsukawa, Yamakita et al. 2000). Perhaps the ROCKs, or other downstream effectors of the active Rho proteins, cause phosphorylation of an unknown protein that causes the degradation of PGP synthase. Alternatively, the ROCKs themselves may be phosphorylating PGP synthase. He and Greenberg have shown that PGP synthase enzyme activity is decreased in response to inositol due to phosphorylation of the PGP synthase enzyme rather than degradation or protein mislocalization (He and Greenberg 2004). Therefore, in cells with Dlc-2 interrupted, the more active ROCKs, due to the more active Rho proteins, may be decreasing PGP synthase enzyme activity through phosphorylation. Ceramide can

activate phosphatases PP1 and PP2A (Birbes, El Bawab et al. 2002), which may then cause dephosphorylation of PGP synthase. It was shown by Xu et al. that the protein phosphatase inhibitors calyculin A and okadaic acid attenuated the ceramide-mediated induction of the PGP synthase enzyme (Xu, Kelly et al. 1999). Therefore, CAPP is involved in the induction of PGP synthase (Xu, Kelly et al. 1999). The western blots in this project do not suggest a strong correlation between ceramide treatment and changes in PGP synthase protein levels. Therefore, the increase in PGP synthase enzyme activity after ceramide treatment shown by Hatch, et al. may be due to the dephosphorylation of the PGP synthase enzyme by CAPP, rather than due to changes in PGP synthase protein levels.

PGP synthase is localized to the inner mitochondrial membrane (Kuchler, Daum et al. 1986). Dlc-2 can localize to the mitochondria via its START domain (Ng, Chan et al. 2006). We have hypothesized that ceramide binds to Dlc-2's START domain because ceramide can bind to CERT's START domain (Hanada, Kumagai et al. 2003). Ceramide can form "lipid rafts" on the lateral plane of lipid bilayers (Futerman and Hannun 2004; Zhang, Li et al. 2009). Therefore, Dlc-2 may be able to interact with PGP synthase through its localization to the mitochondria through its START domain binding to ceramide on lipid rafts. Additionally, ceramide can form protein-permeable channels in mitochondrial membranes (Siskind 2005). These channels may allow for more interactions between Dlc-2, Rho, and PGP synthase.

The effect of lower PGP synthase protein levels in the E91 cells after ceramide treatment would cause a decrease in the amount of CL present in mitochondria. CL is a binding site for cytochrome *c*, caspase-8, and tBid (Garrido, Galluzzi et al. 2006; Gonzalez and Gottlieb 2007; Gonzalez, Schug et al. 2008). Therefore, the decrease in cardiolipin levels may be part of the reason the E91 cell line is more resistant to apoptosis (Hatch, Gu et al. 2008). The tightly-bound cytochrome *c* would no longer be able to peroxidize CL, so the CL would not become exposed on the OMM, which is a sign of apoptosis (Gonzalez and Gottlieb 2007). Caspase-8, which is a pro-apoptosis initiator caspase, would no longer be processed (Gonzalez, Schug et al. 2008). Bid would no longer be cleaved to the pro-apoptotic tBid (Gonzalez, Pariselli et al. 2010). CL is important for proper mitochondrial structure (Gonzalez and Gottlieb 2007). The mitochondria of Barth syndrome patients exhibit abnormal cristae ultrastructure (Claypool, Boontheung et al. 2008). CL is necessary for the function of many mitochondrial enzymes, such as the ETC (Gonzalez and Gottlieb 2007). Therefore, E91 cells would have abnormal mitochondria physically and functionally, which would then affect the cells themselves. The mitochondria provide the energy to cells, which then allows the cells to perform basic functions. The defect in mitochondria in E91 cells may account for the reason the cells grow more slowly than C122 cells.

## 4.5 Future Directions

In terms of transcriptional control, it would be interesting to conduct more Real-Time RT-PCR experiments using the absolute quantification method rather than the relative quantification method. This may allow for less error between cell batches because it determines the actual number of double-stranded DNA (dsDNA) molecules, rather than expression compared to another gene.

For post-transcriptional control, it would be useful to conduct more Real-Time RT-PCR experiments for longer actinomycin D time points. As well, the absolute quantification method would be useful in this case to allow for the determination of mRNA half-lives.

For post-translational control, it would be useful to conduct immunoprecipitation experiments followed by sequencing to verify beyond a doubt that the phage antibodies are detecting PGP synthase. As well, it would be useful to repeat more western blots for the ceramide and ethanol treatment times used in this project to achieve statistical significance. Western blots of additional ceramide and ethanol treatment times would also be useful to allow for determining the patterns of PGP synthase protein levels with ceramide treatment when Dlc-2 is functioning and not functioning. Finally, pulse-chase experiments would be beneficial to determine if the PGP synthase protein decay rates are different with ceramide treatment, or the presence or absence of Dlc-2.

## 4.6 Conclusions

In terms of the first goal of this project, the Real-Time RT-PCR data suggests that transcriptional control of the PGP synthase gene by ceramide and Rho is not taking place. Regarding the second goal of this project, ceramide and Rho do not seem to affect mRNA stability of PGP synthase. For the third goal of this project, ceramide and Rho do seem to exhibit translational or post-translational control over the PGP synthase protein. When Dlc-2 is not functional, ceramide treatment cannot increase protein levels as it may when Dlc-2 is functional. However, due to the inconsistent behaviour of the Cl22 cell line after 4 hours of ceramide treatment, more investigation is required to confirm this trend.

The relationships between Dlc-2 (and Rho), ceramide, and PGP synthase (and CL) are important to understand. All three are involved in cancer and apoptotic responses. The knowledge gained by the experiments discussed in this thesis can contribute to an understanding of how these proteins and lipids interact. This knowledge may then be used in future cancer treatments.

## **CHAPTER 5 – LITERATURE CITED**

- Alpy, F. and C. Tomasetto (2005). "Give lipids a START: the StAR-related lipid transfer (START) domain in mammals." J Cell Sci **118**(Pt 13): 2791-801.
- Anthony, R. V. and J. D. Cantlon (2007). "Ribonucleic acid interference: a new approach to the in vivo study of gene function." J Anim Sci **85**(13 Suppl): E18-9.
- Aspenstrom, P., A. Fransson, et al. (2004). "Rho GTPases have diverse effects on the organization of the actin filament system." Biochem J **377**(Pt 2): 327-37.
- Bartke, N. and Y. A. Hannun (2009). "Bioactive sphingolipids: metabolism and function." J Lipid Res **50** Suppl: S91-6.
- Birbes, H., S. El Bawab, et al. (2002). "Mitochondria and ceramide: intertwined roles in regulation of apoptosis." Adv Enzyme Regul **42**: 113-29.
- Boulter-Bitzer, J. I., H. Lee, et al. (2010). "Single chain variable fragment antibodies selected by phage display against the sporozoite surface antigen S16 of *Cryptosporidium parvum*." Exp Parasitol **125**(2): 124-9.
- Bourne, H. R., D. A. Sanders, et al. (1991). "The GTPase superfamily: conserved structure and molecular mechanism." Nature **349**(6305): 117-27.
- Bratkovic, T. (2010). "Progress in phage display: evolution of the technique and its application." Cell Mol Life Sci **67**(5): 749-67.
- Chen, C. L., C. F. Lin, et al. (2008). "Ceramide induces p38 MAPK and JNK activation through a mechanism involving a thioredoxin-interacting protein-mediated pathway." Blood **111**(8): 4365-74.
- Chicco, A. J. and G. C. Sparagna (2007). "Role of cardiolipin alterations in mitochondrial dysfunction and disease." Am J Physiol Cell Physiol **292**(1): C33-44.
- Ching, Y. P., C. M. Wong, et al. (2003). "Deleted in liver cancer (DLC) 2 encodes a RhoGAP protein with growth suppressor function and is underexpressed in hepatocellular carcinoma." J Biol Chem **278**(12): 10824-30.
- Cho, S. G. and E. J. Choi (2002). "Apoptotic signaling pathways: caspases and stress-activated protein kinases." J Biochem Mol Biol **35**(1): 24-7.
- Christenson, L. K. and J. F. Strauss, 3rd (2001). "Steroidogenic acute regulatory protein: an update on its regulation and mechanism of action." Arch Med Res **32**(6): 576-86.

- Claypool, S. M., P. Boontheung, et al. (2008). "The cardiolipin transacylase, tafazzin, associates with two distinct respiratory components providing insight into Barth syndrome." Mol Biol Cell **19**(12): 5143-55.
- Clontech Laboratories, I. (2007). "TALON Metal Affinity Resins User Manual."
- de Tayrac, M., A. Etcheverry, et al. (2009). "Integrative genome-wide analysis reveals a robust genomic glioblastoma signature associated with copy number driving changes in gene expression." Genes Chromosomes Cancer **48**(1): 55-68.
- Degli Esposti, M. (2004). "Mitochondria in apoptosis: past, present and future." Biochem Soc Trans **32**(Pt3): 493-5.
- Durkin, M. E., V. Ullmannova, et al. (2007). "Deleted in liver cancer 3 (DLC-3), a novel Rho GTPase-activating protein, is downregulated in cancer and inhibits tumor cell growth." Oncogene **26**(31): 4580-9.
- Durkin, M. E., B. Z. Yuan, et al. (2007). "DLC-1: a Rho GTPase-activating protein and tumour suppressor." J Cell Mol Med **11**(5): 1185-207.
- EMD Biosciences, I. (2004). "Novagen BugBuster Protein Extraction Reagent."
- Erlmann, P., S. Schmid, et al. (2009). "DLC1 activation requires lipid interaction through a polybasic region preceding the RhoGAP domain." Mol Biol Cell **20**(20): 4400-11.
- Esteve, P., L. del Peso, et al. (1995). "Induction of apoptosis by rho in NIH 3T3 cells requires two complementary signals. Ceramides function as a progression factor for apoptosis." Oncogene **11**(12): 2657-65.
- Futerman, A. H. and Y. A. Hannun (2004). "The complex life of simple sphingolipids." EMBO Rep **5**(8): 777-82.
- Garet, E., A. G. Cabado, et al. (2010). "Rapid isolation of single-chain antibodies by phage display technology directed against one of the most potent marine toxins: Palytoxin." Toxicon **55**(8): 1519-26.
- Garrido, C., L. Galluzzi, et al. (2006). "Mechanisms of cytochrome c release from mitochondria." Cell Death Differ **13**(9): 1423-33.
- GEHealthcare (2006). "Amersham ECL plus western blotting detection reagents product booklet."
- Gomez-Munoz, A. (2006). "Ceramide 1-phosphate/ceramide, a switch between life and death." Biochim Biophys Acta **1758**(12): 2049-56.
- Gonzalez, I. L. (2005). "Barth syndrome: TAZ gene mutations, mRNAs, and evolution." Am J Med Genet A **134**(4): 409-14.

- Gonzalvez, F. and E. Gottlieb (2007). "Cardiolipin: setting the beat of apoptosis." Apoptosis **12**(5): 877-85.
- Gonzalvez, F., F. Pariselli, et al. (2010). "Mechanistic issues of the interaction of the hairpin-forming domain of tBid with mitochondrial cardiolipin." PLoS One **5**(2): e9342.
- Gonzalvez, F., Z. T. Schug, et al. (2008). "Cardiolipin provides an essential activating platform for caspase-8 on mitochondria." J Cell Biol **183**(4): 681-96.
- Goodison, S., J. Yuan, et al. (2005). "The RhoGAP protein DLC-1 functions as a metastasis suppressor in breast cancer cells." Cancer Res **65**(14): 6042-53.
- Grant, S. and S. Spiegel (2002). "A chicken-or-egg conundrum in apoptosis: which comes first? Ceramide or PKCdelta?" J Clin Invest **109**(6): 717-9.
- Greenberg, M. L., S. Hubbell, et al. (1988). "Inositol regulates phosphatidylglycerolphosphate synthase expression in *Saccharomyces cerevisiae*." Mol Cell Biol **8**(11): 4773-9.
- Hanada, K., K. Kumagai, et al. (2003). "Molecular machinery for non-vesicular trafficking of ceramide." Nature **426**(6968): 803-9.
- Hannun, Y. A. and L. M. Obeid (2008). "Principles of bioactive lipid signalling: lessons from sphingolipids." Nat Rev Mol Cell Biol **9**(2): 139-50.
- Hannun, Y. A., L. M. Obeid, et al. (1993). "The novel second messenger ceramide: identification, mechanism of action, and cellular activity." Adv Lipid Res **25**: 43-64.
- Harlow, E. and D. Lane (1999). Using antibodies: a laboratory manual. Cold Spring Harbor, New York, Cold Spring Harbor Laboratory Press.
- Hatch, G. M. (1996). "Regulation of cardiolipin biosynthesis in the heart." Mol Cell Biochem **159**(2): 139-48.
- Hatch, G. M., Y. Gu, et al. (2008). "StARD13(Dlc-2) RhoGap mediates ceramide activation of phosphatidylglycerolphosphate synthase and drug response in Chinese hamster ovary cells." Mol Biol Cell **19**(3): 1083-92.
- Hauff, K. D. and G. M. Hatch (2006). "Cardiolipin metabolism and Barth Syndrome." Prog Lipid Res **45**(2): 91-101.
- He, Q. and M. L. Greenberg (2004). "Post-translational regulation of phosphatidylglycerolphosphate synthase in response to inositol." Mol Microbiol **53**(4): 1243-9.

- Healy, K. D., L. Hodgson, et al. (2008). "DLC-1 suppresses non-small cell lung cancer growth and invasion by RhoGAP-dependent and independent mechanisms." Mol Carcinog **47**(5): 326-37.
- Hicks, G. G., E. G. Shi, et al. (1995). "Retrovirus gene traps." Methods Enzymol **254**: 263-75.
- Houtkooper, R. H. and F. M. Vaz (2008). "Cardiolipin, the heart of mitochondrial metabolism." Cell Mol Life Sci **65**(16): 2493-506.
- Hubbard, S. C., L. Walls, et al. (1994). "Generation of Chinese hamster ovary cell glycosylation mutants by retroviral insertional mutagenesis. Integration into a discrete locus generates mutants expressing high levels of N-glycolylneuraminic acid." J Biol Chem **269**(5): 3717-24.
- Invitrogen (2003). "SuperScript II Reverse Transcriptase."
- Jackson, A. L. and P. S. Linsley (2004). "Noise amidst the silence: off-target effects of siRNAs?" Trends Genet **20**(11): 521-4.
- Jacob, C. O., R. Arnon, et al. (1985). "Effect of carrier on the immunogenic capacity of synthetic cholera vaccine." Mol Immunol **22**(12): 1333-9.
- Jaffe, A. B. and A. Hall (2005). "Rho GTPases: biochemistry and biology." Annu Rev Cell Dev Biol **21**: 247-69.
- Jimenez, B., M. Arends, et al. (1995). "Induction of apoptosis in NIH3T3 cells after serum deprivation by overexpression of rho-p21, a GTPase protein of the ras superfamily." Oncogene **10**(5): 811-6.
- Kagan, V. E., H. A. Bayir, et al. (2009). "Cytochrome c/cardiolipin relations in mitochondria: a kiss of death." Free Radic Biol Med **46**(11): 1439-53.
- Kam, P. C. and N. I. Ferch (2000). "Apoptosis: mechanisms and clinical implications." Anaesthesia **55**(11): 1081-93.
- Kawai, K., Y. Iwamae, et al. (2009). "Focal adhesion-localization of START-GAP1/DLC1 is essential for cell motility and morphology." Genes Cells **14**(2): 227-41.
- Kawai, K., S. Y. Kitamura, et al. (2009). "START-GAP1/DLC1 is localized in focal adhesions through interaction with the PTB domain of tensin2." Adv Enzyme Regul.
- Kawai, K., M. Kiyota, et al. (2007). "START-GAP3/DLC3 is a GAP for RhoA and Cdc42 and is localized in focal adhesions regulating cell morphology." Biochem Biophys Res Commun **364**(4): 783-9.

- Kawai, K., J. Seike, et al. (2009). "START-GAP2/DLC2 is localized in focal adhesions via its N-terminal region." Biochem Biophys Res Commun **380**(4): 736-41.
- Kawasaki, K., O. Kuge, et al. (1999). "Isolation of a chinese hamster ovary (CHO) cDNA encoding phosphatidylglycerophosphate (PGP) synthase, expression of which corrects the mitochondrial abnormalities of a PGP synthase-defective mutant of CHO-K1 cells." J Biol Chem **274**(3): 1828-34.
- Kawasaki, K., O. Kuge, et al. (2001). "Purification of phosphatidylglycerophosphate synthase from Chinese hamster ovary cells." Biochem J **354**(Pt 1): 9-15.
- Kim, M. R., Y. H. Choeng, et al. (2010). "Heterologous production of streptokinase as a secretory form in *Streptomyces lividans* and nonsecretory form in *Escherichia coli*." J Microbiol Biotechnol **20**(1): 132-7.
- Kim, T. Y., J. W. Lee, et al. (2007). "DLC-1, a GTPase-activating protein for Rho, is associated with cell proliferation, morphology, and migration in human hepatocellular carcinoma." Biochem Biophys Res Commun **355**(1): 72-7.
- Kitatani, K., J. Idkowiak-Baldys, et al. (2008). "The sphingolipid salvage pathway in ceramide metabolism and signaling." Cell Signal **20**(6): 1010-8.
- Ko, F. C., Y. S. Yeung, et al. (2010). "Deleted in liver cancer 1 isoforms are distinctly expressed in human tissues, functionally different and under differential transcriptional regulation in hepatocellular carcinoma." Liver Int **30**(1): 139-48.
- Kuchler, K., G. Daum, et al. (1986). "Subcellular and submitochondrial localization of phospholipid-synthesizing enzymes in *Saccharomyces cerevisiae*." J Bacteriol **165**(3): 901-10.
- Kudo, N., K. Kumagai, et al. (2008). "Structural basis for specific lipid recognition by CERT responsible for nonvesicular trafficking of ceramide." Proc Natl Acad Sci U S A **105**(2): 488-93.
- Kumagai, K., S. Yasuda, et al. (2005). "CERT mediates intermembrane transfer of various molecular species of ceramides." J Biol Chem **280**(8): 6488-95.
- Kwan, J. J. and L. W. Donaldson (2007). "The NMR structure of the murine DLC2 SAM domain reveals a variant fold that is similar to a four-helix bundle." BMC Struct Biol **7**: 34.
- Lebendiker, M. (2006). "The protein purification facility." 2008, from <http://wolfson.huji.ac.il/purification/index.html>.
- Ledeen, R. W. and G. Wu (2008). "Nuclear sphingolipids: metabolism and signaling." J Lipid Res **49**(6): 1176-86.

- Leung, T. H., Y. P. Ching, et al. (2005). "Deleted in liver cancer 2 (DLC2) suppresses cell transformation by means of inhibition of RhoA activity." Proc Natl Acad Sci U S A **102**(42): 15207-12.
- Levade, T., M. C. Tempesta, et al. (1993). "The in situ degradation of ceramide, a potential lipid mediator, is not completely impaired in Farber disease." FEBS Lett **329**(3): 306-12.
- Li, H., K. L. Fung, et al. (2007). "Solution structures, dynamics, and lipid-binding of the sterile alpha-motif domain of the deleted in liver cancer 2." Proteins **67**(4): 1154-66.
- Liao, Y. C., L. Si, et al. (2007). "The phosphotyrosine-independent interaction of DLC-1 and the SH2 domain of cten regulates focal adhesion localization and growth suppression activity of DLC-1." J Cell Biol **176**(1): 43-9.
- Livak, K. J. and T. D. Schmittgen (2001). "Analysis of relative gene expression data using real-time quantitative PCR and the 2(-Delta Delta C(T)) Method." Methods **25**(4): 402-8.
- McMillin, J. B. and W. Dowhan (2002). "Cardiolipin and apoptosis." Biochim Biophys Acta **1585**(2-3): 97-107.
- Millipore (2004). "Amicon Ultra-4 Centrifugal Filter Devices User Guide."
- Moon, S. Y. and Y. Zheng (2003). "Rho GTPase-activating proteins in cell regulation." Trends Cell Biol **13**(1): 13-22.
- Nagaraja, G. M. and R. P. Kandpal (2004). "Chromosome 13q12 encoded Rho GTPase activating protein suppresses growth of breast carcinoma cells, and yeast two-hybrid screen shows its interaction with several proteins." Biochem Biophys Res Commun **313**(3): 654-65.
- Ng, D. C., S. F. Chan, et al. (2006). "Mitochondrial targeting of growth suppressor protein DLC2 through the START domain." FEBS Lett **580**(1): 191-8.
- Nishihara, K., M. Kanemori, et al. (2000). "Overexpression of trigger factor prevents aggregation of recombinant proteins in Escherichia coli." Appl Environ Microbiol **66**(3): 884-9.
- Nixon, G. F. (2009). "Sphingolipids in inflammation: pathological implications and potential therapeutic targets." Br J Pharmacol **158**(4): 982-93.
- Ohtsuka, T., M. Nishijima, et al. (1993). "A somatic cell mutant defective in phosphatidylglycerophosphate synthase, with impaired phosphatidylglycerol and cardiolipin biosynthesis." J Biol Chem **268**(30): 22908-13.

- Ott, M., B. Zhivotovsky, et al. (2007). "Role of cardiolipin in cytochrome c release from mitochondria." Cell Death Differ **14**(7): 1243-7.
- Pangborn, M. (1942). "Isolation and purification of a serologically active phospholipid from beef heart." J Biol Chem **143**: 247-256.
- Paradies, G., G. Petrosillo, et al. (2009). "Role of cardiolipin peroxidation and Ca<sup>2+</sup> in mitochondrial dysfunction and disease." Cell Calcium **45**(6): 643-50.
- Perona, R., S. Montaner, et al. (1997). "Activation of the nuclear factor-kappaB by Rho, CDC42, and Rac-1 proteins." Genes Dev **11**(4): 463-75.
- Pierce Biotechnology, I. (2005). "MBS and sulfo-MBS."
- Pierce Biotechnology, I. (2007). "Zeba desalt spin columns ".
- Ponting, C. P. and L. Aravind (1999). "START: a lipid-binding domain in StAR, HD-ZIP and signalling proteins." Trends Biochem Sci **24**(4): 130-2.
- Popescu, N. C. and M. E. Durkin (2004). "Rho GTPase activating protein cDNA on chromosome 13q12 is the deleted in liver cancer (DLC2) gene." Biochem Biophys Res Commun **315**(4): 781.
- Qiagen (2005). "QuantiTect SYBR Green PCR Handbook."
- Qiagen (2006). "Qiagen RNeasy Mini Handbook, Fourth Edition."
- Qiao, F. and J. U. Bowie (2005). "The many faces of SAM." Sci STKE **2005**(286): re7.
- Richter, C. and P. Ghafourifar (1999). "Ceramide induces cytochrome c release from isolated mitochondria." Biochem Soc Symp **66**: 27-31.
- Riedl, S. J. and G. S. Salvesen (2007). "The apoptosome: signalling platform of cell death." Nat Rev Mol Cell Biol **8**(5): 405-13.
- Sabbir, M. G., N. Wigle, et al. (2010). "Identification and characterization of Dlc1 isoforms in the mouse and study of the biological function of a single gene trapped isoform." BMC Biol **8**(1): 17.
- Schlame, M., D. Rua, et al. (2000). "The biosynthesis and functional role of cardiolipin." Prog Lipid Res **39**(3): 257-88.
- Schmandke, A. and S. M. Strittmatter (2007). "ROCK and Rho: biochemistry and neuronal functions of Rho-associated protein kinases." Neuroscientist **13**(5): 454-69.
- Schug, Z. T. and E. Gottlieb (2009). "Cardiolipin acts as a mitochondrial signalling platform to launch apoptosis." Biochim Biophys Acta **1788**(10): 2022-31.

- Scorrano, L. (2008). "Caspase-8 goes cardiolipin: a new platform to provide mitochondria with microdomains of apoptotic signals?" J Cell Biol **183**(4): 579-81.
- Sigma-Aldrich (2005). "Bicinchoninic acid protein assay kit product information."
- Siskind, L. J. (2005). "Mitochondrial ceramide and the induction of apoptosis." J Bioenerg Biomembr **37**(3): 143-53.
- Smith, D. J., H. Ng, et al. (2008). "The mitochondrial gateway to cell death." IUBMB Life **60**(6): 383-9.
- Sorice, M., A. Circella, et al. (2004). "Cardiolipin and its metabolites move from mitochondria to other cellular membranes during death receptor-mediated apoptosis." Cell Death Differ **11**(10): 1133-45.
- Sumitomo, M., M. Ohba, et al. (2002). "Protein kinase Cdelta amplifies ceramide formation via mitochondrial signaling in prostate cancer cells." J Clin Invest **109**(6): 827-36.
- Tanaka, T., D. Nishimura, et al. (2006). "Nuclear Rho kinase, ROCK2, targets p300 acetyltransferase." J Biol Chem **281**(22): 15320-9.
- Tomassini, B. and R. Testi (2002). "Mitochondria as sensors of sphingolipids." Biochimie **84**(2-3): 123-9.
- Totsukawa, G., Y. Yamakita, et al. (2000). "Distinct roles of ROCK (Rho-kinase) and MLCK in spatial regulation of MLC phosphorylation for assembly of stress fibers and focal adhesions in 3T3 fibroblasts." J Cell Biol **150**(4): 797-806.
- Ullmannova, V. and N. C. Popescu (2006). "Expression profile of the tumor suppressor genes DLC-1 and DLC-2 in solid tumors." Int J Oncol **29**(5): 1127-32.
- Vermeulen, K., D. R. Van Bockstaele, et al. (2005). "Apoptosis: mechanisms and relevance in cancer." Ann Hematol **84**(10): 627-39.
- Villalonga, P. and A. J. Ridley (2006). "Rho GTPases and cell cycle control." Growth Factors **24**(3): 159-64.
- Wennerberg, K., K. L. Rossman, et al. (2005). "The Ras superfamily at a glance." J Cell Sci **118**(Pt 5): 843-6.
- Winter, G. (2002). Datasheet: Human single fold scFv I and J libraries (Tomlinson I and J). MRC Laboratory of Molecular Biology and the MRC Centre for Protein Engineering, Cambridge, UK.

- Wong, C. M., J. W. Yam, et al. (2005). "Rho GTPase-activating protein deleted in liver cancer suppresses cell proliferation and invasion in hepatocellular carcinoma." Cancer Res **65**(19): 8861-8.
- Xu, F. Y., S. L. Kelly, et al. (1999). "N-Acetylsphingosine stimulates phosphatidylglycerolphosphate synthase activity in H9c2 cardiac cells." Biochem J **337** ( Pt 3): 483-90.
- Yam, J. W., F. C. Ko, et al. (2006). "Interaction of deleted in liver cancer 1 with tensin2 in caveolae and implications in tumor suppression." Cancer Res **66**(17): 8367-72.
- Yuan, B. Z., X. Zhou, et al. (2003). "DLC-1 gene inhibits human breast cancer cell growth and in vivo tumorigenicity." Oncogene **22**(3): 445-50.
- Yuan, J. S., A. Reed, et al. (2006). "Statistical analysis of real-time PCR data." BMC Bioinformatics **7**: 85.
- Zhang, Y., X. Li, et al. (2009). "Ceramide-enriched membrane domains--structure and function." Biochim Biophys Acta **1788**(1): 178-83.
- Zhong, D., J. Zhang, et al. (2009). "The SAM domain of the RhoGAP DLC1 binds EF1A1 to regulate cell migration." J Cell Sci **122**(Pt 3): 414-24.